Application and Evaluation of Local and Global Analysis for Dynamic Models of Infectious Disease Spread

A Thesis Submitted to the
College of Graduate Studies and Research
in Partial Fulfillment of the Requirements
for the Degree of Master of Science
in the Department of Computer Science
University of Saskatchewan
Saskatoon

By
Qian Zhang

Permission to Use

In presenting this thesis in partial fulfilment of the requirements for a Postgraduate degree from the University of Saskatchewan, I agree that the Libraries of this University may make it freely available for inspection. I further agree that permission for copying of this thesis in any manner, in whole or in part, for scholarly purposes may be granted by the professor or professors who supervised my thesis work or, in their absence, by the Head of the Department or the Dean of the College in which my thesis work was done. It is understood that any copying or publication or use of this thesis or parts thereof for financial gain shall not be allowed without my written permission. It is also understood that due recognition shall be given to me and to the University of Saskatchewan in any scholarly use which may be made of any material in my thesis.

Requests for permission to copy or to make other use of material in this thesis in whole or part should be addressed to:

Head of the Department of Computer Science
176 Thorvaldson Building
110 Science Place
University of Saskatchewan
Saskatoon, Saskatchewan
Canada
S7N 5C9

Abstract

In this thesis, we applied local analysis tools (eigenvalue and eigenvalue elasticity analysis, global function elasticity/sensitivity analysis), and global analysis tools (deriving the location and stability of fixed points) to both aggregate and individual-level dynamic models of infectious diseases. We sought to use these methods to gain insight into the models and to evaluate the use of these methods to study their short-term and long-term dynamics and the influences of parameters on the models.

We found that eigenvalues are effective for understanding short-term behaviours of a nonlinear system, but less effective in providing insights of the long-term impacts of a parameter change on its behaviours. In term of disease control, local changes of behaviours, yielded from the changes of parameters based on eigenvalue elasticity, are able to alter behaviours in a short-term, especially in the period of a disease outbreak. While eigenvalue elasticity analysis can be helpful for understanding the impact of parameter changes for simple aggregate models, such analyses prove unwieldy and complicated, particularly for models with large number of state variables; and easily fall prey to eigenvalue multiplicity problems for large individual-based models, and distracting artifacts associated with small denominators. In response to these concerns, we introduced other local methods (global function elasticity/sensitivity analyses) that capture many of the advantages of eigenvalue elasticity methods with much greater simplicity. Unfortunately, parameter changes guided by these local analysis techniques are often insufficient to alter behaviours in the longer-term, such as when system behaviours approach stable endemic equilibria. By contrast, the global analytic tools, such as fixed point location and stability analysis, are effective for providing insights into the global behaviours of disease spread in the long-term, as well as their dependence on parameters. Using all of the above analysis as a toolset, we gained some possible insights into combination of local and global approaches. Choice of applying local or global analysis tools to infectious disease models is dependent on the specific target of policy makers as well as model type.

Acknowledgements

I have had the most wonderful fortune of having Dr. Nathaniel D. Osgood as my supervisor. I deeply appreciate for his support and guidance to both my study and research, his counsel and example, his humor and patience. Dr. Osgood's truly scientific intuition and abundant experiences greatly enriches me as a student, ensures my research being on the right track, and inspired me to carry out productive researches and to choose my future study.

I would like to thank all members of my thesis committee, Dr. Winfried Grassmann, Dr. Raymond J. Spiteri and Dr. Kevin G. Stanley, for their helpful comments, suggestions, and encouragement throughout my research and thesis writing. I am very grateful to have had the opportunity to learn from and interact with them.

I have had the good fortune to study in Software Research Lab with Dr. Brian de Alwis, Yu Gao, Andriy Hnativ, Ian Hopkins, David Noete, Jeeva Paudel, Andrew Sutherland, David Vickers and Jin Zhang for their help and suggestions in both computer science and health science. I would also like to thank Canadian people and all my friends in Canada for your friendship and kindness.

Finally, I owe the deepest gratitude to my parents for their forever love and supports, and to all my friends in Beijing and my hometown for their sincere help and encouragements, without which I would not have been able to pursue my dreams.

For my parents, who offered me unconditional love and support throughout the course of this thesis.

Contents

List of Tables

List of Figures

List of Abbreviations

ABM	Agent-based Model
CTL	Cytotoxic T Lymphocyte
DFE	Disease-free Equilibrium
HIV	Human Immunodeficiency Virus
HSV	Herpes Simplex Virus
IBM	Individual-based Model
SARS	Severe Acute Respiratory Syndrome
SD	System Dynamics
SIR	Susceptible-Infected-Recovery
TB	Tuberculosis

Chapter 1

Introduction

1.1 Motivations

We are living in a dangerous world due to infectious diseases: while in the past we faced bubonic plague, smallpox and typhoid, today we face Human Immunodeficiency Virus (HIV), Severe Acute Respiratory Syndrome (SARS) and chlamydia. Many researchers from diverse research areas have contributed many new ideas to the research on the spread of infectious disease and disease control.

Infectious diseases exhibit complex dynamic behaviours (e.g., sudden outbreak, oscillations, periods of quiescence, sudden die off) [1]. They also respond to control measures in complex and sometimes unexpected ways. This complexity can render some well-intentioned policies ineffective, and complicated policy choices. Therefore, we need mathematical models to capture complexities and hidden dynamic characteristics and structures of the outbreak, spread, and response to policies of infectious diseases.

Classic aggregate or compartmental models of infectious disease, such as SIR model firstly developed by W. Kermack and G. McKendrick in 1927 [1], seek to model the progress of an epidemic in a large population by representing the shift of the population between different compartments, for example representing individuals in natural history of infection. More elaborate versions of the Kermack-McKendrick model and other aggregate models that better reflect the actual biology of a given disease have been researched in terms of mathematics for a long time [1].

While powerful, aggregate infectious disease models pose difficulties in characterizing the detailed impacts of network contact between individuals in the population

on the progress of disease spread, especially for some sexually transmitted diseases, of which the transmission exhibits distinct complex dynamics in some sub-groups such as a particular ethnic group or a group of sex trade workers [2]. In terms of disease control, policy makers should consider different policies for these special groups of people from the occasionally infected patients.

One of the new lines of inquiry is social network analysis, and its close variant of network analysis in static agent-based models. Network analysis can help us identify the significant people in the network to whom public health field nurses or policy makers should pay more attention. However, classic social network analysis mainly emphasizes static network properties and characteristics of nodes in the network, and therefore cannot provide insight into the best time and important factors of each individual to control the spread of infectious diseases. In addition, most agent-based models use discrete rules to describe inner state transitions for each agent in the network, which typically have only coarse representations of individual-level dynamics, such as the dynamics of infection, building of naturally acquired or vaccine introduced immunity, and waning of immunity.

Meanwhile in the level of individual biological dynamic processes, mathematical models of disease dynamics in aspect of immunology and virology have recently begun to provide details of dynamics of infected cells, uninfected cells, virus, and immune responses by differential equations models. Within this study we study a new type of model that combines agent-based models and immunological dynamic models to establish a relatively detailed "immune-epidemiological" dynamic model of infectious diseases spread.

Fixed point and stability analysis have been widely applied to mathematical models of compartmental infectious disease models and some individual-based models. Such methods provide evidence for understanding the long-term outcome of disease control strategies. Thus we analyze equilibria and their stability to find out the global attributes of our infectious disease models. Application of eigenvalue analysis, which has been applied in linear and simple nonlinear dynamical models, could be taken into consideration to analyze local behaviours and characteristics of both

compartmental and individual-based models of infectious disease spread. Furthermore, in terms of local disease control, we investigate eigenvalue elasticity and global function elasticity with respect to parameters in hopes of identifying parameters that have great influences on the disease spread.

The thesis is arranged as follows: Chapter 2 reviews past literature concerning eigenvalue elasticity analysis, mathematical modeling of infectious diseases, agent-based modeling, and equilibrium and stability analysis of infectious disease models. Chapter 3 provides details on these methodologies. Chapter 4 analyzes an aggregate model and an individual-based virus dynamic model with eigenspace and eigenvalue elasticity methods. Chapter 5 presents a novel global function elasticity analysis for both an SIR model and an individual-based virus dynamic model. Finally Chapter 6 gives conclusions and future directions for our study.

1.2 An Overview of Eigenvalue Elasticity Analysis

Eigenvalue elasticity analysis methods originated in control theory and control engineering [25]. In 1982, N. Forrester proposed and applied eigenvalue elasticity analysis (EEA) to system dynamics models as a tool to analyze the relationship between the strength (gains) of feedback loops and the behaviour modes of a linearized system [7]. Forrester focused on the gains of the causal links which constitute the basic structure of the system. A gain matrix was presented that is similar to a Jacobian matrix of a nonlinear system near an equilibrium point. He used EEA to explore how the eigenvalues change as link gains change, and described the relationship between model structure and behaviour by eigenvalues and corresponding eigenvectors of the gain matrix.

In addition, eigenvalue elasticities with respect to parameters were used to identify the influential parameters of a model. In Forrester's study, such elasticities to parameter changes helped confirm the dominant role of inventory adjustment in a business cycle [7]. In our study, eigenvalue elasticities with respect to parameters are mainly discussed to identify the timing and character of effective public health

interventions. Although it is possible to re-run simulations with different parameter settings to investigate the importance of a parameter, as classic parameter sensitivity experiments do, for a large system, like an individual-based model with a large population size, such the method is time-consuming. Therefore, we use elasticity analysis to gain characteristics of parameters at the same time when the simulation runs.

1.3 An Overview of Individual-based Modeling

A multi-agent system is a system consisting of multiple interacting agents, where an agent is defined as "a system component that has autonomy in its actions and has a social ability to interact with other agents in the system through some patterns like cooperation, coordinations and negotiation" [35]. An agent-based model (ABM) is a multi-agent system acting as a computational model for simulating actions of individual agents and interactions between agents in a network. The most distinct aspect of agent-based modeling is the interaction between individual agents. The model simulates the simultaneous operations of agents and their interactions in an attempt to re-create and anticipate the system's complex high-level behaviours. This behaviour reflects the emergence of the system dynamics from a micro level to a macro level; as a disaggregated modeling technique, a central aim of the agent-based modeling is to discover the global consequences emerging from local actions [4]. Agent-based modeling has been applied in fields such as logistics, ecology, modeling of consumer behaviour, vehicle traffic analysis, and the spread of epidemics [23].

Given the above definition of agents, it is apparent that an individual actor (e.g. a human being or an animal) can be abstracted and represented as a situated agent for many purposes. However, in this thesis, we thus prefer to use the term "individual-based models" to "agent-based model" because 1) "agent-based models" is often used to denote models using discrete objects and interacting rules, the terms sometimes carry implications not just about the level of aggregate of the model, but also its implementation techniques. In our study, distinctive from traditional

agent-based models which are usually described by state charts, the model of this study use differential equations to describe dynamics of the number of virus, infected cells and T cells for each individual in a network rather than discrete behaviour changes; 2) individual-based models can be formulated by using either classic state-equation methods (as used in system dynamics) or traditional agent-based modeling techniques [23]. 3) In the health science, the term "agent" is widely used with a distinct meaning as a factor, such as a microorganism or chemical substance, whose presence or relative absence can result in the occurrence of a disease [19].

1.4 Epidemiological Background

Most extant dynamic infectious disease models can be classified as either compartmental models or individual-level network models [15]. The dynamics of compartmental models are usually described by ordinary differential equations, an example being the SIR model (Susceptible-Infected-Recovered) [34]. This type of model presents dynamics of infectious disease transmission at an aggregated level, and such models commonly impose assumption of continuous mixing of population within compartments [26]. SIR models and their variants are epidemiological models that compute the theoretical number of people who are infected with an infectious disease in a closed population over time [34]. One of the simplest and earliest examples of SIR models is the Kermack-McKendrick model [14]. This model describes the spread of an infectious disease in an aggregated level in a closed group of people: it involves state equations relating the number of susceptible people $S(t)$, the number of infected people $I(t)$, and the number of recovered people $R(t)$. Many variants of this model exist, with multiple classes of infective and susceptible individuals [24].

Network models explicitly represent individuals with connections and mainly describe the influence of topology or structure of a network on the spread of infectious disease. One type of network model is individual-based dynamic models. This type of model mathematically describes changes over time in the epidemiology and natural history of infectious diseases at a level of population members. In such models,

network structure frequently is based on the reported contacts of individuals [20].

In immunology, cytotoxic T lymphocytes (CTL) are regarded as a kind of white blood cell whose function is mainly to induce the death of infected cells and attack viruses. CTLs proliferate following an infection. Like other T lymphocytes, CTLs kill cells infected with viruses or other pathogens and dysfunctional cells. We use the term 'immune responsiveness' to describe the rate at which an individual mounts an immune response to a given virus, and 'CTL responsiveness' is the average rate at which specific CTLs proliferate after encountering infected cells [22].

Virus dynamics describes how viruses spread from cell to cell. This micro-level epidemiology provides a novel perspective from which to understand infectious diseases in terms of dynamical systems using characterized mathematical tools such as differential equations. The purpose of research in this field is to reveal the basic laws that control the spread of infectious agents within an individual, their interactions with the immune system, and their responses to treatment [22]. In this thesis, we build on a simple model of virus dynamics that considers the populations of uninfected cells, infected cells, free virus particles, and the effect of CTL responses that can eliminate infected cells. Based on the basic model for an individual, we follow an individual-based network model developed in [33] with the assumption that interactions between individuals result in flow of free virus particles among those people.

1.5 Thesis Contributions

In this study, we seek to use analytic techniques to better understand mathematical models simulating the spread of infectious disease in the population. Specifically, by applying both global techniques (fixed points and their stability analysis) and local techniques (eigenspace analysis, eigenvalue elasticity analysis, and global function elasticity analysis) to both aggregate and individual-based infectious disease models, we aim to address the following questions: 1) how well do linear eigenspace-based approaches for assessing the sensitivity of model behaviours to a parameter function

when applied to nonlinear models of infectious disease spread? 2) In light of the large number of different eigenvalues associated with larger state-variable models, can elasticity with respect to parameters of summary measures of model functioning help provide high-level insight into the short-term impact of parameter changes on model behaviours? 3) Can symbolic or (if required) numeric analysis of the location and stability of equilibria help provide insight into how the long-term behaviour of models depends on parameter values?

Within this thesis, eigenvalue and eigenvalue elasticity analysis are applied to analyze the evolution of the system behaviours of nonlinear infectious disease models as a tool of parameter sensitivity analysis in order to identify parameters that have great impacts on the system, as well as proper time points to perturb these parameters with the purpose of altering the system evolution. Drawing on eigenspace techniques employed in previous studies of model behaviour, we find that for nonlinear systems, eigenvalues are effective to understand short-term behaviours, but form a poor tool determining for the long-term impacts of a change on behaviours. This reflects the fact that, for a non-linear system far from equilibrium, eigenvalues of the Jacobian matrix at a particular time point only represent local behaviour modes for a short period of time. In addition, we find that in an individual-based model, because of similar equations for individuals in the network, the multiplicity of eigenvalues of the Jacobian matrix occurs frequently, that may hamper the efficiency of eigenspace analysis on individual-based models. In eigenvalue elasticity analysis, while changes of parameters based on eigenvalue elasticities could yield significant changes to eigenvalues in a short period of time, such changes may not directly change state behaviours. In terms of disease control, local changes of eigenmodes are able to alter behaviours in a short-term, especially in the period of the disease outbreak, though such changes may not be sufficient to decrease the prevalence or average infection among the population in the later stages of disease spread, as system behaviours approach to stable endemic equilibria. We found that for highly nonlinear systems, a focus on the dominant eigenvalues – or even all eigenvalues – alone may not be sufficient to describe the dynamics of the system even in a short time period,

given that the structure of eigenvectors, as well as coefficients, could mediate and moderate the impacts of such an eigenvalue change on state variables in important ways. This difficulty poses particular challenges for larger systems, because of the large number of state variables and eigenvalues, as well as their associated coefficients and eigenvectors.

Inspired by some of the difficulties associated with the eigenvalue elasticity analysis method, we developed global function elasticity and sensitivity in order to better anticipate the impacts of parameters on the global behaviours of a large system. We then applied this method to analyze both aggregate and individual-based models. With perturbations of parameters at time points when the elasticities or the sensitivities have high values, the trajectory of the global function achieves significant changes in a short period of time after the perturbations. This result is especially useful during the period of disease outbreak. But in the long-term, such perturbations may not bring the significant changes of the global function because the changes based on these locally high global function elasticities or sensitivities cannot guarantee either changes of the position of the endemic equilibrium nor significant global changes to the system trajectory. Even when large trajectory deviations can be achieved, the global structure of the system may cause the shifted trajectory to exhibit a changed elasticity from what was originally expected.

In contrast to the local understanding afforded by eigenspace methods, fixed points and stability analysis give insights into the global behaviours of disease spread in the long-term, as well as their dependence on parameters. A change of one parameter when all other parameters are left unchanged might change the positions or stability of equilibria for a model, thereby shifting the position of the trajectory in the long run. To help understand this dependence, we derived formulas for the location of fixed points for both aggregate and individual-based models, and suggest how they may be generalized for individual-based models with arbitrarily large population size but simple network structure. Similarly, we performed numeric analysis of eigenvalue structure for such models around equilibria, in order to understand how network structure and selected parameters impact the stability of equilibria.

Following the Routh-Hurwitz Criterion, we derived a series of ranges for all perturbed parameters, within which an increment or a decrement of a parameter will not change the stability of the equilibrium.

With fixed points analysis and eigenspace analysis, as well as global function elasticity, we gained some possible insights into combination of local and global approaches. If the value of a global function (such as prevalence) at a fixed point is directly related with the parameter to be perturbed, any change of the parameter could result in shifting the global function in the long run. The time point at which the global function elasticity has the largest absolute value could be considered as an advantage deadline to change the parameter. Any perturbation of the parameter before that time point may allow the global function to rapidly approach to the shifted fixed point in time.

Chapter 2

Literature Review

Anderson and May [1] described mathematical models of the transmission of infectious agents with human populations which can help policy makers to interpret observed epidemiological trends, understand and control the process of the spread of diseases, such as measles, malaria, river blindness, sleeping sickness, and schistosomiasis, and the advent of AIDS/HIV and other emerging viruses. They dealt with the dynamics of the basic linear and nonlinear model of infectious diseases and focused on the non-seasonal oscillations in incidence observed for many infections. Spectral analysis was applied to analyze the data for measles, pertussis, and mumps that showed that well-determined cycles explained most of the variability of these data; and the estimated period of damped oscillations of the basic model for endemic infections, described in the form of $T \simeq 2\pi[(D + D')A]^{1/2}$ (where $D + D'$ is the duration of the latent plus infectious intervals, A is the average age at infection and D is the period between oscillations in years), was in good agreement with the observed periods of oscillations for these diseases.

In the paper of Korobeinikov et al [17], the stability of compartment infectious disease models was studied using a SIRS (susceptive-infection-recover-susceptive) model and a SEIRS (E for exposed host) model. With the assumption that the incidence rate can be represented by an arbitrary function $f(S, I, N)$ and the population size is constant, they showed that these models exhibit asymptotically stable steady states and proved that the concavity of the incidence rate with respect to the number of infective individuals is a sufficient condition for stability, i.e., the models have either a unique and stable endemic equilibrium state or no endemic equilibrium at all. In [32] and [21], authors of two papers separately analyzed the equilibrium

of compartmental models of infectious diseases transmission, and indicated that the basic reproduction number R_0 is a threshold for the stability of the models. The disease-free state is asymptotically stable when $R_0 < 1$ and unstable if $R_0 > 1$, and whether the stability of such equilibrium is global or local depends on the model structures. In addition, it was proved out that there was a unique endemic state for the two-stage model studied in the paper and such state is globally asymptotically stable if $R_0 > 1$.

The methodology of eigenvalue elasticity analysis in the field of system dynamics was first used by N. Forrester in 1982 [7]. In his PhD thesis, he proposed the concept of eigenvalue elasticity and used this concept relative to the model feedback structure to understand model behaviours. He described the magnitude of 'the loop elasticity' as a measurement of the significance of a feedback loop to a dynamic behaviour mode. Because the sum of all link elasticities arriving at one node equals the sum of all link elasticities departing this node, 'link elasticity' was defined as a sum of all loop elasticities passing through a link. With this definition, it is possible to set up a linear system to identify the loop elasticities of the model for each eigenvalue of the system matrix. Forrester applied this methodology in a linear system and a nonlinear system which was linearized for particular time points.

Recent work on loop dominance analysis was contributed by Saleh [28, 29]. In his work, he refined many aspects of the eigenvalue analysis, especially in nonlinear models. In [28], he suggested that eigenvalue elasticity analysis is also suited for nonlinear systems by noting how the eigenvalues change as causal link gains change in the linearized model in addition to conventional computation of eigenvalues of the Jacobian matrix at particular time points. Eigenvalues can be regarded as defining different behaviour modes, the superposition of which describes the overall behaviour of the system. Eigenvalue elasticity analysis provides a method to find the dominant structures (e.g., loops) in the model [29].

As an improvement of formal dynamic model analysis tools, Guneralp [11, 10] proposed a ten-step procedure to measure all modes of the model and to calculate the elasticity values with a normalized method, which overcomes the drawbacks,

particularly the computational expenses, of the traditional experimental iterative analysis of models. The methodology is able to track the loop dominance dynamics over time and the influences of feedback loops on a specific variable. This method also made it possible to plot relative loop elasticities over time for visualization of how loop dominance dynamics unfold through simulation [11]. His analysis is useful in understanding the impact of the structural causes underlying oscillations and the other modes of system behaviour, as well as potential policy options for prevention and management of an economic system. However, the methodology was shown to be effective only for simple nonlinear systems with a small number of state variables (less than ten), and the influences of evolutions of eigenvectors and coefficients on the system analysis were not discussed.

In recent years, more and more scholars begin to concern the pros and cons of two approaches to system modeling: aggregated compartmental modeling (such as is classically the focus of the methodology of System Dynamics) and disaggregated agent-based modeling. Demirel [4] analyzed a supply chain model by both system dynamics method and agent-based modeling techniques. In this work, he proved that there are some factors and effects captured by the aggregate method that emerge in an agent-based model, but there are also cases where aggregate models cannot capture certain dynamics generated by agent-based modeling, even at an aggregate level [4]. In addition, aggregate models cannot capture all detailed dynamics and make no distinction among agents; it is therefore unable to capture context-based rational choices and autonomy of the agents. The results suggested that a macro-level approach to dynamical systems can show dynamics at an aggregated level but misses the heterogeneity among agents emerging from the increase of rationality.

There are pitfalls of traditional compartmental modeling techniques in epidemiology, e.g., it assumes that each individual in a population has an equal chance of spreading the disease to others within a compartment. Meyers, etc. [20] indicated that conventional compartmental models to SARS have resulted in estimates of the fundamental quantity of the basic reproductive number R_0 [1] were not consistent with the observed value. This paper gave explanations of the inconsistency between

predictions and the observed epidemiology and applied the powerful quantitative methods of network epidemiology to illustrate that a single R_0 in the same parameter setting may produce very different epidemiological outcomes [20]. Thus, the application of disaggregated individual-based network provides a valuable perspective to the research on epidemiology.

Recent study of infectious disease modeling focuses on individual-based models, where viral dynamics of each individual in the population is described by differential equations. Glasser et al [9] put forward dynamic individual-based models with current US age distributions and typical spatially distributed social structures based on biologically realistic systems that reproduced the spatiotemporal pattern of the importation of smallpox into Yugoslavia in 1972. In this study, the disease models were represented by compartments and ordinary differential equations, and they modeled hypothetical current US communities of "village", "town" and "city" with different populations and municipal constructions that included hospitals. Age-appropriate activities determined social connections between neighbourhoods and schools or workplace, and other interconnections were considered dynamically with different probabilities of individuals to be exposed to social activities within their community and between neighbour communities. With exposure of 10, 50, or 10,000 people in various settings, surveillance and containment (S&C) coupled with vaccination of hospital-based health care workers (HCWs) within 2 days after the first diagnosis were modeled. If 90% of patients were isolated within days after their initial symptom onset and 75% of contacts were vaccinated and monitored, S&C would reduce cases by 82%-99%. But immunization of HCWs, closing schools would contribute little to control the disease. Therefore, they suggested in this paper that for policy makers, stockpiling vaccine, training HCWs, improving laboratory capacity and further understanding of S&C should be emphasized [9]. In addition, [18] modeled each individual in a population based on an immune response model described by ordinary differential equations and studied the effect of individual responses on the disease spread at the population level. The simulation results showed that the immune responses of infection in an individual are not necessarily valid when the

individuals are connected in a network. The length of an infection and the viral load peak values in the network changed from the single individual case, and it is possible for a few individuals with weak immune response to maintain the infection in the whole population. Based on the conclusion, the paper gave explanations of chronic infections reappearing in large group of people in a certain environment. In addition, the paper also provided the prerequisite to stable infection-free equilibriums of the models.

Chapter 3

Methodology

3.1 Background of Dynamical Systems

System Dynamics is an approach to understanding the behaviour of complex systems over time. It deals with internal feedback loops and time delays that affect the behaviour of the entire system [12, 31]. Different from other methods to study complex systems, System Dynamics employs feedback loops and stocks and flows to describe the structure of a dynamic system. A stock is an accumulation or integration of its inflows and outflows. In term of mathematics, the structure of stock and flows can be represented to the following equations [31]:

$$\begin{aligned} \text{Stock}(t) &= \int_{t_0}^{t} [\text{Inflow}(s) - \text{Outflow}(s)]\mathrm{d}s + \text{Stock}(t_0) \\ \frac{\mathrm{d}\text{Stock}(t)}{\mathrm{d}t} &= \text{Inflow}(t) - \text{Outflow}(t) \end{aligned}$$

Examples of such systems are common in chaos theory and social dynamics [13, 27]. Although the key elements of System Dynamics are feedback, accumulation of flows into stocks, and time delay which can be abstracted graphically, the details of these elements are described by ordinary differential equations, frequently nonlinear ones. Therefore, a system analyzed by System Dynamics can be considered as a dynamical system in which the system state can be represented as a point in state space, each of whose axes corresponds to a particular state variable. Mathematically, the evolution of such a system can be studied with differential equations methods.

3.1.1 Eigenvalues and Eigenvectors of Linear Constant-Coefficient Systems

The simplest linear system with N states can be written as

$$\dot{\mathbf{x}} = A\mathbf{x} \tag{3.1}$$

where $\mathbf{x}$ is the vector of state in the system like

$$\begin{pmatrix} x_1 \\ x_2 \\ \vdots \\ x_N \end{pmatrix}$$

A is a constant matrix of $N \times N$ dimension, which is called the coefficient matrix of the system. If A is time-variant but a constant matrix at a particular time point, Eq. 3.1 can be written as

$$\dot{\mathbf{x}} = A(t)\mathbf{x} \tag{3.2}$$

For both Eq. 3.1 and Eq. 3.2, at a particular time point, the system matrix is a constant matrix, and its eigenvalues and eigenvectors describe the normal dynamic mode of behaviours inherent in this linear constant-coefficient system at that time point (for simplicity we call such linear constant-coefficient systems "linear systems" later in this thesis). The non-zero vector $\mathbf{r}$ is defined to be a right eigenvector of the matrix A if it satisfies the eigenvalue equation $A\mathbf{r} = \lambda\mathbf{r}$ for some scalar λ. In this situation, the scalar λ is called an eigenvalue of A corresponding to the eigenvector $\mathbf{r}$ [16]. In principle, the eigenvalues can be determined by computing the roots of the characteristic equation

$$\det(A - \lambda I) = 0$$

where I is the identity matrix of $N \times N$ dimension. For small systems (of fewer state variables), it is frequently possible to derive symbolic expressions for eigenvalues in terms of model parameters; however, for large systems this is typically not possible.

In the common case when the λs are distinct the eigenvalue solutions of the linear system given in Eq. 3.1 is a linear combination of N linearly independent solutions

of Eq. 3.1 each of which evolves as $\mathbf{x}_i = e^{\lambda_i t}\mathbf{r}_i$ [6]:

$$\mathbf{x} = c_1 e^{\lambda_1 t}\mathbf{r}_1 + c_2 e^{\lambda_2 t}\mathbf{r}_2 + \cdots + c_N e^{\lambda_N t}\mathbf{r}_N = \sum_{i=1}^{N} c_i e^{\lambda_i t}\mathbf{r}_i \tag{3.3}$$

each $c_i (i = 1, \cdots, N)$ is a constant. Therefore, the overall behaviour of the state variables in a linear system can be computed with this linear combination of the modes described by eigenvalues of the coefficient matrix A.

3.1.2 Nonlinear Systems and Jacobian Matrix

In our real physical world, truly linear systems are rare and nonlinear systems dominate. However, such systems very frequently act in a linear fashion within the commonly experienced operating range. Even when the non-linearity plays an important role in the observed dynamics, we can often use linearization to understand their behaviour around a particular time point or point in state space. A subset of nonlinear systems can be expressed with first order ordinary differential equations, in the form

$$\dot{x_i} = f_i(x_1, x_2, \cdots, x_N)x_i \tag{3.4}$$

where N is the number of state variables in the system and f_i is a nonlinear function of the state variables.

One simple example of such a nonlinear system is the Lotka-Volterra equations (also known as the predator-prey equations) [13], mathematically described as:

$$\begin{aligned} \dot{x} &= x(\alpha - \beta y) \\ \dot{y} &= -y(\gamma - \delta x) \end{aligned} \tag{3.5}$$

where y is the population size of some predator, x is the population size of its prey and α, β, γ, δ are parameters associated with the demographics and interaction of two species. To analyze the behaviour modes of this nonlinear system as we do for a linear system, we linearize the system at each time point using the Jacobian matrix.

The Jacobian matrix is defined as the matrix of all first-order partial derivatives of a vector-valued function. For the vector-valued function $(f_i)_{N\times 1}$ in Eq. 3.4, its

Jacobian matrix is

$$\begin{pmatrix} \frac{\partial f_1}{\partial x_1} & \cdots & \frac{\partial f_1}{\partial x_N} \\ \vdots & \ddots & \vdots \\ \frac{\partial f_N}{\partial x_1} & \cdots & \frac{\partial f_N}{\partial x_N} \end{pmatrix}$$

The Jacobian matrix J is constant for linear systems and is equivalent to A in Eq. 3.1 for that case. For nonlinear systems, the Jacobian matrix depends on the values of state variables and $J(\mathbf{x})$ represents the linear approximation to a differentiable function near a particular point, i.e., for the system Eq. 3.4, $\dot{\mathbf{x}} = J(\mathbf{x}_0)\mathbf{x}$ is almost linear in $\mathbf{x}$ in sufficiently small neighbourhoods around the point $\mathbf{x}_0$. For example, for the nonlinear Lotka-Volterra equations, the Jacobian matrix is

$$\begin{pmatrix} \alpha - \beta y & -\beta x \\ \delta y & \delta x - \gamma \end{pmatrix}$$

which is time-variant depending on the values of x and y.

3.1.3 Transfer an Inhomogeneous System to a Homogeneous System

In the above sections, we discuss homogeneous systems, but inhomogeneous systems are more common in our real world. For a nonlinear system, a linearized model at a particular time point t_0 can be derived by a Taylor expansion around t_0:

$$\dot{\mathbf{x}}|_{t_0} = f(\mathbf{x}_{t_0}) + J_{\mathbf{x}_{t_0}} \cdot (\mathbf{x} - \mathbf{x}_{t_0}) + H.O.T. \tag{3.6}$$

Where, $J_{ij} = \partial \dot{x}_i / \partial x_j$ is the entry in the ith row and jth column of the Jacobian matrix of the system at the time point t_0. By omitting the higher order terms, Eq. 3.6 can be approximated as an inhomogeneous system:

$$\dot{\mathbf{x}} = J_{\mathbf{x}_{t_0}}\mathbf{x} + \mathbf{b} \tag{3.7}$$

For simplicity of expression, we denote $J_{\mathbf{x}_{t_0}}$ as J, and $\mathbf{b} = -J\mathbf{x}_{t_0} + f(\mathbf{x}_{t_0})$ is a constant vector at time t_0.

With differentiation with t in both sides of Eq. 3.7, we obtain

$$\ddot{\mathbf{x}} = J\dot{\mathbf{x}} \tag{3.8}$$

Suppose λ_i is one eigenvalue of J, and $\mathbf{r}_i$ is its corresponding (right) eigenvector ($i = 1 \ldots N$). In eigenspace, $\dot{\mathbf{x}}$ can be expressed as a linear combination of the right eigenvectors [10], i.e.,

$$\dot{\mathbf{x}} = \sum_{i=1}^{N} c_i \mathbf{r}_i \tag{3.9}$$

where c_i is the coefficient of the linear combination for the eigenvector $\mathbf{r}_i$. Differentiating Eq. 3.9 on both sides, we obtain

$$\ddot{\mathbf{x}} = \sum_{i=1}^{N} \dot{c}_i \mathbf{r}_i \tag{3.10}$$

Equating the righthand sides for $\ddot{\mathbf{x}}$ given by Eq. 3.8 and Eq. 3.10, and using the definition of $\dot{\mathbf{x}}$ in Eq. 3.9, we have

$$J \sum_{i=1}^{N} c_i \mathbf{r}_i = \sum_{i=1}^{N} \dot{c}_i \mathbf{r}_i$$

Because $\mathbf{r}_i$ are the eigenvectors of J, and $J\mathbf{r}_i = \lambda_i \mathbf{r}_i$ $\therefore$

$$\sum_{i=1}^{N} c_i \lambda_i \mathbf{r}_i = \sum_{i=1}^{N} \dot{c}_i \mathbf{r}_i$$

$\therefore$

$$\dot{c}_i = \lambda_i c_i \qquad (i = 1 \cdots N)$$

$\therefore$

$$c_i = c_i(t_0) e^{\lambda_i (t - t_0)} \qquad (i = 1 \cdots N) \tag{3.11}$$

With Eq. 3.9 and Eq. 3.11, we have

$$\dot{\mathbf{x}} = \sum_{i=1}^{N} c_i(t_0) e^{\lambda_i (t - t_0)} \mathbf{r}_i \tag{3.12}$$

From the above, it can be observed that the slope trajectory (the rate of a state variable changing) is composed of several behaviour modes, each expressed by an eigenvalue and its associated right eigenvector [10]. For nonlinear system, its change rates over a period of time can also be approximated by eigenvalues and eigenvectors.

To express the formula for $\mathbf{x}(t)$, we must deal with the non-homogeneous constant term in Eq. 3.7. We proceed Eq. 3.7 by rewriting:

$$\dot{\mathbf{x}} = J(\mathbf{x} - J^{-1}\mathbf{b}) \tag{3.13}$$

Suppose $\mathbf{X} = \mathbf{x} - J^{-1}\mathbf{b}$. We have $\dot{\mathbf{X}} = \dot{\mathbf{x}}$. Therefore, we have a homogeneous linear system

$$\dot{\mathbf{X}} = J\mathbf{X} \tag{3.14}$$

The eigenvalue solution of Eq. 3.14 is

$$\mathbf{X} = \sum_{i=1}^{N} C_i(t_0) e^{\lambda_i (t-t_0)} \mathbf{r}_i$$

and therefore

$$\mathbf{x} = \sum_{i=1}^{N} C_i(t_0) e^{\lambda_i (t-t_0)} \mathbf{r}_i + J^{-1}\mathbf{b} \tag{3.15}$$

We note that the constant term does not affect the behaviours (eigenmodes) of the system. For our eigenspace analysis at a particular point of time with a small time interval in the next chapters, this constant term can be neglected because the interventions of parameters based on eigenvalue elasticities aim to alter behaviour patterns, as captured by eigenvalues. Therefore, in following sections, we do not take the constant terms into consideration.

3.2 Eigenvalue Elasticity Analysis

3.2.1 Eigenvalue Analysis

For a linear system, eigenvalues of its system matrix correspond to elemental behaviour modes of the system, and the overall behaviour of the system is a superposition of these elemental behaviour modes. Table 3.1 presents five forms of eigenvalues of a linear system and their corresponding behaviour modes. When the imaginary part of an eigenvalue is zero and the real part is nonzero, i.e., in exponential growth or decay mode, the inverse of the real part is the time constant of growth or the negative inverse of real part is the time constant of decay. When both the imaginary and real parts of the eigenvalue are nonzero, the observed frequency of oscillation equals to the absolute value of the imaginary parts of the eigenvalues, and when the behaviour mode is convergent oscillation, such a frequency is called the damped frequency [7].

Table 3.1: Eigenvalue classes and corresponding behaviour modes.

Eigenvalue Class	**Behaviour Mode**
0	Constant
$a + 0 \cdot i, a > 0$	Exponential Divergent Growth
$a + 0 \cdot i, a < 0$	Exponential Convergent Decay
$0 \pm b \cdot i, b \neq 0$	Sustained Oscillation
$a \pm b \cdot i, a > 0, b \neq 0$	Divergent Oscillation
$a \pm b \cdot i, a < 0, b \neq 0$	Convergent Oscillation

Because the total system behaviours are determined by the superposition of all the eigenmodes, it becomes more difficult to study all eigenvalues when the size of state variables of a large complex system grows, and we therefore seek to focus attention on the 'important' eigenvalues. When the real parts of all eigenvalues of a linear system are negative, the magnitude of variations in system behaviours will die away and the system eventually approaches equilibrium. If not all eigenvalues are negative, the eigenvalue with the largest real part will also eventually dominate the system behaviours [7]. Therefore, we term the eigenvalue with the largest real part the 'dominant eigenvalue' of the system, as it will determine the behaviour mode of a linear system. In this study, we assume that there is a unique dominant eigenvalue, and if the dominant eigenvalue is complex we treat that conjugate pair of complex eigenvalues as the same dominant eigenvalue.

With an eye towards identifying these 'important' eigenvalues, we define dominant eigenvectors as the following.

Definition 1 *For a linear system*

$$\dot{\mathbf{x}}(t) = A\mathbf{x}(t)$$

where A is the constant system matrix, its general solution [6] is

$$\mathbf{x} = \sum_i c_i \mathbf{r_i} e^{\lambda_i t}$$

*Where c_i are constants and are called the **coefficients** of the eigenvectors $\mathbf{r}_i$. The eigenvalue with the largest real part is called the **dominant eigenvalue**, and its corresponding eigenvector is termed the **dominant eigenvector**.*

For a nonlinear continuous system, the linearization of it in the immediate vicinity period of the point around which the linearization is performed is adequate to describe system behaviours in that period of time [7]. Therefore, in the short term[1], the superposition of eigenmodes of the Jacobian matrix approximates the observed behaviour of the nonlinear system in a particular time period. The dominant eigenvalue and eigenvector, as well as its coefficient, together determine the most important behaviour mode of the nonlinear system in this period.

3.2.2 Eigenvalue Sensitivity and Elasticity

Eigenvalue elasticities measure transient-response sensitivities of the model to parameters [10]. And since the values of elasticities are dimensionless, they can be compared with each other. This can aid us identifying the parameters which could greatly influence the system.

3.2.2.1 Eigenvalue Sensitivity with Respect to a Parameter

We define sensitivity of an eigenvalue with respect to a parameter as the partial derivative of the eigenvalue with respect to that parameter.

Definition 2 (Eigenvalue Sensitivity) *For a linear system*

$$\dot{\mathbf{x}} = A\mathbf{x}$$

*where λ_i is the ith eigenvalue of the system matrix A, where $i = 1, \cdots, N$ and N is the dimension of the state vector $\mathbf{x}$, the **eigenvalue sensitivity** S_i with respect to the jth parameter of the system p_j is defined as:*

$$S_i(p_j) = \lim_{\Delta p_j \to 0} \frac{\Delta \lambda_i}{\Delta p_j} = \frac{\partial \lambda_i}{\partial p_j} \tag{3.16}$$

[1]The time constant associated with "short term" will depend on the the particulars of the system, and specifically, on the speed with which the system's Jacobian evolves.

We define $[\bullet]$ denoting the unit of $\bullet$ and we can observe that eigenvalue sensitivity is not dimensionless:

$$[S_i(p_j)] = \frac{[\lambda]}{[p]}$$

which indicates that eigenvalue sensitivity prevents comparisons across different parameters with different dimension.

3.2.2.2 Eigenvalue Elasticity with Respect to a Parameter

In contrast to eigenvalue sensitivity (which measures the ratio of the absolute change in an eigenvalue to the absolute change in a parameter), eigenvalue elasticity measures the ratio of the proportional (e.g. percentage) change in the eigenvalue to the proportional (e.g. percentage) change in a parameter. As defined in [7], the ***eigenvalue elasticity with respect to a parameter*** is defined as the partial derivative of the eigenvalue with respect to that parameter normalized for the size of the parameter and the size of the eigenvalue. And with this definition, assuming a non-zero value of the parameter, the elasticity of eigenvalue could also be described as the product of the eigenvalue sensitivity and the ratio of the eigenvalue and parameter. Thus the eigenvalue elasticity of λ_i, with respect to a parameter p_j is as Eq. 3.17.

$$\epsilon_i(p_j) = \lim_{\Delta p_j \to 0} \frac{\frac{\Delta \lambda_i}{\lambda i}}{\frac{\Delta p_j}{p_j}} = \frac{\frac{\partial \lambda_i}{\lambda_i}}{\frac{\partial p_j}{p_j}} = \frac{\partial \lambda_i}{\partial p_j} \cdot \frac{p_j}{\lambda_i} = S_i(p_j) \cdot \frac{p_j}{\lambda_i} \tag{3.17}$$

In this definition, since $[\partial \lambda_i] = [\lambda_i]$ and $[\partial p_j] = [p_j]$, eigenvalue elasticity is dimensionless, enabling us to compare elasticities of the eigenvalue with respect to different parameters. Therefore, if an eigenvalue elasticity with respect to one parameter is larger than for others, it means that behaviour mode is more sensitive to a certain proportional change in that parameter than to similar proportional changes in other parameters. A similar comparison of elasticities is also possible between different time points. Thus, a large elasticity might suggest that:

1. Extra effort should be made to obtain a good estimate of parameter;

2. The parameter should be investigated as a possible policy lever [7];

3. The time when the elasticity arrives at a peak might be the 'best' time to exercise this possible policy lever.

In the next chapter, we use the largest eigenvalue elasticity rather than the elasticity of the dominant eigenvalue because the eigenvalue with the largest elasticity does not always correspond to the dominant eigenvalue. For example, in an individual-based model of infectious disease spread with 3 persons, the dominant eigenvalue differs from the second and the third dominant eigenvalue a little, and their values of elasticities with respect to a parameter are close to each other. Therefore, we apply the largest eigenvalue elasticity to distinguish the greatest impact of a parameter on system behaviours.

3.2.2.3 Implementation Issues

It is difficult to calculate eigenvalue sensitivity or elasticity with Eq. 3.17, because for all but the smallest systems of state equations the computation of derivatives of an eigenvalue is complicated. Specifically, it is not in general possible to derive expressions for eigenvalues in closed form, and numeric differentiation is associated with its own difficulties. The following part of this section tries to simplify the expression of eigenvalue elasticities for the purpose of convenient and accurate computation.

Suppose J is the Jacobian matrix of a nonlinear system, and $\lambda_i, (i = 1, \cdots, N)$ are eigenvalues of J. The matrix Λ is a diagonal matrix whose diagonal elements are all eigenvalues of J, the eigenvalue sensitivity matrix $S(p_j)$ is a diagonal matrix whose entries are eigenvalue sensitivities $S_i(p_j), (i = 1, \cdots, N)$ and the matrix $R = [\mathbf{r}_1, \mathbf{r}_2, \cdots, \mathbf{r}_N]$ is a matrix of eigenvectors $\mathbf{r}_i$ of J.

$$\because J\mathbf{r}_i = \lambda_i \mathbf{r}_i$$

$$\therefore JR = R\Lambda$$

$$\therefore \Lambda = R^{-1}JR \tag{3.18}$$

then by applying the chain rule for matrices we can derive the following:

$$S(p_j) = \frac{\partial \Lambda}{\partial p_j} = \frac{\partial R^{-1}JR}{\partial p_j} = R^{-1}\frac{\partial J}{\partial p_j}R + R^{-1}J\frac{\partial R}{\partial p_j} + \frac{\partial R^{-1}}{\partial p_j}JR \tag{3.19}$$

As proven in [27], supposing $M(t)$ is a matrix depending on the variable t, the following identity holds:

$$\frac{dM(t)^{-1}}{dt} = -M(t)^{-1}\frac{dM(t)}{dt}M(t)^{-1}$$

Thus, Eq. 3.19 can be written as:

$$\frac{\partial\Lambda}{\partial p_j} = R^{-1}\frac{\partial J}{\partial p_j}R + R^{-1}J\frac{\partial R}{\partial p_j} + (-R^{-1}\frac{\partial R}{\partial p_j}R^{-1}JR) \tag{3.20}$$

and finally applying Eq. 3.18 twice we have:

$$\frac{\partial\Lambda}{\partial p_j} = R^{-1}\frac{\partial J}{\partial p_j}R + \Lambda R^{-1}\frac{\partial R}{\partial p_j} - R^{-1}\frac{\partial R}{\partial p_j}\Lambda \tag{3.21}$$

Suppose $\mathbf{l}_i$ is the left eigenvector of J corresponding to the eigenvalue λ_i (i.e. $\mathbf{l}_i{}^T J = \lambda_i \mathbf{l}_i{}^T$) whose right eigenvector is $\mathbf{r}_i$, and L is an $N \times N$ matrix, $L = [\mathbf{l}_1, \mathbf{l}_2, \cdots, \mathbf{l}_N]$. With an assumption that the left and right eigenvectors are in unit length, we have [28]:

$$L^T = R^{-1} \tag{3.22}$$

With Eq. 3.22, Eq. 3.21 can be written as:

$$\frac{\partial\Lambda}{\partial p_j} = L^T\frac{\partial J}{\partial p_j}R + \Lambda R^{-1}\frac{\partial R}{\partial p_j} - R^{-1}\frac{\partial R}{\partial p_j}\Lambda \tag{3.23}$$

Now we focus on the last two terms of the right part of Eq. 3.23. Given A is a square matrix and Λ is a diagonal matrix, the matrix $A\Lambda$ has the same entries in the diagonal with the matrix ΛA. Therefore, we have

$$\Lambda(R^{-1}\frac{\partial R}{\partial p_j}) - (R^{-1}\frac{\partial R}{\partial p_j})\Lambda = \begin{pmatrix} 0 & * & \dots & * \\ * & 0 & * & \dots \\ \vdots & \vdots & \ddots & * \\ & \dots & * & 0 \end{pmatrix} \tag{3.24}$$

.

As a result, we can say that in Eq. 3.23 the diagonal entries of the left hand side of Eq. 3.23 equal the diagonal entries of the first term of the right side, i.e.

$$S_i(p_j) = \frac{\partial\lambda_i}{\partial p_j} = \mathbf{l}_i{}^T\frac{\partial J}{\partial p_j}\mathbf{r}_i \tag{3.25}$$

And Eq. 3.17 can be written as Eq. 3.26

$$\epsilon_i(p_j) = \mathbf{l}_i{}^T \frac{\partial J}{\partial p_j} \mathbf{r}_i \frac{p_j}{\lambda_i} \tag{3.26}$$

With this equation, eigenvalue elasticity with respect to a parameter can be computed using left and right eigenvectors and the partial derivatives of the linearized Jacobian matrix with respect to a parameter. Because J and $\frac{\partial J}{\partial p_j}$ can often be easily determined symbolically and because the eigenvalues can be computed for particular parameter values and points in time, both eigenvalue elasticity and sensitivity with respect to a parameter can be computed without the need to either compute closed-form expressions for eigenvalues nor to perform numeric differentiations. In previous work on eigenvalue elasticity analysis of Forrester [7], Saleh [28] and Guneralp [11], Eq. 3.25 and Eq. 3.26 were applied without explanations. To clarify them we have given the deduction of these two equations in the above.

3.3 Improvements: Global Function Elasticity and Sensitivity Analysis

For a large system with many state variables, the number of eigenvalues is too large to analyze one by one in combination with each parameter. In addition, due to the variation of coefficients, the eigenvalue with the largest real part alone may not describe the dominant behaviour of the system over a short period of time, and there might be several eigenvalues of the system Jacobian matrix that jointly determine the behaviour pattern.[2] In such cases, it is difficult to analyze eigenvalue elasticities to find significant parameters of the system. In this section, we introduce global function in state space and its sensitivity and elasticity to analyze a large system. In contrast to previous sections which synthesized and recast findings from other contributions, the work presented in this section is novel to this thesis.

A global function in state space is defined as a scalar function summarizing the global state of a system ($G : \Re^N \mapsto \Re$, where N is the number of state variables in the

[2]More explanations on this point are provided in Ch. 4.

system) at particular time points, e.g. the average viral load in population members, the total number of infected people, or cumulative mortality in the application field of epidemiology. In a fashion similar to the definition of eigenvalue sensitivity with respect to parameters, we define global function sensitivity as

$$g_s = \lim_{\Delta p \to 0} \frac{\Delta G}{\Delta p} = \frac{\partial G}{\partial p} \tag{3.27}$$

And the global function elasticity is defined as

$$g_e = \lim_{\Delta p \to 0} \frac{\frac{\Delta G}{G}}{\frac{\Delta p}{p}} = \frac{\frac{\partial G}{G}}{\frac{\partial p}{p}} = \frac{\partial G}{\partial p}\frac{p}{G} = g_s \frac{p}{G} \tag{3.28}$$

The derivative of a global function over time can also describe the global behaviour of the system by indicating the rate of change of the global function. Explicating this, we define the elasticity of the global function's rate of change with respect to a parameter to show how much the rate of growth or decrease of a global function could be affected by a small change in a parameter. In this study, this elasticity or sensitivity is called $\dot{G}$ elasticity or $\dot{G}$ sensitivity.

$$\dot{g}_s(p) = \lim_{\Delta p \to 0} \frac{\Delta \dot{G}}{\Delta p} = \frac{\partial \dot{G}}{\partial p} \tag{3.29}$$

$$\dot{g}_e(p) = \lim_{\Delta p \to 0} \frac{\frac{\Delta \dot{G}}{\dot{G}}}{\frac{\Delta p}{p}} = \frac{\frac{\partial \dot{G}}{\dot{G}}}{\frac{\partial p}{p}} = \frac{\partial \dot{G}}{\partial p}\frac{p}{\dot{G}} = \dot{g}_s \frac{p}{\dot{G}} \tag{3.30}$$

Using the total differential and Eq. 3.7, $\dot{G}$ could be written as

$$\dot{G} = \frac{dG}{dt} = \frac{\partial G}{\partial t} + \sum_{i=1}^{N} \frac{\partial G}{\partial x_i}\dot{x}_i \tag{3.31}$$

We note that each of the $\dot{x}_i$ is specified by the series of differential equations. With proper choice or construction of a global function, the term $\frac{\partial G}{\partial t}$ and $\frac{\partial G}{\partial x_i}$ could be computed symbolically prior to the start of simulation. Based on these definitions, we can analyze the impact of a parameter on the system on some global summaries of the system states. When there are high-level global functions of clear interest, this method provides a more direct view than eigenvalue elasticity analysis for informing policy to control the spread of an infectious disease.

Chapter 4

Eigenspace Analysis of Infectious Disease Models

As indicated in Section 1.4, most epidemiological models can be classified into compartmental models and network models. In this chapter, an aggregate compartmental model and an individual-based model within a network are studied using eigenspace methods.

4.1 Eigenspace Analysis of an Aggregate Infectious Disease Model

An SIRS model is a basic aggregate epidemiological model describing dynamic changes of the number of people at different stages of disease exposure and progression in a relatively closed population over time. Because this basic model includes just three state variables, it is relatively easy to quantitatively analyze. But the SIRS model is also of value in serving as representative of a larger and somewhat more elaborate class of infectious disease models. This section studies the systematic behaviours and parameter sensitivity of an SIRS model by analyzing eigenvalues and their corresponding eigenvectors of the linearized SIRS model over time, as well as the eigenvalue elasticities with respect to parameters of the model.

4.1.1 An Improved SIRS Model: Description

Elaborating the typical SIR model of Kermack-McKendrick [14], this study added several parameters with consideration of health care workers, young children, and people who have died from infectious diseases. Much of the model structure draws on the work of [24]. Fig. 4.1 shows a stock-and-flow diagram of the model used in this section. For some serious infectious diseases, such as SARS, hepatitis B and

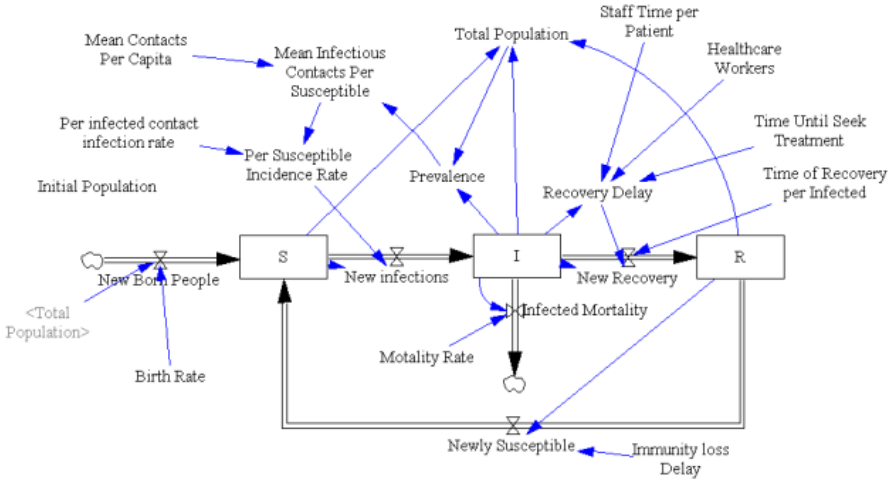

Figure 4.1: The stock-flow diagram of an SIRS model.

C, and potentially many sexually transmitted infections, limitations of health care capacity (and particularly contact tracing) can play a major role in the evolution of an epidemic. For such pathogens, factoring limitations of health care workers into a model is reasonable. Another change in this model relates to the recovery of individuals. The recovery is partitioned into two parts: 1) `Recovery Delay`, which is the time delay due to medical treatment, including a period from the time a patient is infected until the time the patient seeks treatment and a period for a patient to be treated by health workers once presenting for treatment; 2) `Time of Recovery per Infected` which is the time for an individual to physically clear the disease once treated. The third change of the model is a flow from `Recovery` to `Susceptible`, because for many infections, such as flu and many sexually transmitted diseases, patients cannot get lifelong immunity despite recovery. The model representation also assumes that in this model only infected people die off. Because this SIRS model

Table 4.1: Parameter settings of an SIRS model.

Parameter	Full Name	Default Value	Unit
β	Per Infected Contact Infection Rate	0.01	1/person
c	Mean Contacts Per Capita	12	person/day
τ	Immunity Loss Delay	275	day
p	Staff Time Per Patient	0.5	hcw $\cdot$ day/person
q	Time Until Seek Treatment	2	day
h	Health Care Workers	10	hcw
d	Time of Recovery Per Infected	7	day
μ	Mortality Rate	0.02	1/day
σ	Birth Rate	0.01	1/day

has not been calibrated with empirical data drawn from a particular epidemiological context, this model is a stylized general model used for testing and exploring our methodology and considerations of time delay of patients treatment, and will likely behave in a manner representative of a particular real-world context.

Eq. 4.1 provides the state equations of the model in Fig. 4.1.

$$\begin{aligned} \dot{S} &= \frac{R}{\tau} - \beta c \frac{I}{N} S + \sigma N \\ \dot{I} &= \beta c \frac{I}{N} S - \frac{I}{q + \frac{pI}{h} + d} - I\mu \\ \dot{R} &= \frac{I}{q + \frac{pI}{h} + d} - \frac{R}{\tau} \end{aligned} \tag{4.1}$$

where $N = S + I + R$, and the initial values are $S(0) = 200,000$, $I(0) = 200$ and $R(0) = 0$. We also define $Prevalence = I/N$.

The parameters of the model are explained in Table 4.1[1], that are based on the work of [24]. All state variables are of unit 'person'.

4.1.2 Equilibrium and Stability Analysis of an SIRS Model

Epidemiological models of the spread of infection in a population are usually associated with a threshold quantity: the basic reproductive constant R_0, defined

[1] 'hcw' in this table means Health Care Worker

as the mean number of secondary infections resulting from the introduction of one infected individual into an otherwise susceptible population [1]. If $R_0 < 1$, the introduced infection will die out in the long run and the disease-free equilibrium (DFE) is asymptotically stable; if $R_0 > 1$ the level of infection will grow in the population and the DFE is unstable [17, 21, 32]. A general-purpose methodology exists for deriving R_0 from the structure of the system [32].

We define the next generation matrix of an SIRS model to be a matrix whose the (i, j) entry is the expected number of new infections in compartment i produced by the infected individual originally introduced into compartment j [32]. Following [32] and [5], we derive the next generation matrix at the DFE ($S = N, I = 0, R = 0$) for the model Eq. 4.1:

$$\begin{pmatrix} 0 & -\frac{\beta c}{\frac{1}{d+q}+\mu} & 0 \\ 0 & \frac{\beta c}{\frac{1}{d+q}+\mu} & 0 \\ 0 & 0 & 0 \end{pmatrix}$$

R_0 is defined as the spectral radius of the next generation matrix, therefore in this SIRS model

$$R_0 = \frac{\beta c}{\frac{1}{d+q} + \mu} \tag{4.2}$$

This result is identical to the symbolic expression of R_0 derived from the heuristic method of multiplying the infection rate and the mean duration of the infection [32]. With the parameter settings in Table 4.1, $R_0 = 0.9153 < 1$.

We can derive the fixed points of the system by setting the derivatives of the state variables to zero, and solving for values of S, I and R. The equations in this SIRS model are associated with one endemic equilibrium, where the size of infected population and recovered population are in balance with the size of the susceptible population:

$$\begin{aligned} \hat{S} &= \frac{h\mu(\mu\sigma\tau + \mu - \sigma)((\mu - \sigma)\beta c(q + d) - \mu(q + d)^2 - \sigma\tau\beta c - \mu)}{p\sigma(\mu + \sigma\tau\beta c)(\mu^2 + \sigma\beta c - \mu\beta c)} \\ \hat{I} &= \frac{h((\mu - \sigma)\beta c(q + d) - \mu(q + d)^2 - \sigma\tau\beta c - \mu)}{p(\mu^2 + \sigma\beta c - \mu\beta c)} \\ \hat{R} &= \frac{h\tau((\mu - \sigma)\beta c(q + d) - \mu(q + d)^2 - \sigma\tau\beta c - \mu)}{p(\mu + \sigma\tau\beta c)} \end{aligned} \tag{4.3}$$

With the parameter settings in Table 4.1, the endemic equilibrium listed in Eq. 4.3 is (to the nearest integer):

$$\hat{S} = 3183, \quad \hat{I} = 8570, \quad \hat{R} = 5387 \tag{4.4}$$

and the numeric eigenvalues of the Jacobian matrix at the endemic equilibrium are

$$-0.036795, \quad -0.011122, \quad -0.0034814$$

Because all eigenvalues are negative at this point, this endemic equilibrium is asymptotically stable with respect to the current parameter settings.

By contrast, the eigenvalues of the Jacobian matrix at the DFE ($\tilde{S} = N, \tilde{I} = 0, \tilde{R} = 0$) are:

$$\lambda_1 = \sigma, \quad \lambda_2 = -\frac{1}{\tau}, \quad \lambda_3 = \beta c - \mu - \frac{1}{d+q}$$

Because all parameters are non-negative, λ_1 is positive if the birth rate is positive, λ_2 is always negative, and λ_3 may be positive if an infective person infects other people faster than the infected people recover or die. With respect to the current parameter settings, there is at least one eigenvalue with positive real part (λ_1) and the DFE is unstable.

It departs from the normal intuition stated above that the DFE is unstable when $R_0 < 1$. The underlying reason is the varying population size. In our model, the death rate is different from the birth rate and we assume only infective people will die. Given the parameters at hand, the value of N grows over time and the DFE is unstable. To factor out the effects of the changing population size, we look at the fraction of the population that is infected, susceptible or recovered.

We consider the fractions of individuals in the three compartments, namely

$$s = S/N, \quad i = I/N, \quad r = R/N \tag{4.5}$$

Eq. 4.1 becomes

$$\begin{aligned} \dot{s} &= \sigma - \beta csi + \frac{r}{\tau} - \sigma s + \mu si \\ \dot{i} &= -\mu i - g(I)i + \beta csi + \sigma i + \mu i^2 \\ \dot{r} &= -\frac{r}{\tau} + g(I)i - \sigma r + \mu ir \end{aligned} \tag{4.6}$$

where $g(I) = (d + q + pI/h)^{-1}$ and $s + i + r = 1$. For the DFE of this system, $\tilde{s} = 1, \tilde{i} = 0, \tilde{r} = 0$ (corresponding to $\tilde{S} = N, \tilde{I} = 0, \tilde{R} = 0$), and the eigenvalues of the Jacobian matrix at DFE is

$$\lambda_1 = -\sigma, \quad \lambda_2 = -\frac{1 + \sigma\tau}{\tau}, \quad \lambda_3 = \beta c - \mu - \sigma - \frac{1}{d + q}$$

With the current parameter settings, they are

$$\lambda_1 = -0.01, \lambda_2 = -0.0136, \lambda_3 = -0.0211$$

The DFE for the fractional model is stable. The endemic equilibrium of the fractional model is $\hat{s} = 0.1857, hati = 0.5, \hat{r} = 0.3143$. This corresponds to the fractional values of each state variable at the endemic equilibrium in the original model (Eq. 4.4). Similar to the original model, the endemic equilibrium is stable because the real parts of all eigenvalue of the Jacobian matrix at the endemic equilibrium are negative. As indicated in [3], there are two different ways of considering a disease as being controlled in a population of varying size. The stricter way requires that the population of infective $I(t) \to 0$, while the weaker way requires the proportion of infective within the whole population $i(t) \to 0$. For our model and parameter settings, because of varying population size, the infective population cannot be completely eliminated, but the fraction of infective population to the whole population can approach to 0, i.e., the DFE of the fractional model is stable but that of the original model is unstable.

Later in this section, based on eigenvalue elasticity, we will perturb each parameter to increase or decrease its value based on its eigenvalue elasticity, which would change both position and stability of the endemic equilibrium. According to the Routh-Hurwitz Criterion [8], if we fix values of other parameters, we may be able to derive a range of one specific parameter's value. While any change of the value of this parameter within this range may shift the location of the endemic equilibrium within state space, it is guaranteed not to change the stability of that equilibrium. Based on the parameter settings listed in Table 4.1, we can obtain the range of each

parameter respectively if all other parameters are kept constant:

$$\beta: \ (0.00333, \quad \infty) \qquad p: \ (0, \quad \infty)$$
$$h: \ (0, \quad \infty) \qquad \tau: \ (0, \quad \infty)$$
$$\sigma: \ (0.00258, \quad 0.0167) \qquad c: \ (4, \quad \infty)$$
$$d: \ (0, \quad 435.5) \qquad q: \ (0, \quad 430.5)$$
$$\mu: \ (0.01101, \quad 0.0895) \cup (0.0939, \quad 0.10899)$$

Therefore, the stability of the endemic equilibrium does not change if we increase or decrease one parameter by 10% from its default value and keep other parameters unchanged at the same time.

4.1.3 Eigenvalue Analysis of an SIRS Model

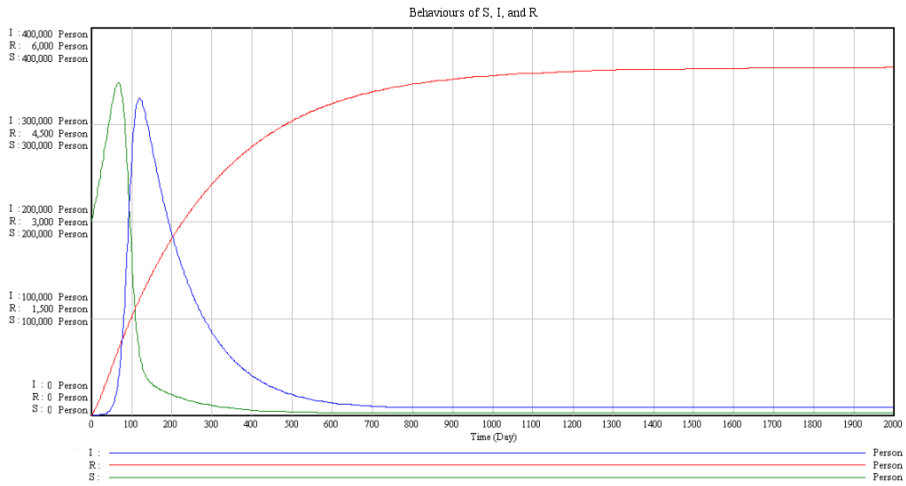

Figure 4.2: The value of S, I, and R over time for an SIRS model.

For the SIRS model described above, Fig. 4.2 shows the trajectories of three states in the system, where the X-axis is time and the Y-axis represents the number of susceptible/infected/recovered people. The numerical simulations for the following analysis were carried out with the Euler method with step size 1. In order to evaluate the adequacy of this step size, we also did simulations for the system with the Euler method with step size 0.1 and 0.01. These simulations produced very close results to that with the same method with step size 1. We approximated the system

to be a linear one at regularly spaced time points with the Jacobian matrix, and obtained eigenvalues of the Jacobian matrix over time. Fig. 4.3 shows all eigenvalues of the Jacobian matrix of the SIRS model over time, where the horizontal axis is time and the vertical axis shows the value of the real and imaginary components of the eigenvalues. In this figure, three solid lines represent real parts of three eigenvalues; meanwhile the dashed line is the magnitude of the imaginary part of complex eigenvalues. Because the Jacobian matrix has three eigenvalues and complex eigenvalues come in conjugate pairs, the imaginary part of eigenvalues is unique if the system has complex eigenvalues. Fig. 4.4 presents the largest real part of the eigenvalues over time. Here the horizontal axis is also the time axis and the vertical axis represents the value of the largest real part of the three eigenvalues.

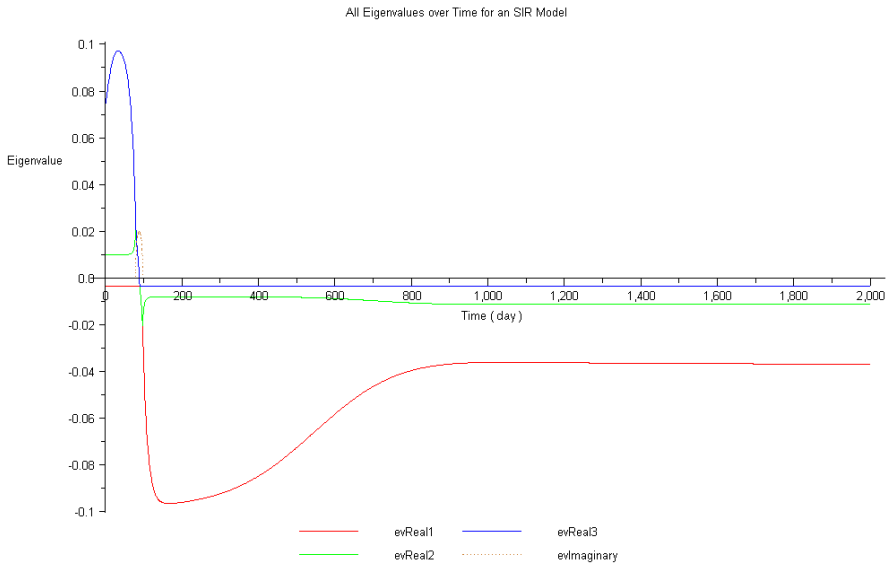

Figure 4.3: All eigenvalues of the Jacobian matrix of an SIRS model over time.

From $time = 82$ to $time = 101$, the imaginary parts of two eigenvalues are nonzero. Correspondingly, as shown in Fig. 4.2, there are oscillations in this short period of time of S and I. However, the value of R does not oscillate during that time period. The reason for this is that the component of the dominant eigenvector representing R has a very small value, and this behaviour mode exerts little influence

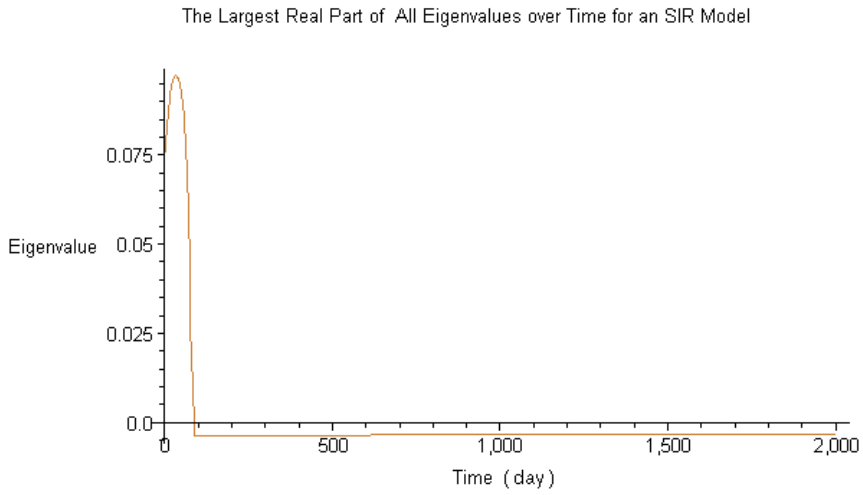

Figure 4.4: The largest real components of eigenvalues of the Jacobian matrix of an SIRS Model over time.

on R. For example, at $time = 82$, three eigenvalues of the Jacobian matrix are:

$$\lambda_{1,2} = +2.21361 \times 10^{-2} \pm 5.720 \times 10^{-3} i, \quad \lambda_3 = -3.63619 \times 10^{-3}$$

and the pair of conjugate eigenvalues has the largest real part. And their corresponding eigenvectors are defined as dominant eigenvectors, namely

$$\begin{pmatrix} -9.24918 \times 10^{-1} \\ -3.60966 \times 10^{-1} \\ 3.92696 \times 10^{-6} \end{pmatrix}$$

Because two eigenvalues are conjugate, they have identical real components for the entries of the eigenvectors. For this mode at $time = 82$, the system oscillates divergently, and since the entries of S and I in the dominant eigenvector are relatively large, the changes of S and I are dramatically controlled by the mode, and oscillate in pronounced manner. And because the third entry of the dominant eigenvector is almost zero, the variable R which it represents is not significantly controlled by this mode, and does not oscillate. From $time = 97$ to $time = 101$, the real part of the conjugate eigenvalues becomes negative, and the system tends to oscillate convergently. Because the rate of convergence is sufficiently high, the oscillations are not apparent. From $time = 102$ forward, all eigenvalues are real, and the largest

real part of eigenvalues are negative, therefore the system tends to be convergent, as Fig. 4.3 and Fig. 4.4 show.

4.1.4 Eigenvalue Elasticity Analysis of an SIRS Model

From the above section, we know that there are 9 parameters for this SIRS model. This section analyzes the elasticity of eigenvalues with respect to selected parameters.

As indicated in the last chapter, the elasticity of all eigenvalues with respect to a parameter can be computed using Eq. 3.26. Because the eigenvalue elasticity with respect to a parameter describes the proportional change of eigenvalues with respect to the proportional change of the parameter, the imaginary parts of the eigenvalues might also be altered by the change of the parameter. Fig. 4.5 and Fig. 4.6 show eigenvalue elasticities with respect to β and p over time. In these graphs, solid red, green, and blue lines represent real parts of elasticities of three eigenvalues, and dashed black is the imaginary part. As above, because complex eigenvalues come in pairs, two eigenvalues are complex conjugates of each other, and the third is real. A single specification of the imaginary component is adequate. From Eq. 4.1, the parameter q and d have same position in the governing equations, thus the symbolic expressions of elasticity with respect to q and d are same, and the values of this elasticity are also same. Similarly, perturbation of the parameter c has similar effects to identical perturbation of the parameter β, because c and β are in the mathematically identical positions. In the following analysis, the parameter d and c are therefore neglected.

By computing eigenvalue elasticities with respect to parameters, we found that q, h and τ have little impacts on eigenvalues, i.e., eigenvalues of the system are not sensitive to these parameters, thus we neglect their influences in this discussion. In the following section, we choose the parameter β and p to analyze the changes of state variables over time resulting from perturbation of these two parameters at times when the values of eigenvalue elasticity are large.

The perturbation of a parameter at $time = t^*$ here means to increase or decrease

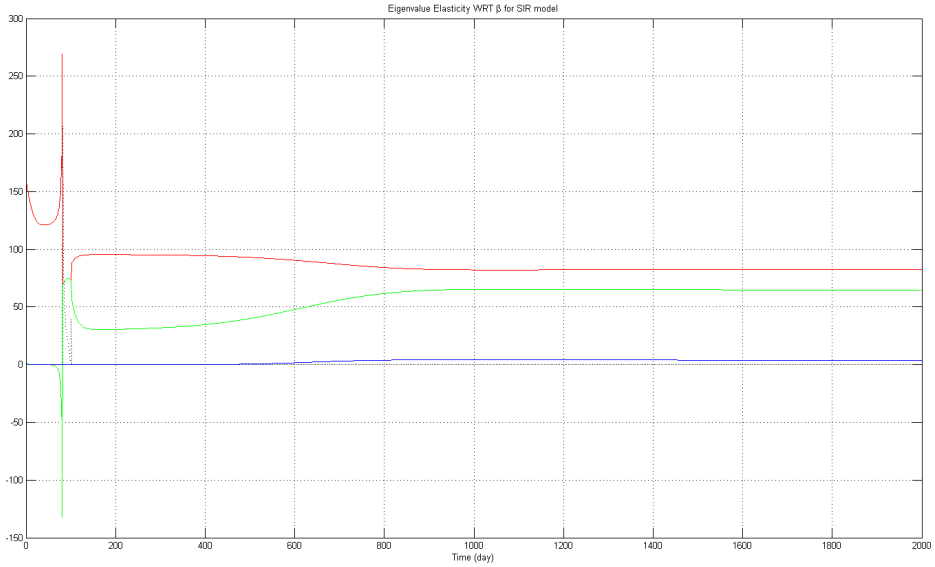

Figure 4.5: Eigenvalue elasticity with respect to β (`Per Infected Contact Infection Rate`) of the SIRS model over time.

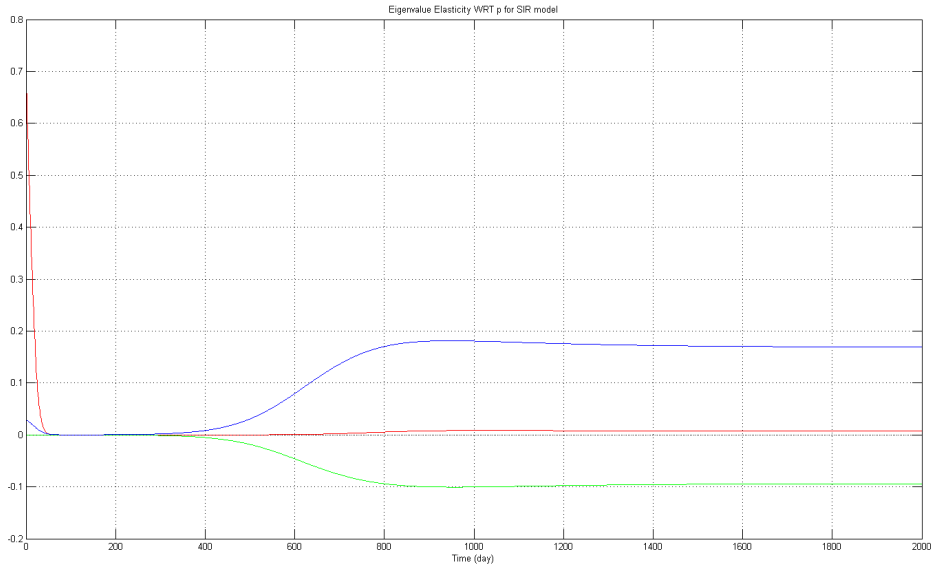

Figure 4.6: Eigenvalue elasticity with respect to p (`Staff Time Per Patient`) of the SIRS model over time.

it by 10% of its value from $time = t^*$ to the end of the simulation. In our elasticity analysis, the parameter is perturbed not at one short period of time, but changed for a long time. Through experiments, we have found that a perturbation of a parameter for a vary brief interval of time can not visibly change the behaviour of state variables. Although it has the shortcoming of causing a long-term effects in that the perturbation of a parameter at one particular time may be accumulated or offset

in later stages, such persistent perturbation of a parameter can help us study the local and global changes of the state behaviours. We note that because the eigenvalue elasticity with respect to a parameter quantifies the impact of a parameter change on the eigenvalues rather than directly on state variables, the impacts of perturbation of the parameter on state variables depend on eigenvalues, the coefficients, and the structure of the eigenvector associated with that eigenmode in the rates of state change.

4.1.4.1 Eigenvalue Elasticity with Respect to β for an SIRS model

As depicted in Fig. 4.5, eigenvalue elasticity with respect to β (`Per Infected Contact Infection Rate`) is quite large at $time = 81$ for the real parts (with values of 269.4 and -132.4) and $time = 82$ for the imaginary part (with a value of 206.9). Thus we perturb β to decrease it by 10% at $time = 81$. The trajectory of the state variables is perturbed as shown in Fig. 4.7 to Fig. 4.10. From these figures, it can be seen that the decrease in β altered the trajectory of S, I and $Prevalence$, but has little effect on R. As indicated in above section, at $time = 82$ the dominant eigenvector has a very small value on the third entry representing R, and large changes of the eigenvalues with largest real parts will not have correspondingly large influences on R. The same condition also obtains at $time = 81$.

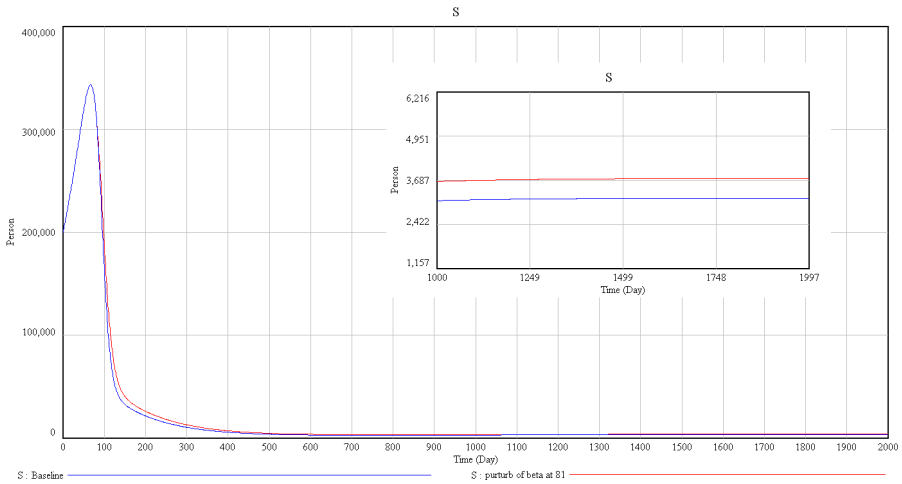

Figure 4.7: The value of S with a perturbation (decreasing by 10%) of β (`Per Infected Contact Infection Rate`) at $time = 81$.

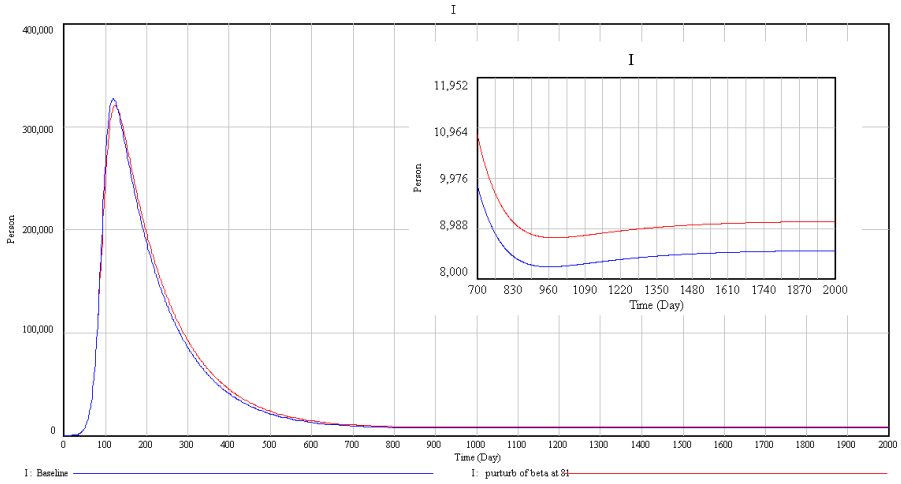

Figure 4.8: The value of I with a perturbation (decreasing by 10%) of β (`Per Infected Contact Infection Rate`) at $time = 81$.

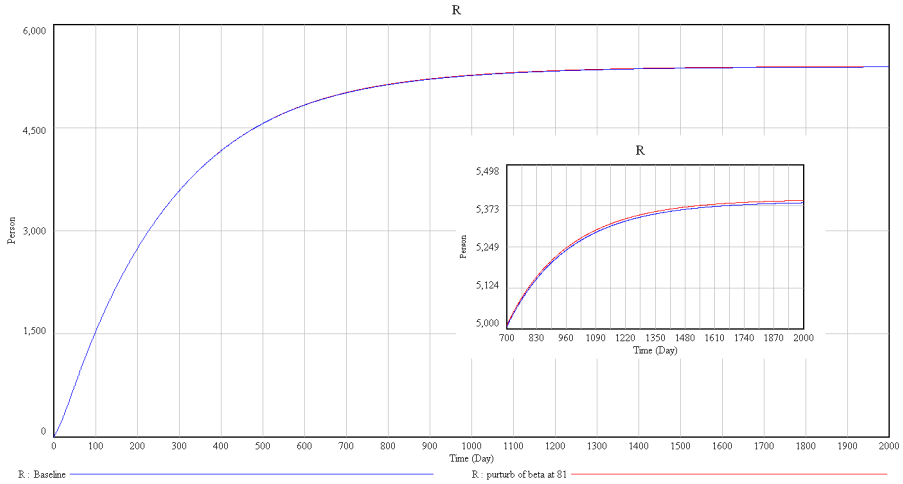

Figure 4.9: The value of R with a perturbation (decreasing by 10%) of β (`Per Infected Contact Infection Rate`) at $time = 81$.

Decreasing β (`Per Infected Contact Infection Rate`) by 10% changes the endemic equilibrium in Eq. 4.3 to be

$$\hat{S}|_{\beta^*} = 3750, \quad \hat{I}|_{\beta^*} = 9144, \quad \hat{R}|_{\beta^*} = 5394$$

where $\hat{S}$, $\hat{I}$, and $\hat{R}$ are increased by 17.8%, 6.7%, and 0.13% respectively from their values without perturbations. As would be anticipated from the eigenvalue elasticity, such change decreases the number of infected people for a short period of time. However, after $time = 101$, the reduced level of β increases the number of infected people. For S, this perturbation increases the number of susceptible people.

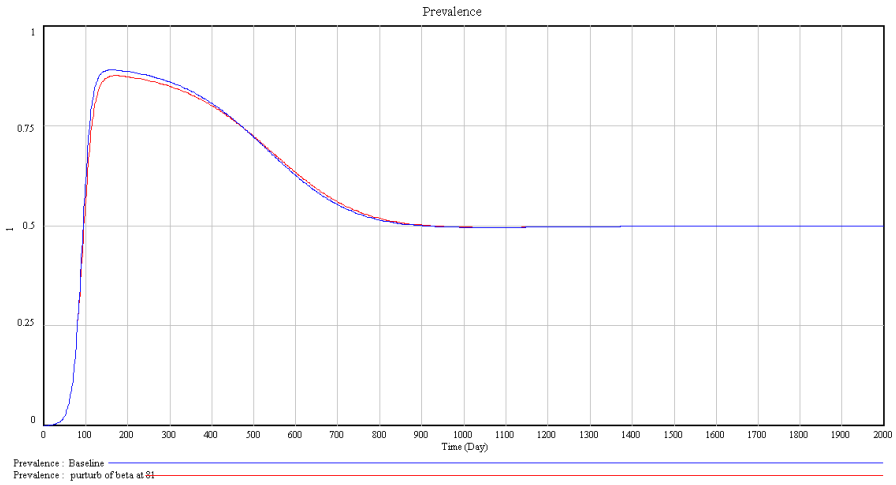

Figure 4.10: The value of *Prevalence* with a perturbation (decreasing by 10%) of β (`Per Infected Contact Infection Rate`) at $time = 81$.

Therefore a small decrease of the rate contacting infection for an infected patient can increase the number of infected and susceptible people in the longer term, with the epidemic playing out more slowly with an decreased infection rate for per infected contact than with the original rate.

4.1.4.2 Eigenvalue Elasticity with Respect to p for an SIRS model

As shown in Fig. 4.6, eigenvalue elasticity with respect to p (`Staff Time Per Patient`) has the largest values at $time = 0$, $time = 946$ and $time = 957$ (with values of 0.7032, 0.18125 and -0.10058 respectively). Based on Eq. 4.3, increasing p will lower the values of state variables at the endemic equilibrium, and 10% increment of p shifts the endemic equilibrium to be

$$\hat{S}|_{p^*} = 2894, \quad \hat{I}|_{p^*} = 7791, \quad \hat{R}|_{p^*} = 4897$$

where $\hat{S}$, $\hat{I}$, and $\hat{R}$ are decreased by 9.1% respectively from their values without perturbations. If we increase p at $time = 0$, the value of R changes from the starting time point, as Fig. 4.11 shows. We now analyze perturbation of p at $time = 946$. Fig. 4.12 to Fig. 4.15 show the effects of the perturbation of increasing p by 10%. Different from perturbation of β, perturbation of p has small effects on S and I, but

greatly changes the trajectory of R. Most of the increase in *Prevalence* could be attributed to the great change of R.

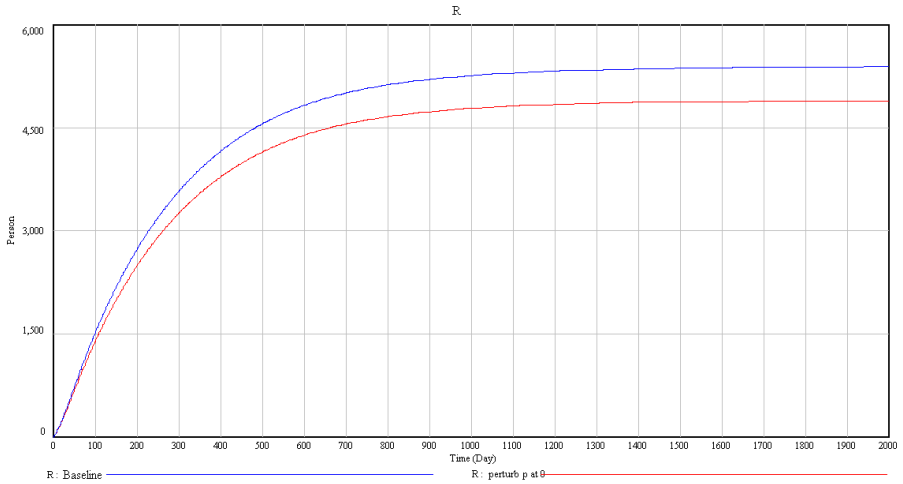

Figure 4.11: The value of R with a perturbation (increasing by 10%) of p (`Staff Time Per Patient`) at $time = 0$.

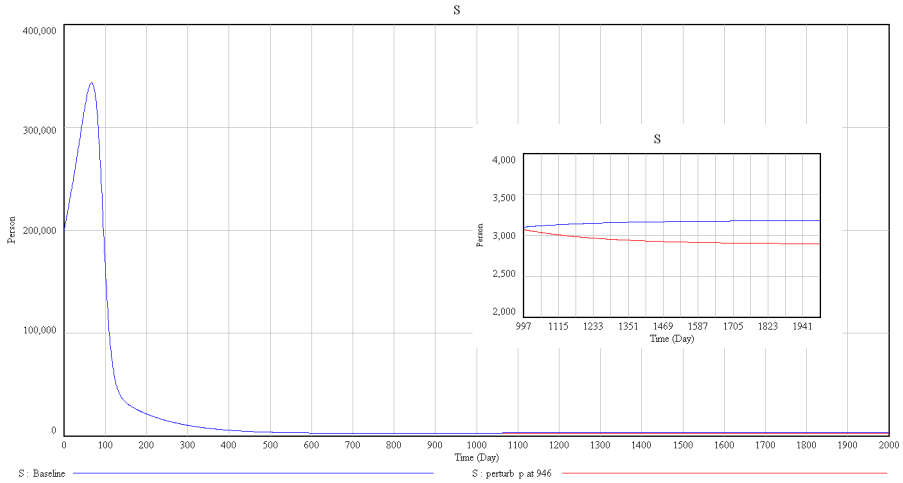

Figure 4.12: The value of S with a perturbation (increasing by 10%) of p (`Staff Time Per Patient`) at $time = 946$.

At $time = 946$, the large elasticities of eigenvalues with respect to p correspond to the 2nd and 3rd eigenvalues: -1.1218×10^{-2} and -3.46976×10^{-3}. The corresponding eigenvectors are

$$\begin{pmatrix} +5.07910 \times 10^{-2} \\ -9.98687 \times 10^{-1} \\ +6.68735 \times 10^{-3} \end{pmatrix}, \begin{pmatrix} +1.69634 \times 10^{-1} \\ +9.42675 \times 10^{-1} \\ +2.87382 \times 10^{-1} \end{pmatrix}$$

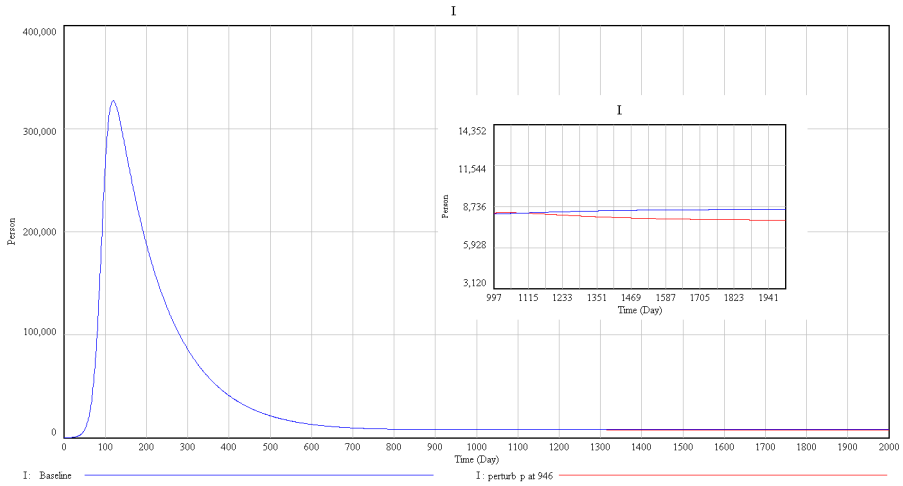

Figure 4.13: The value of I with a perturbation (increasing by 10%) of p (`Staff Time Per Patient`) at $time = 946$.

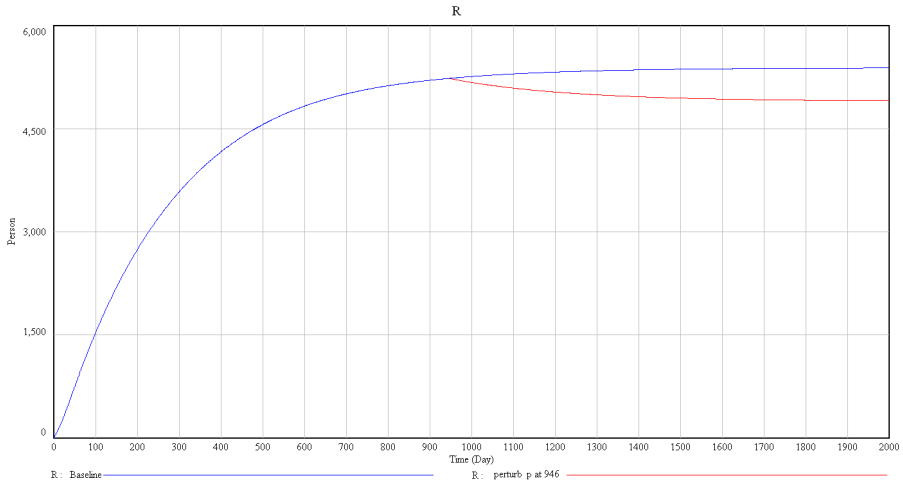

Figure 4.14: The value of R with a perturbation (increasing by 10%) of p (`Staff Time Per Patient`) at $time = 946$.

where the third entries of two eigenvectors, representing R, are much larger than the third entry of the eigenvector corresponding to the largest eigenvalue elasticity at $time = 82$ (a time point that was of interest for eigenvalue elasticity with respect to β) in Section 4.1. The corresponding coefficients of the eigenvectors are 1.97632 and 1.86503. The second entries of two eigenvectors, which represent I, have opposite values, with similar coefficients, the change of eigenvalues on I brought by perturbation of p thus almost offset each other. Although the first entries of the two eigenvectors have relatively large values, S also has relatively small proportional changes possibly because of the time delay associated with the loss of immunity from

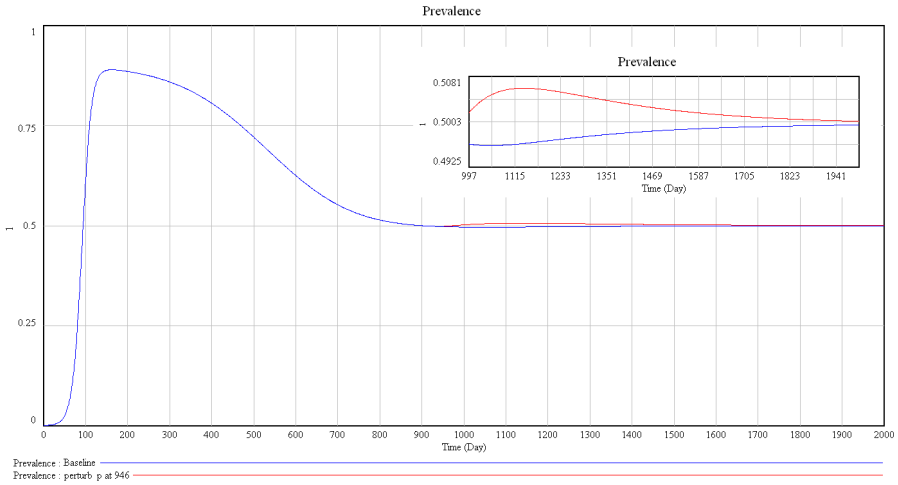

Figure 4.15: The value of *Prevalence* with a perturbation (increasing by 10%) of p (`Staff Time Per Patient`) at $time = 946$.

R to S. Direct change of p alters the third entries greatly.

This experiment suggests that given the number of health care workers assumed, a bit longer time of treatment on an individual patient will result in a significant decrease in the total number of recovered people and an increase in *Prevalence*. Thus, timely treatments are necessary to guarantee that people recover from the disease.

4.1.5 Discussion

In this section we studied eigenvalues and eigenvalue elasticity with respect to parameters for an SIRS model. Despite its nonlinearity, the behaviours of the system could be quantitatively described by eigenvalues of its Jacobian matrix over time. In addition to experiments listed in above sections, we also perturbed other parameters at time points when the values of their eigenvalue elasticities are large. Because of the space limitation we do not list the experimental results in this thesis and only discuss the experimental results briefly in this section.

Eigenvalue elasticity analysis reveals that the parameter β (`Per Infected Contact Infection Rate`) has great impacts on S and I. Its decrease temporarily lowers the values of S and I in a short period after perturbation, but increases them in the long run. In fact, *Prevalence* is the variable i in Eq. 4.6, the fraction of infectives in the

population. Based on Eq. 4.3, we have the endemic equilibrium of Eq. 4.6:

$$\hat{s} = \frac{(\beta\, c\mu - \sigma\, \beta\, c - \mu^2)\, \sigma\, \tau}{\mu\ (\sigma\, \tau\, \beta\, c + \mu)},\ \hat{i} = \frac{\sigma}{\mu},\ \hat{r} = \frac{\mu\, \sigma\, \tau - \sigma + \mu}{\sigma\, \tau\, \beta\, c + \mu}$$

The fixed point of *Prevalence* will not be changed by decreasing β. Commonly it is believed that if the infection rate of an infective patient can be controlled by behaviour change, the total infective population could be decreased. However, for the model with varying population size, such a policy is not globally effective because the overall measurement *Prevalence* keeps constant in the long-term. However, during a period of disease outbreak, during which *Prevalence* and I grow quickly, decreasing β decreases the number of infected people, and the prevalence in the short-term. If we aim at decreasing the value of *Prevalence* or I in the long-term around the endemic equilibrium, the value of β should be increased, i.e., we should increase the infection rate for each contacted infective, and the number of infected people would increase when the disease outbreaks massively.

The parameter p (`Staff Time per Patient`) has significant influences on R. Increasing the treatment time for each patient will decrease the population of susceptible, infected, and recovered people in the long run. Because long time waiting for infected people will increase their chances to die and to infect susceptible peoples, more infected patients die and the total population declines. Such perturbation also increases *Prevalence* shortly after the perturbation, though it does not eventually change the location of the fixed point of *Prevalence*. Therefore, the efficiency of health workers is very important to control the number of infected and susceptible people.

We mentioned in Section 3.2.2 that the eigenvalue elasticity with respect to a parameter is dimensionless and can be compared with that with respect to another parameter to determine which parameter has more important impacts on the system. From Fig. 4.5 and Fig. 4.6, we expect that because of high elasticities, the change of β should produce more significant changes than the change of p. However, because of the effects of eigenvectors and coefficients, the comparison of the importance of two parameters is not given by the values of eigenvalue elasticities alone if the largest

elasticities appear at different times.

There are other parameters with relatively small values of eigenvalue elasticities for this model, such as the number of health care workers h and the immunity loss delay τ. However, perturbations of these parameters could also change the trajectories of state variables. From Eq. 4.3, the position of the endemic equilibrium is associated with h and τ. An increment of h will increase the value of $\hat{S}$, $\hat{R}$ and $\hat{I}$ by saving lives, but does not change the position of *Prevalence*. An increment of τ does not change *Prevalence* either, but decreases $\hat{I}$, and the direction of change of $\hat{S}$ or $\hat{R}$ depends on the specific amount of increment and parameter values assumed. If we increase the values of parameters h and τ by 10% and decrease p by 10% at $time = 0$, when the eigenvalue elasticities are -0.03516, -0.0037 and 0.7032 respectively, we can get illustrating results of the changes of R shown in Fig. 4.16. The application of perturbation on a parameter with a high eigenvalue elasticity can generate more significant changes of the trajectories of state variables in the short-term. Because the eigenvalue elasticity is dimensionless we can anticipate the importance of a parameter for the system over a short time based on the value of its eigenvalue elasticity. Such values can be thus employed for a sort of dynamic

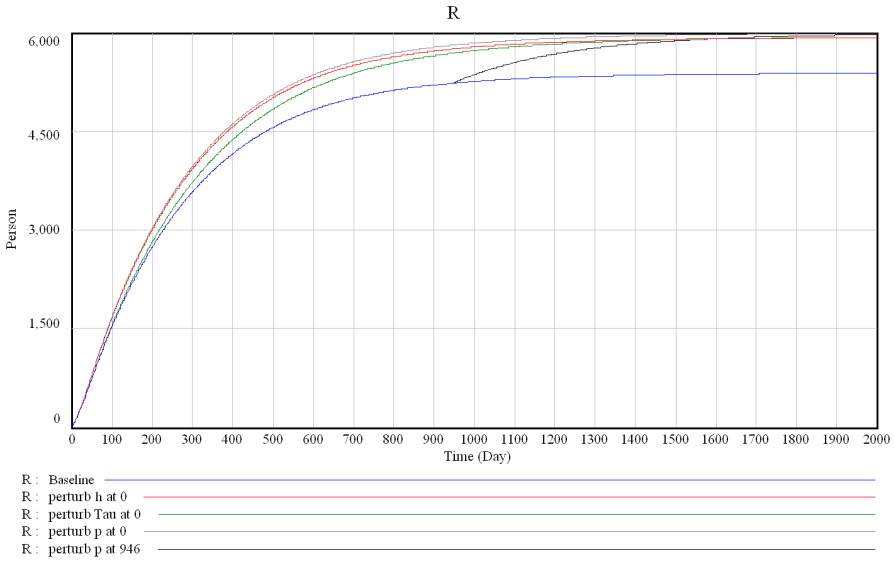

Figure 4.16: The comparison of the value of R with perturbations of h (`Health Care Workers`), p (`Staff Time Per Patient`) and τ (`Immunity Loss Delay`).

sensitivity analysis.

In terms of the value of elasticity, at $time = 0$ the absolute value of elasticity of p is almost as 20 times as that of h, and as 180 times as that of τ, but in the behaviours of R under those three scenarios of perturbations, such differences are not reflected. One reason for this is that eigenvalues indicate the behaviour modes of the system, and changes of a parameter based on its eigenvalue elasticity only affect the behaviour mode but not directly behaviours. Another reason is that the linearization of a nonlinear system is local but we change the parameter for a long period. Therefore the immediate effects of the perturbation of a parameter at time when the elasticity is high might be accumulated or offset in the later stage. Ultimately, the trajectories for this model all approach the endemic equilibria, and the long-term behaviour is more shaped by the dependence of the fixed point location on the parameters than by elasticities.

4.2 Eigenspace Analysis of an Individual-based Infectious Disease Model

In this section, we use an individual-based system dynamics model to describe the spread of an infectious disease within a given population in which a nonlinear CTL response characterizes each population member's individual immune response to an infectious disease.

4.2.1 An Individual-based Viral Dynamic Model: Description

The base virus dynamic model for an individual contains four state variables: the population size of uninfected cells x, the population size of infected cells y, the number of free virus particles v, and CTL z. The state equations of the model are based on those of [22].

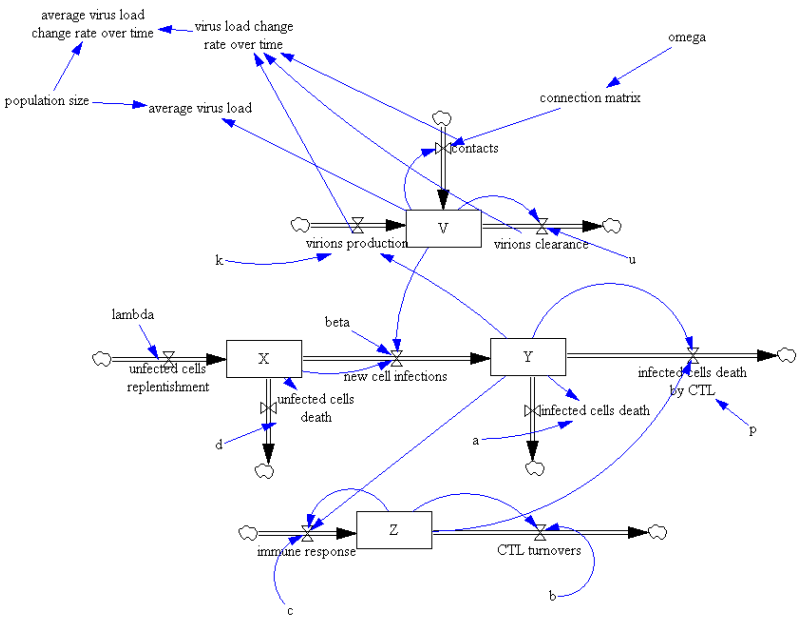

Figure 4.17: The stock-flow diagram of an individual-based viral dynamic model.

$$\begin{aligned}
\dot{x} &= \lambda - dx - \beta xv \\
\dot{y} &= \beta xv - ay - pyz \\
\dot{v} &= ky - uv \\
\dot{z} &= cyz - bz
\end{aligned} \tag{4.7}$$

The unit for x, y, v, and z is cells, cells, virions, and CTLs respectively. Explanations and initial settings of parameters are listed in Table 4.2.

The simulations in the following for individual-based models are carried out with a Runge-Kutta method of order 4 with step size 0.0625. We checked simulations with the same methods with smaller step size, which produced very close results to the simulation with step size 0.0625. There are two reasons for us to use the Runge-Kutta method for individual-based models rather than the Euler method, which is used for the SIRS model in the above section. Firstly numeric results for the model with the Runge-Kutta method of order 4 with step size 0.0625 are as the same as that with the Euler method with step size 0.0078125. Thus to reduce computational costs, we chose the Runge-Kutta method of order 4 with step size 0.0625. Another reason is that solving systems with imaginary eigenvalues of local Jacobian by the

Table 4.2: Parameter settings of an individual-based viral dynamic model.

Parameter	Full Name	Value	Units
β	the rate of uninfected cells to be infected	10^{-5}	1/day·virions
k	the rate of infected cells to produce free virus	3	virions/day·cells
d	the death rate of uninfected cells	0.1	day^{-1}
u	the death rate of free virus	3	day^{-1}
a	the death rate of infected cells	0.5	day^{-1}
λ	the replenishing uninfected cell rate	10^5	cells/day
p	the rate of infected cells to be eliminated by the CTL response	1	1/day·CTLs
c	the production rate of CTL	0.7	1/day·CTLs
b	the death rate of CTL	0.05	day^{-1}

Euler method sometimes gives unstable solutions [30]. In terms of this system, we observed that simulation with the Euler method with step size 0.0625 gave infinite values of state variables.

Fig. 4.18 describes the early stage of dynamical changes of the state variables of the individual in one person model described by Eq. 4.7. The initial conditions for this one person model are $x(0) = 10^6, y(0) = 0, v(0) = 0.01, z(0) = 1$. Infected by initial viruses, and then by endogenous viruses, the number of infected cells, y, increases exponentially at the beginning of the system evolution and at the same time the number of uninfected cells, x decreases. Shortly after the rise of infected cells, y, the viral load, v, begins to increase exponentially because of the release of virions from infected cells. Later the value of z, representing the number of CTLs, grows, reflecting CTLs proliferation in response to the rise of infected cells. z declines more slowly than y and v so that the individual largely clears the infection and receives some degree of protective immunity. Because the number of infected cells decreases, the immune response begins to decline. As their protective immunity wanes, a 'critical' point is reached at which the rate of the death of infected cells falls below the rate of infection of cells and y begins to increase again. The amount of CTLs does not decline to zero because when it is decreasing infected cells start to

increase. Because of the immune memory built up in response to the first infection, the second peak value of y is much smaller than the first one. We should note here the scale of infected cells, viral loads and CTLs in this figure are relatively small compared with that of uninfected cells because of our default parameter settings. Practically, the values of parameters vary over different types of diseases, and for the purpose of methodology study we did not calibrate the model and parameter settings with real data. The reader can choose to view the state variables and parameters as associated with specific dimensions but arbitrary units.

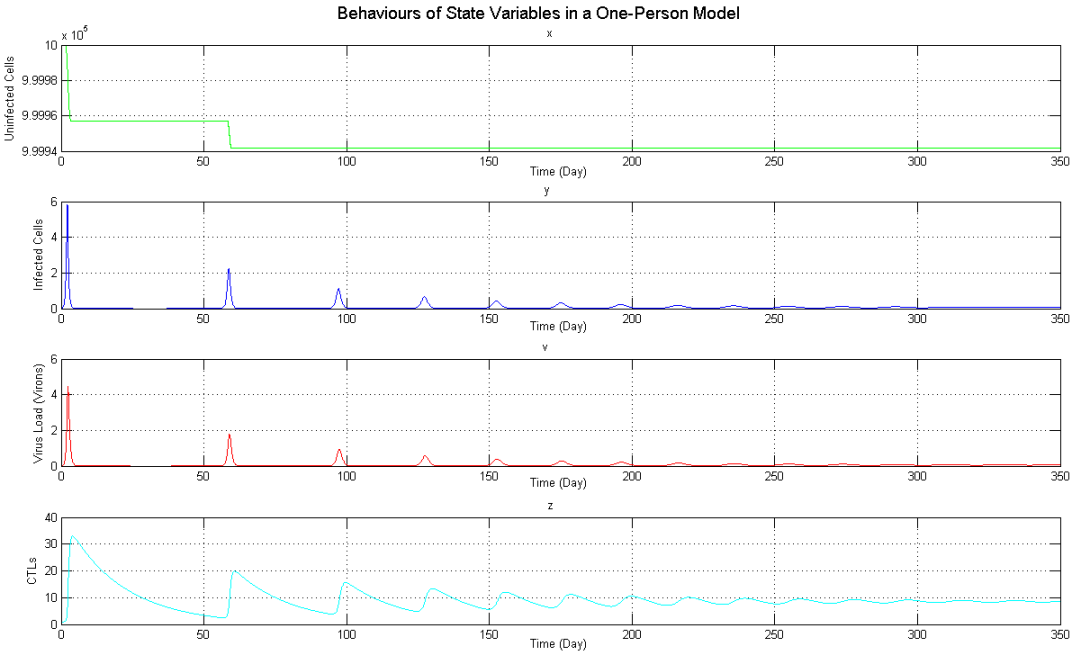

Figure 4.18: Dynamic behaviours of state variables in one-person model.

To understand the implications of individual viral dynamics to infection spread in the population, we follow the multi-individual model depicted in [33], whose state equations are shown as Eq. 4.8. In this model, an individual interacts with others in

form of exchanging free virus v.

$$\begin{aligned}
\dot{x_i} &= \lambda - dx_i - \beta x_i v_i \\
\dot{y_i} &= \beta x_i v_i - a y_i - p y_i z_i \\
\dot{v_i} &= k y_i - u v_i + \omega \sum_{i \neq j} \sigma_{ij} v_j \\
\dot{z_i} &= c y_i z_i - b z_i
\end{aligned} \tag{4.8}$$

Where, $i, j = 1, \cdots, P$ and P is the size of population.

σ_{ij} indicates whether the i^{th} individual and the j^{th} individual are connected. This parameter varies for different individuals in the network, and we assume that $\sigma_{ij} = \sigma_{ji} (i \neq j)$ and $\sigma_{ii} = 0$. ω is the connection weight between individuals, with the unit of 1/day.

In individual-based models, the behaviours of state variables for each individual are influenced not only by values of parameters, but also by network structures and population size.

If we call the individual in the above one person model `Person 1` and add another person (`Person 2`), who is free from disease initially, i.e., $x_2 = 10^6, y_2 = 0, v_2 = 0, z_2 = 1$. Connect those two individuals with connection weight (ω) 10^{-6}, the resulting connection matrix is:

$$(\sigma_{ij})_{2\times 2} = \begin{pmatrix} 0 & 1 \\ 1 & 0 \end{pmatrix}$$

The behaviours of state variables of `Person 1` will change only slightly, as Fig. 4.19 and Fig. 4.20 illustrate. But if we add the third person connected to `Person 2` with the same weight and initial conditions (to form a line-shape three-person model), the connection matrix becomes:

$$(\sigma_{ij})_{3\times 3} = \begin{pmatrix} 0 & 1 & 0 \\ 1 & 0 & 1 \\ 0 & 1 & 0 \end{pmatrix}$$

The behaviours of state variables of `Person 1` in this three-person model remain the same as in the two-person model (all new introduced individuals have no virus

initially, i.e., $v(0) = 0$ and other initial conditions and parameters are as same as the first individual). We select the viral load (v) of `Person 1` in these three models with different population size and illustrate it in Fig. 4.19. In this figure the magnitudes of oscillations of v in three models do not change. In the very beginning of system evolution, the behaviours of v for `Person 1` are almost same, but later on the oscillations of v in two-person and three-person models appear a bit earlier than in the one-person model. This information reflects the fact that connecting additional persons to an infected individual will not cause his/her infection to deteriorate, but will shift slightly earlier the oscillations of the viral load in late stages of system evolution. The first surges of the viral loads for two indirectly infected individuals are delayed because of the process of transmitting virus from `Person 1` and necessary time for infection to take off. However, the new introduced individuals have relatively larger magnitudes of viral loads than the first individual in the early period, as Fig. 4.20 presents. Later on, the magnitudes of viral loads for each individual differ very little, although the timing remains significantly offset. The trajectories of y (infected cells) also show similar behaviour patterns as v. We could conclude that an uninfected individual might be severely sick during "primary infection" when he/she is firstly contact with an infected person.

Connection weight (ω) plays an important role in disease spread. A large connection weight means an infected individual could transmit a high rate of virions to other people connected with him/her. We here focus on the simplest connection model, in which two individuals are connected with each other. `Person 1` is exactly same as in the above analysis; `Person 2` has no virus initially but is otherwise identical to initial conditions and parameters to `Person 1`. Fig. 4.21 shows the behaviours of v for the first individual in the models with different connection weights. With increasing time, the oscillation of the viral load for the first individual appears earlier for the model with larger connection weight than that with smaller connection weight, and the magnitude of the oscillation slightly decreases when the connection weight increases. Meanwhile a large value of ω could shorten the interval between the oscillations of different individuals (Fig. 4.22) and increase the average viral loads

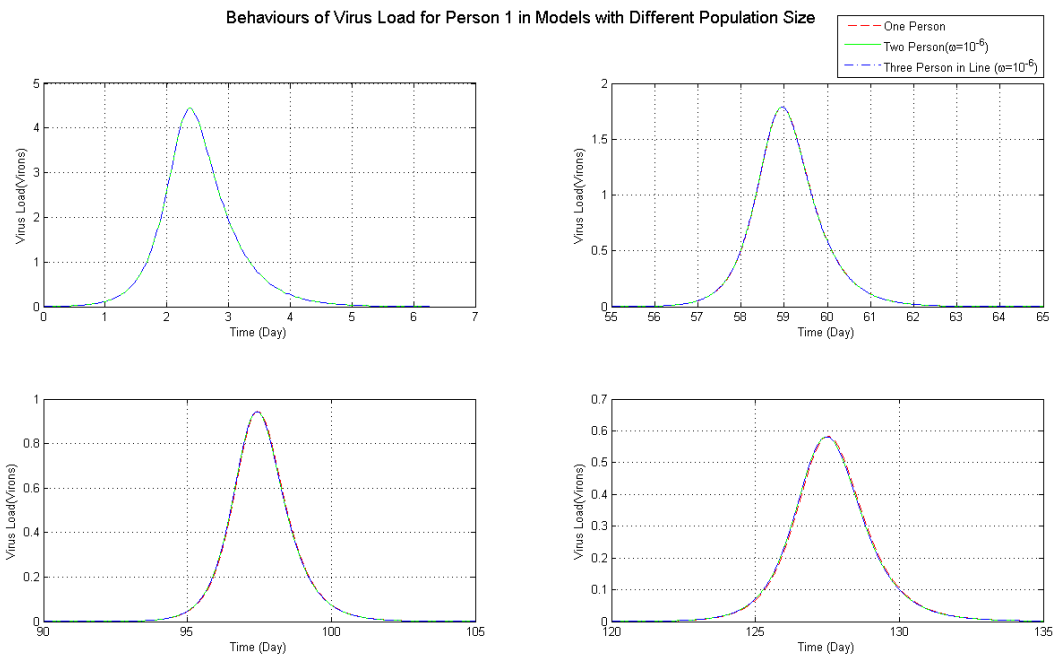

Figure 4.19: Dynamic behaviours of v for `Person 1` in models with different population size, and different subfigures show successive oscillations.

of the population (Fig. 4.23). In practice, the information bolster intuition that in a place where individuals are in close contact, like a classroom in a primary school, the period of infectious disease outbreak could be shorter but the disease might be more serious.

Network structure of an individual-based model also affects the accumulation of the population-wide viral loads [33]. Here we analyze two simple three-person models with different connection types: one line-shape model as described above and another full connection model in which the second and third individuals in the line-shape model are connected with the same connection weight (10^{-6}), i.e., the connection matrix appears as:

$$(\sigma_{ij})_{3\times 3} = \begin{pmatrix} 0 & 1 & 1 \\ 1 & 0 & 1 \\ 1 & 1 & 0 \end{pmatrix}$$

The magnitudes of the viral load (v) of `Person 1` do not change in the early periods, but the oscillation of v appears a bit earlier for the first person in the full connection

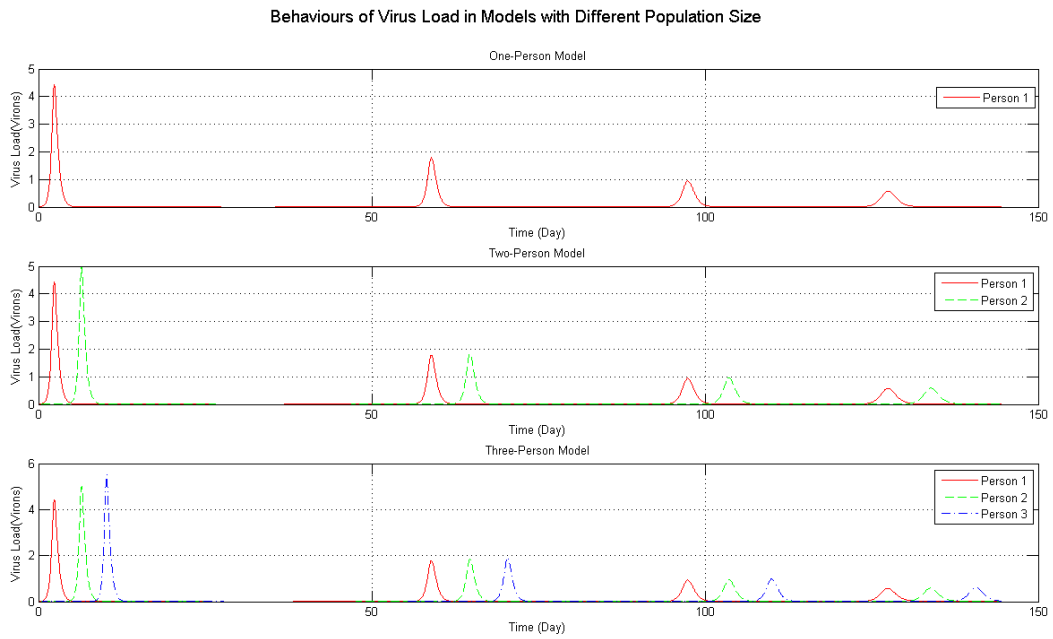

Figure 4.20: Dynamic behaviours of v in models with different population size.

model than in the line-shape model in a long run, as shown in Fig. 4.24. In the line-shape model, `Person 3` begins to be infected after the infection of `Person 2` and initially has a relatively larger magnitude of viral load oscillation. In the full connection model, `Person 2` and `Person 3` are in symmetric position therefore their behaviours are same (Fig. 4.25). Therefore, in the level of population, the time duration of oscillations of the average viral load in the full connection model is shorter than in the line-shape model but with a larger peak value of the magnitude of oscillations (Fig. 4.26).

4.2.2 Equilibrium and Stability Analysis

We define the basic reproduction rate R_0 for this viral dynamic model as the number of newly infected cells that are infected by any one infected cell when all other cells are uninfected [22]. To distinguish the parameter λ from the symbol of eigenvalue, we use $\bar{\lambda}$ to represent the eigenvalue in the following sections. For the one-person model described by Eq. 4.7, the rate at which an infected cell produces

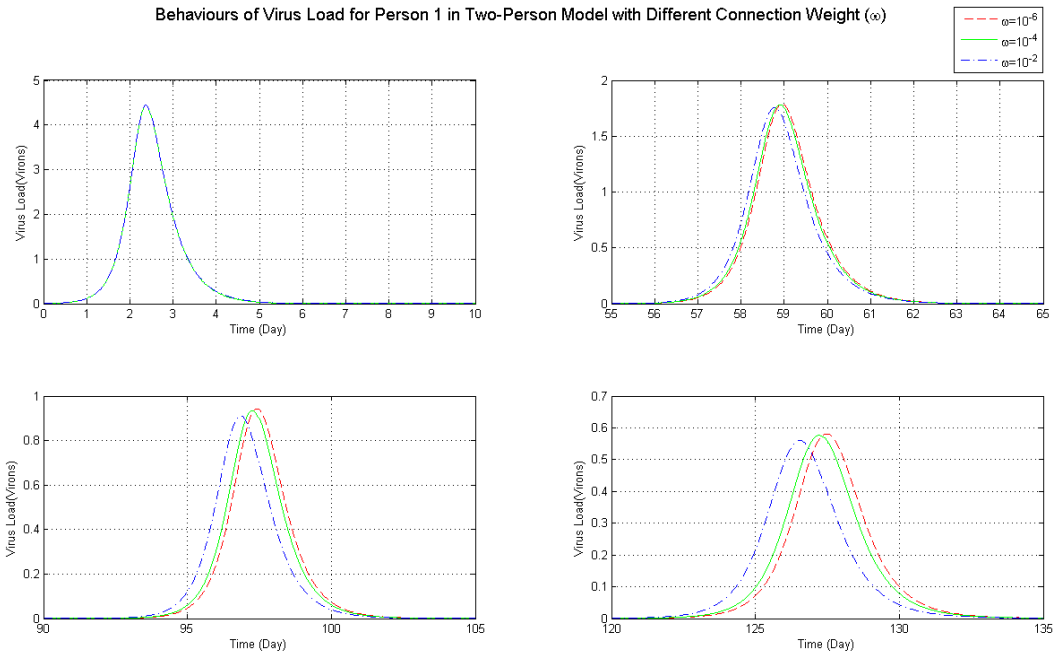

Figure 4.21: Dynamic behaviours of v for `Person 1` in two-person models with different connection weights, and different subfigures show successive oscillations.

new virus is k, the new born free virions and uninfected cells produce new infected cells at rate β via mass-action dynamics, and meanwhile the life duration of an virus is $1/u$, therefore the infection incidence rate is $\beta kx/u$: the number of newly infected cells caused by one infected cell per day. Initially, $x = \lambda/d$ when there are no infected cells. The life duration of an infected cell is $1/a$, therefore we have

$$R_0 = \frac{\beta\lambda k}{adu}$$

The equations of the one-person model are associated with three equilibrium states. The disease-free equilibrium, where no cell is infected and there is no free virus, as well as CTL cells are absent, is:

$$\hat{x} = x(0) = \frac{\lambda}{d},\ \hat{y} = 0,\ \hat{v} = 0, \hat{z} = 0 \tag{4.9}$$

The symbolic expressions of the eigenvalues of Jacobian matrix at the DFE are:

$$\bar{\lambda}_1 = -d,\ \bar{\lambda}_2 = -b$$

$$\bar{\lambda}_3 = -\frac{1}{2}\left(u + a - \sqrt{(u-a)^2 + 4\frac{\lambda}{d}\beta k}\right),\ \bar{\lambda}_4 = -\frac{1}{2}\left(u + a + \sqrt{(u-a)^2 + 4\frac{\lambda}{d}\beta k}\right)$$

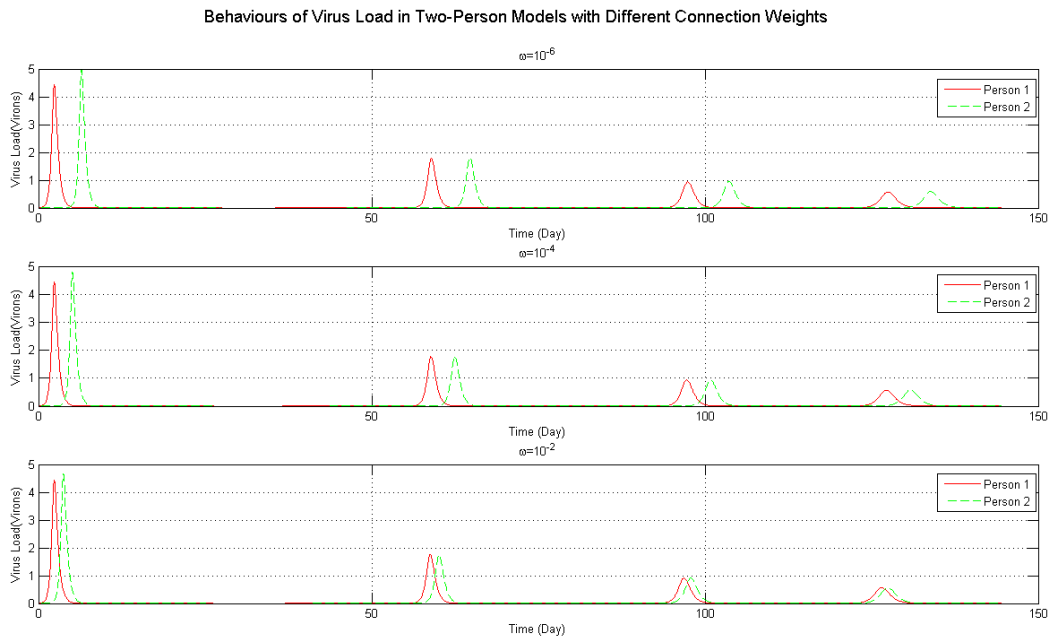

Figure 4.22: Dynamic behaviours of v in two-Person models with different connection weights.

Because the parameters u, a, d and b are all non-negative, the stability of the DFE depends on the third eigenvalue. With our assumption that all parameters are positive for the one-person model, $\bar{\lambda}_3$ is negative if

$$u + a > \sqrt{(u-a)^2 + 4\frac{\lambda}{d}\beta k}$$

$$\therefore ua > \frac{\lambda}{d}\beta k$$

$$\therefore R_0 = \frac{\lambda\beta k}{adu} < 1$$

Therefore, as expected, we derive that if $R_0 < 1$ the DFE is asymptotically stable and the DFE is unstable when $R_0 > 1$. With parameter settings listed in Table 4.2, $R_0 = 20 > 1$ and the DFE is unstable.

The second equilibrium is called a "defense-free" equilibrium [33] where CTLs absent and the individual is unable to eliminate infected cells:

$$x^* = \frac{au}{\beta k},\ y^* = \frac{\lambda\beta k - dau}{a\beta k},\ v^* = \frac{\lambda\beta k - dau}{a\beta u},\ z^* = 0$$

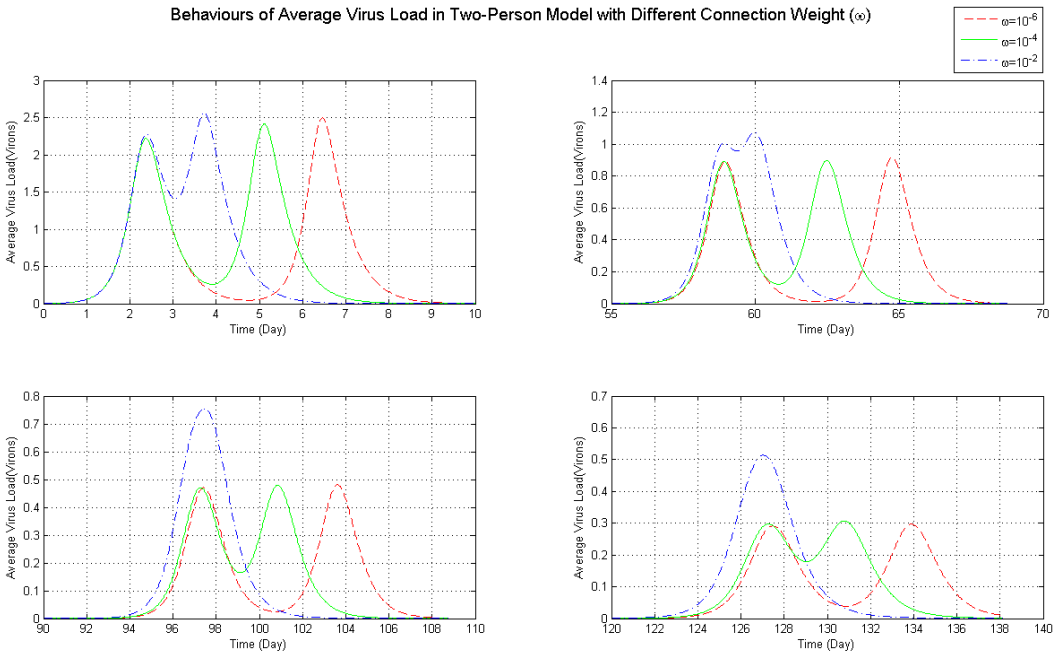

Figure 4.23: Dynamic behaviours of average v in two-Person models with different connection weights, and different subfigures show successive oscillations.

If $R_0 < 1$ this defense-free equilibrium is physically meaningless, as it implies non-physical values of y^* and v^*. Because of the complicated expressions of the defense-free equilibrium, we did not derive the symbolic expressions of the eigenvalues of Jacobian matrix. With current parameter settings, the numeric eigenvalues of Jacobian matrix at this equilibrium are:

$$\bar{\lambda}_{1,2} = -0.8059 \pm 0.29\,i,\ \bar{\lambda}_3 = -3.8882,\ \bar{\lambda}_4 = 1.33 \times 10^5$$

Because $\bar{\lambda}_4 > 0$, the defense-free equilibrium is unstable. The endemic equilibrium is given as

$$\tilde{x} = \frac{\lambda uc}{duc + \lambda kb},\ \tilde{y} = \frac{b}{c},\ \tilde{v} = \frac{kb}{uc},\ \tilde{z} = \frac{\beta\lambda ck - a\beta kb - adcu}{p(dcu + \beta kb)}$$

Similar to the defense-free equilibrium, symbolic expressions for eigenvalues could not be obtained, and here we only focus on their numeric values based on current parameter settings. The endemic equilibrium is asymptotically stable because all

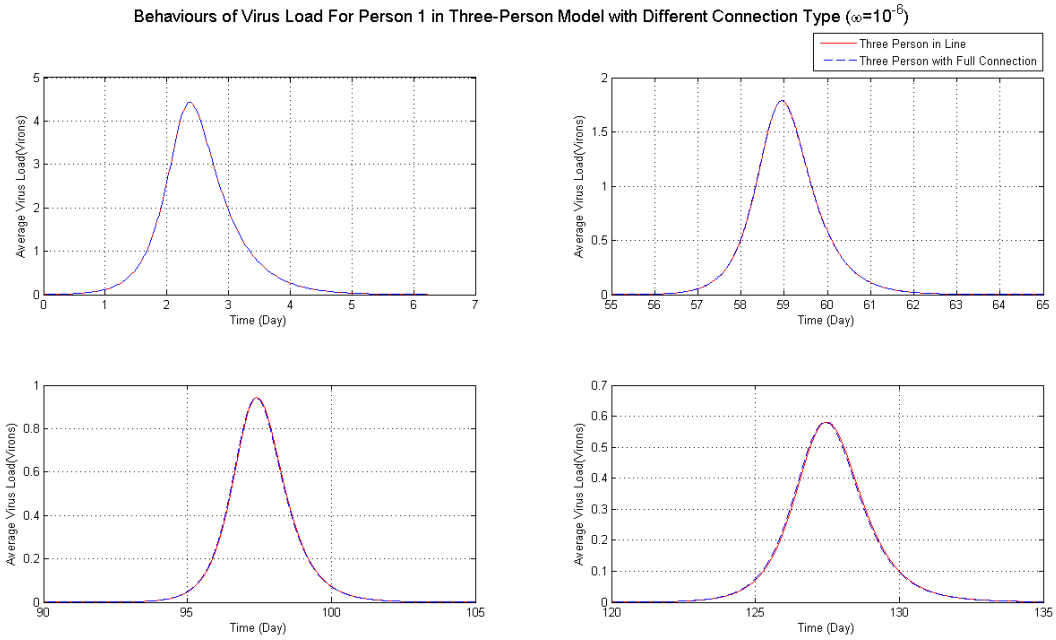

Figure 4.24: Dynamic behaviours of v for `Person 1` in three-person models with different connection types, and different subfigures show successive oscillations.

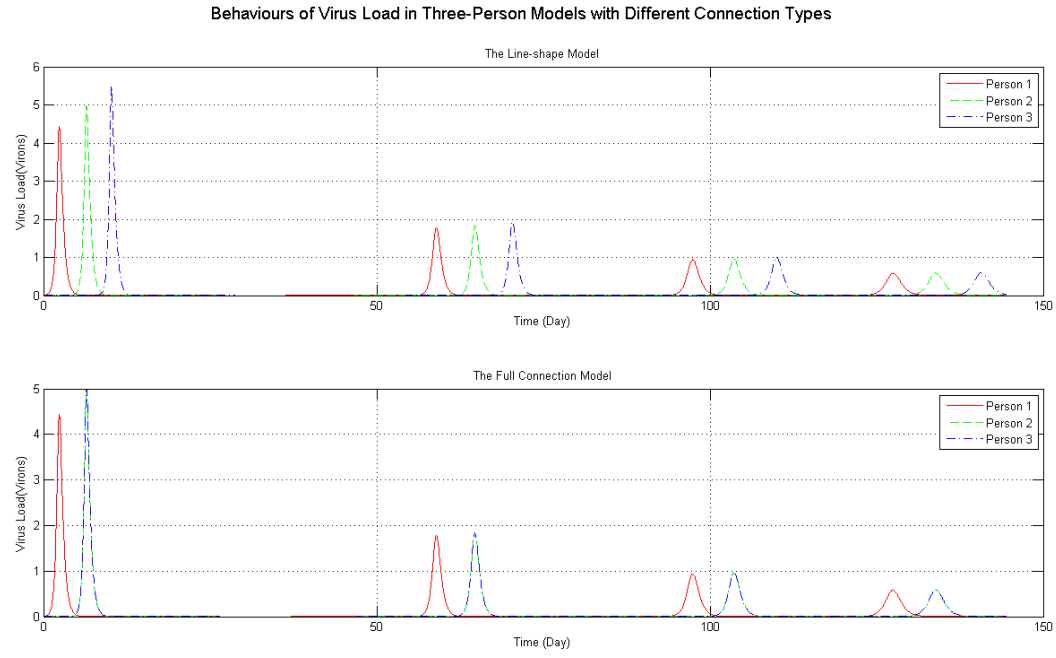

Figure 4.25: Dynamic behaviours of v in three-person models with different connection types.

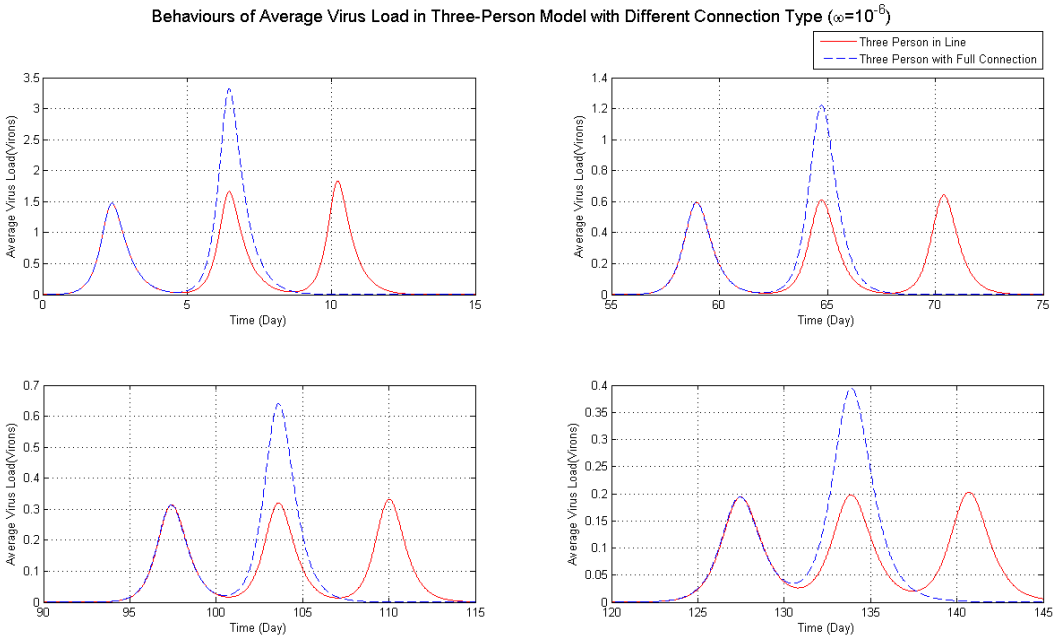

Figure 4.26: Dynamic behaviours of average v in three-person models with different connection types, and different subfigures show successive oscillations.

real parts of the numeric eigenvalues of Jacobian matrix at this point are negative:

$$\bar{\lambda}_{1,2} = -0.0141 \pm 0.3311\, i,\ \bar{\lambda}_3 = -0.1,\ \bar{\lambda}_4 = -12.97$$

For an individual-based viral dynamic model with population size larger than one, described by Eq. 4.8, the number of equilibrium states grows geometrically with population size. A model with population size P has at most 3^P equilibrium states, associated with each possible combination of equilibria in one-person model. There is a unique disease-free equilibrium of the multi-person model, in which state variables in each system of equations representing an individual share the same values as Eq. 4.9, and similarly the stability of this unique DFE depends on R_0. The multi-person model is associated with a unique endemic equilibrium, in which state variables for each individual have similar values of the endemic equilibrium in one-person model with slight differences on x, v and z because of the connections with other individuals (examples will be given later). For any other 'combined' equilibrium state, it could be stable only when state variables in this equilibrium representing ev-

ery individual correspond to a stable disease-free/defense-free/endemic equilibrium. Because both the DFE and the defense-free equilibrium in the one-person model are unstable, for the multi-person model in our analysis, only the unique endemic equilibrium could be stable.

For the connected two-person model, the endemic equilibrium is

$$\begin{aligned}
\tilde{x}_1 = \tilde{x}_2 &= \frac{\lambda c(u-\omega)}{dc(u-\omega)+\beta kb} \\
\tilde{y}_1 = \tilde{y}_2 &= \frac{b}{c} \\
\tilde{v}_1 = \tilde{v}_2 &= \frac{kb}{c(u-\omega)} \\
\tilde{z}_1 = \tilde{z}_2 &= \frac{\beta\lambda ck - a\beta kb - adc(u-\omega)}{p(dc(u-\omega)+\beta kb)}
\end{aligned} \tag{4.10}$$

For the three-person model with a line-shape, the endemic equilibrium is located at

$$\begin{aligned}
\tilde{x}_2 &= \frac{\lambda c(u^2-2\omega^2)}{dc(u^2-2\omega^2)+\beta kb(u+2\omega)},\ \tilde{x}_1 = \tilde{x}_3 = \frac{\lambda c(u^2-2\omega^2)}{dc(u^2-2\omega^2)+\beta kb(u+\omega)} \\
\tilde{y}_1 &= \tilde{y}_2 = \tilde{y}_3 = \frac{b}{c} \\
\tilde{v}_2 &= \frac{kb(u+2\omega)}{c(u^2-2\omega^2)},\ \tilde{v}_1 = \tilde{v}_3 = \frac{kb(u+\omega)}{c(u^2-2\omega^2)} \\
\tilde{z}_2 &= \frac{\beta\lambda ck(u+2\omega) - a\beta kb(u+2\omega) - adc(u^2-2\omega^2)}{p(dc(u^2-2\omega^2)+\beta kb(u+2\omega))} \\
\tilde{z}_1 = \tilde{z}_3 &= \frac{\beta\lambda ck(u+\omega) - a\beta kb(u+\omega) - adc(u^2-2\omega^2)}{p(dc(u^2-2\omega^2)+\beta kb(u+\omega))}
\end{aligned} \tag{4.11}$$

The endemic equilibrium for the three-person model with full connections is located at

$$\begin{aligned}
\tilde{x}_1 = \tilde{x}_2 = \tilde{x}_3 &= \frac{\lambda c(u-2\omega)}{dc(u-2\omega)+\beta kb} \\
\tilde{y}_1 = \tilde{y}_2 = \tilde{y}_3 &= \frac{b}{c} \\
\tilde{v}_1 = \tilde{v}_2 = \tilde{v}_3 &= \frac{kb}{c(u-2\omega)} \\
\tilde{z}_1 = \tilde{z}_2 = \tilde{z}_3 &= \frac{\beta\lambda ck - a\beta kb - adc(u-2\omega)}{p(dc(u-2\omega)+\beta kb)}
\end{aligned} \tag{4.12}$$

For an individual-based model with population size P, it is difficult to derive the symbolic expression of the endemic equilibrium because the expressions will depend on network structure. However, for the model with full connections, because the

endemic equilibrium of each individual is located at the same position, and because each individual is connected with other $P-1$ individuals in a symmetric fashion, the system equations Eq. 4.8 at the endemic equilibrium are equivalent to:

$$\begin{aligned}
\dot{\tilde{x}}_i &= \lambda - d\tilde{x}_i - \beta\tilde{x}_i\tilde{v}_i \\
\dot{\tilde{y}}_i &= \beta\tilde{x}_i\tilde{v}_i - a\tilde{y}_i - p\tilde{y}_i\tilde{z}_i \\
\dot{\tilde{v}}_i &= k\tilde{y}_i - u\tilde{v}_i + \omega(P-1)\tilde{v}_i \\
\dot{\tilde{z}}_i &= c\tilde{y}_i\tilde{z}_i - b\tilde{z}_i
\end{aligned} \tag{4.13}$$

where $i = 1, \cdots, P$. Forcing the equations of Eq. 4.13 to be equal to zero, we get the general formula of the endemic equilibria for the P-person fully connected model:

$$\begin{aligned}
\tilde{x}_i &= \frac{\lambda c(u-(P-1)\omega)}{dc(u-(P-1)\omega)+\beta kb} \\
\tilde{y}_i &= \frac{b}{c} \\
\tilde{v}_i &= \frac{kb}{c(u-(P-1)\omega)} \\
\tilde{z}_i &= \frac{\beta\lambda ck - a\beta kb - adc(u-(P-1)\omega)}{p(dc(u-(P-1)\omega)+\beta kb)}
\end{aligned} \tag{4.14}$$

The state variables x, v and z at the endemic equilibrium of an individual-based model are shifted from the positions of the corresponding state variables at the endemic equilibrium of the one-person model and offset by the connection weight ω. For the values of ω and P explored in this thesis, this offset will be small. Eq. 4.11 and Eq. 4.12 indicate that the position of the endemic equilibrium for an individual-based model depends on the network structure. In our study, the network graph is undirected and no individual is connected with him/herself, i.e., the connection matrix is a symmetric matrix with all zero diagonal entries. Therefore, for an individual-based model with population size P, there are a total of $2^{\frac{P(P-1)}{2}}$ types of connection.

Network structure affects not only the location, but also the stability of the equilibria. One particular concern is the stability of the endemic equilibrium for different connection types, which is dependent on eigenvalues of the Jacobian matrix for the particular network topology. Here we examine the largest real parts of the

eigenvalues of Jacobian matrix at the endemic equilibrium for each connection type of the individual-based model with population size of 2, 3 and 4 respectively (all parameter values are based on Table 4.2).

The two-person model has only two types of connection if the connection weight ω is fixed to be 10^{-6}: connected and not connected. The largest real part of the eigenvalues of Jacobian matrix at the endemic equilibrium of these two scenarios are $-0.140751814\times10^{-1}$ and $-0.140751769\times10^{-1}$ respectively. The endemic equilibrium is stable for each scenario. With connection between two persons, the largest real part of the eigenvalues of Jacobian matrix at the endemic equilibrium decreases by a factor of 10^{-7}. For the model with three persons, there are eight types of connections. The largest real part of the eigenvalues of Jacobian matrix at the endemic equilibrium varies between $-0.140751861 \times 10^{-1}$ and $-0.140751769 \times 10^{-1}$. As for the single-person model, the scenario of full connection shares the smallest value of this range, and the scenarios in which the initially infected person (`Person 1`) has no connection with others shares the largest value of the range. The maximum absolute difference between these largest real parts of the eigenvalues at the endemic equilibrium is of the order of 10^{-7}.

Similarly, the range of the largest real part of the eigenvalues of Jacobian matrix at the endemic equilibrium for the model with four persons is

$$\left[-0.140751907 \times 10^{-1}, -0.140751769 \times 10^{-1}\right]$$

As before, the case of full connection shares the smallest value of this range, and the cases where `Person 1` has no connection with others shares the largest value of the range. As above, the length of this range is of the order of 10^{-7}. If we increase the value of the connection weight ω to be 10^{-4} and 10^{-2} respectively for the model with four persons, correspondingly this range becomes

$$\left[-0.14076553 \times 10^{-1}, -0.140751769 \times 10^{-1}\right]$$

whose length is with the order of 10^{-5}, and

$$\left[-0.14213103 \times 10^{-1}, -0.140751769 \times 10^{-1}\right]$$

in which the largest real part of the eigenvalues at the endemic equilibrium for the fully connected case decreases by a factor of 10^{-3}.

In fact, the largest real part of eigenvalues of the Jacobian matrix at the endemic equilibrium for the one-person model is $-0.140751769 \times 10^{-1}$. For a multi-person model in which the initially infected person (`Person 1` in our study) has no contact with any other person, the largest real part of eigenvalues of the Jacobian matrix at the endemic equilibrium is as the same as in the one-person model, though the lack of connection prevents the system from approaching to the endemic equilibrium, because all individuals except the initially infected one will not come in contact with the virus. If this person is connected to anyone else in the model, the largest real part of eigenvalues of Jacobian matrix at the endemic equilibrium will decrease a little. If the connection is stronger, the largest real part of eigenvalues becomes smaller. If the connection becomes weaker, the largest real part of eigenvalues is closer to that in the scenario of no connection.

The less stability of the case of no connection has an epidemiological interpretation that medical treatments could change the states of an individual in the model; however, in the fully connected case, because of connections to other infected individuals, the effects of changing states by medical treatment could be offset by newly transmitted viruses from neighbours and the endemic equilibrium is relatively more stable. For example, consider a family without immune memory to Herpes Simplex Virus (HSV), where all family members live together and virus are able to be transmitted in their daily life. The effects of medical treatments could be blunted by virions obtained from other family members suffering from reactivation. In contrast, if all family members are quarantined from each other, medical treatments (e.g., Acyclovir) could kill virus and produce new CTLs, and each member would not be influenced by others, permitting an easier "escape" from the endemic equilibrium. In such case, the state variables of each individual at the endemic equilibrium could also be slightly altered. Thus, if this family were to achieve to the endemic equilibrium, this endemic equilibrium would be more stable in the case of full connections than in the case of no connection. Therefore we suggest (although do not prove)

that if the one-person model is stable at the endemic equilibrium, any multi-person model, in which all the parameters share the same values, will also be stable at the endemic equilibrium.

When we change other parameters in the one-person model, like c (`the production rate of CTL`), if such change does not alter the stability of the endemic equilibrium of the one-person model, we suggest that it likely does not alter the stability of the endemic equilibrium for a multi-person model with the same parameter settings. Based on the Routh-Hurwitz Criterion, if the value of c is in the range $(0.545, \infty)$ or the value of u is in the range $(0, 60)$ when all other parameter values are fixed, any change of exactly one of these two parameters within in its respective range (leaving the value of the other constant) will not alter the stability of the endemic equilibrium for the one-person model. Following our analysis above, the stability of the endemic equilibrium for other multi-person models will not be changed if one of these two parameters is perturbed within this range. The default values of c and u in our models is 0.7 and 3, therefore if we increase or decrease them by a very small amount the stability of the endemic equilibrium does not change.

4.2.3 Eigenvalue Analysis of an Individual-based Viral Dynamic Model with 3 Persons

In a very short period around a particular point of time, a linearized model can be an excellent approximation to its associated nonlinear model [7]. The following sections describe dynamic behaviours of the individual-based model through eigenvalues and eigenvalue elasticities of a linearized individual-based model described at each time point.

For the model described by Eq. 4.8, there are $N = 4P$ states and correspondingly $4P$ eigenvalues of the system's Jacobian matrix. It is difficult to study all states and eigenvalues clearly for a system with a large population, therefore in this section, we start the study with a model of small populations: the line-shape three-person model, where $P = 3$.

Behaviours of state variables in the system over time are plotted in Fig. 4.27, where the X-axis is time and Y-axis represents the number of viral loads/uninfected cells/infected cells/CTLs.

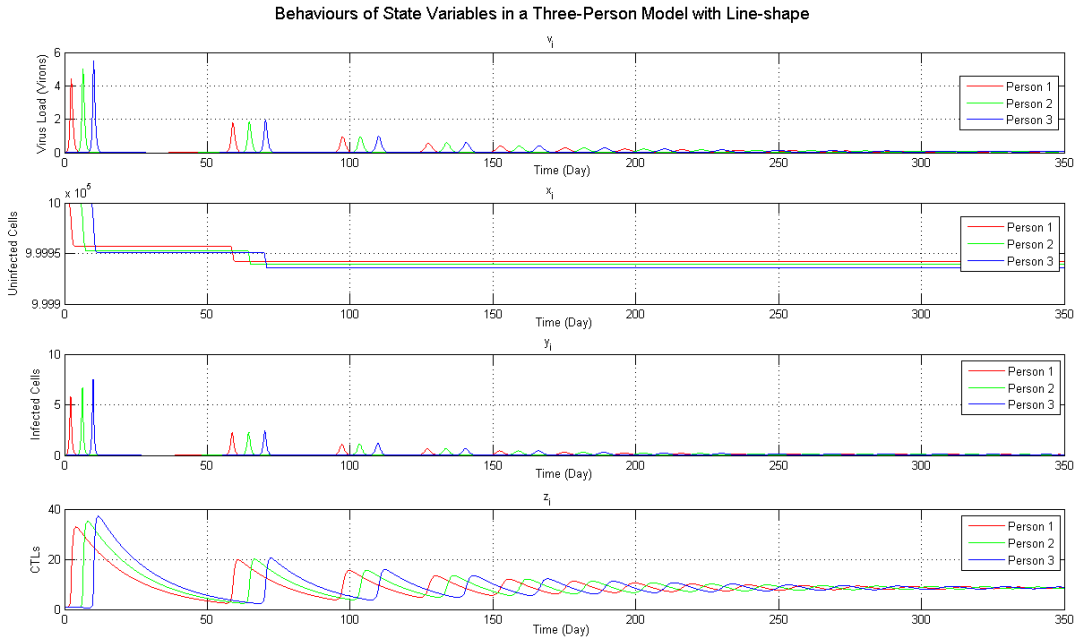

Figure 4.27: Behaviours of state variables for an individual-based model with 3 persons in line-shape.

4.2.3.1 Eigenvalue Clustering

Approximating the system to be a linear one at regularly spaced time points with the Jacobian matrix, we obtained eigenvalues of the Jacobian matrix over time.

Fig. 4.28 shows all real components of eigenvalues of the Jacobian matrix of the model over time, where the horizontal axis is time and the vertical axis shows the value of real components of eigenvalues. With time increasing, the magnitude of oscillation of the eigenvalues becomes quite small,which means the system tends towards the endemic equilibrium. Because there are twelve real parts of eigenvalues and at most six imaginary parts of eigenvalues it is difficult to see clearly how these eigenvalues evolve. Fig. 4.29 shows the eigenvalues of system Jacobian matrix in the

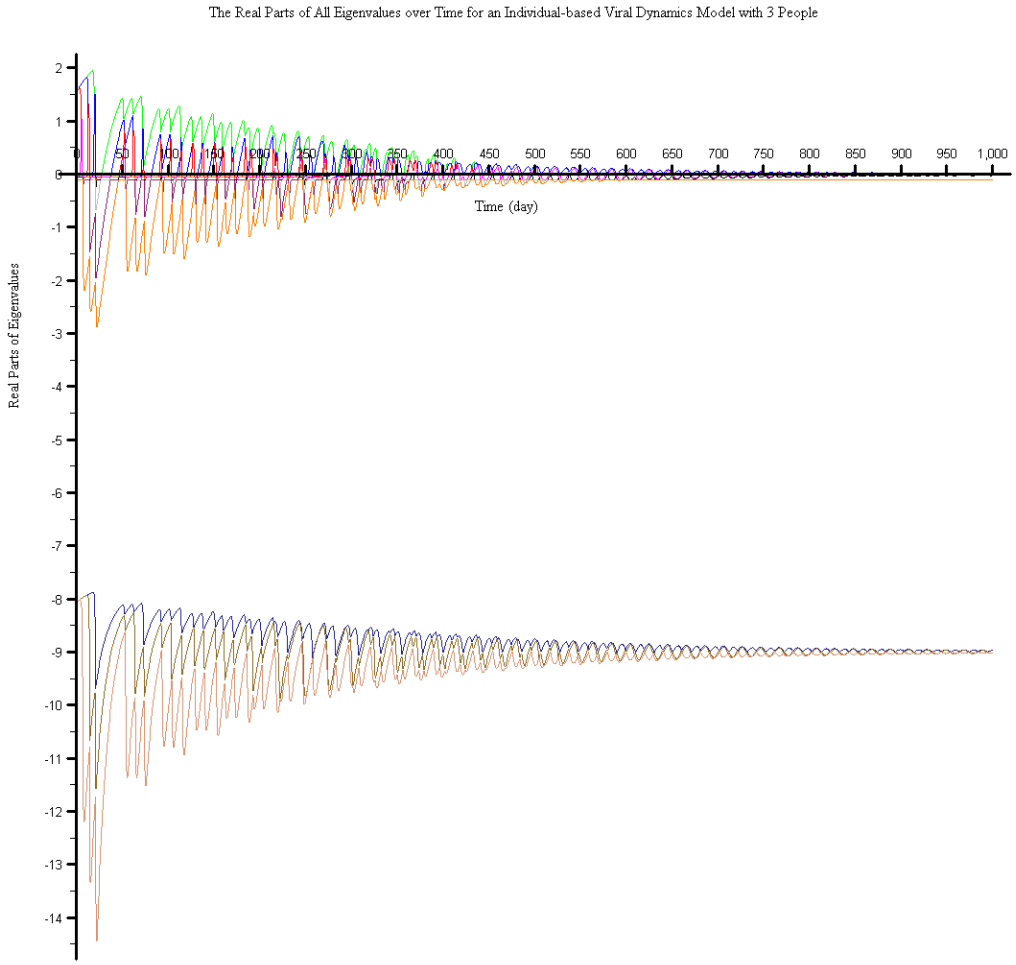

Figure 4.28: The real components of all eigenvalues over time for an individual-based viral dynamic model with 3 persons in line-shape.

complex plane at different times.[2] From these four figures, it can be appreciated that the 12 eigenvalues of the system Jacobian matrix are generally clustered in four groups, representing the four system behaviours associated with each person. The first group of eigenvalues are real and oscillate between -8 and -10, yielding strong exponential damping toward equilibrium. The second group of eigenvalues are also real and oscillate in the region $(-0.5, 0)$. The third and the fourth group contain conjugate pairs of eigenvalues; eigenvalues in these final two groups could have nonzero imaginary parts at some time points, which contribute to the oscillations of the state

[2] A video recording the evolution and clustering of eigenvalues of the Jacobian matrix of the system can be found at http://homepage.usask.ca/~qiz765/eigenvalueClustering.htm

variables.

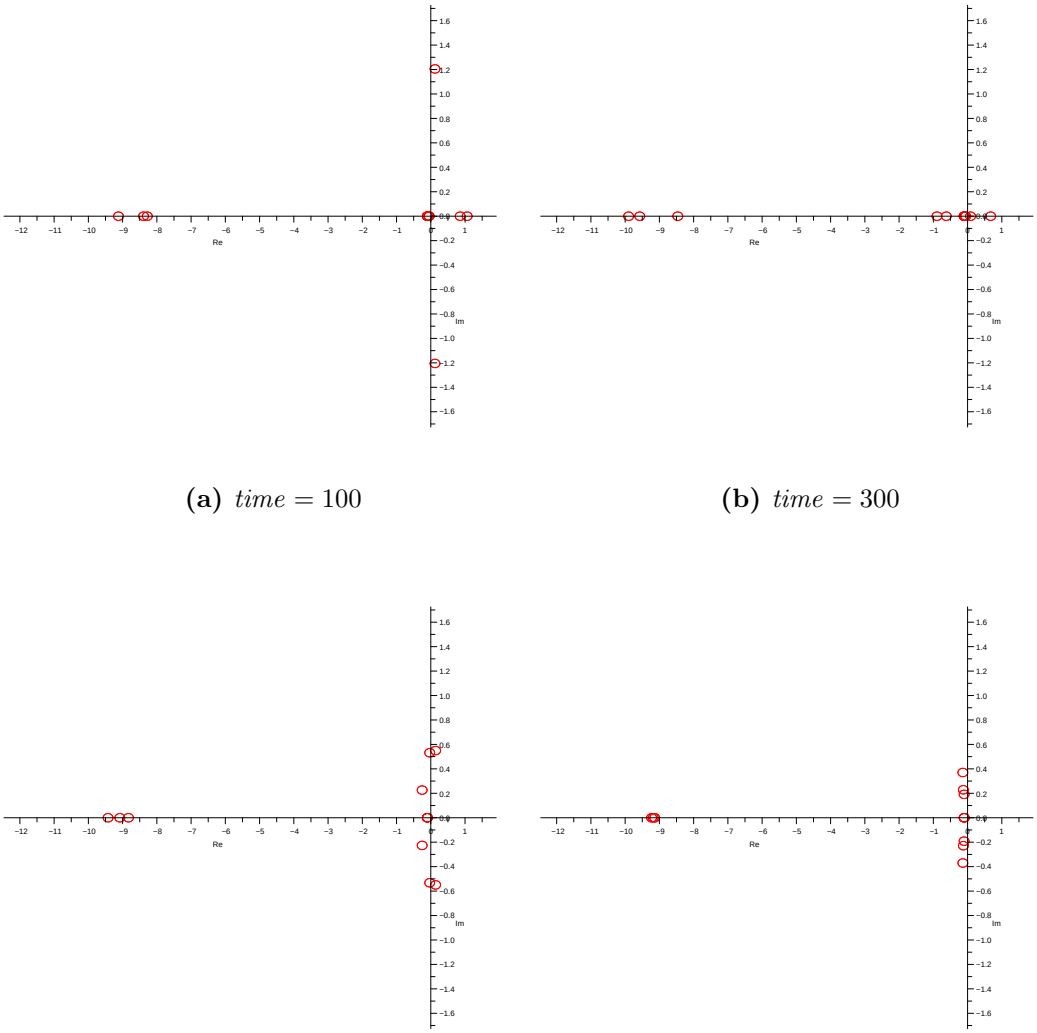

(a) *time* = 100 **(b)** *time* = 300

(c) *time* = 721 **(d)** *time* = 960

Figure 4.29: Eigenvalues of system's Jacobian matrix in the complex plane for an individual-based viral dynamic model with 3 persons in line-shape.

4.2.3.2 Eigenspace Analysis

Because of the large number of eigenvalues in the system, the relationship between the system behaviours and eigenvalues is still not intuitively clear. In the following part of this section, we focus on the dominant eigenvalues, i.e. eigenvalues with the

largest real parts. Fig. 4.30 gives both the real and imaginary parts of the dominant eigenvalues over time for the 3-people model, where the horizonal axis is time axis and the vertical axis presents the value of real and imaginary parts of the eigenvalues.

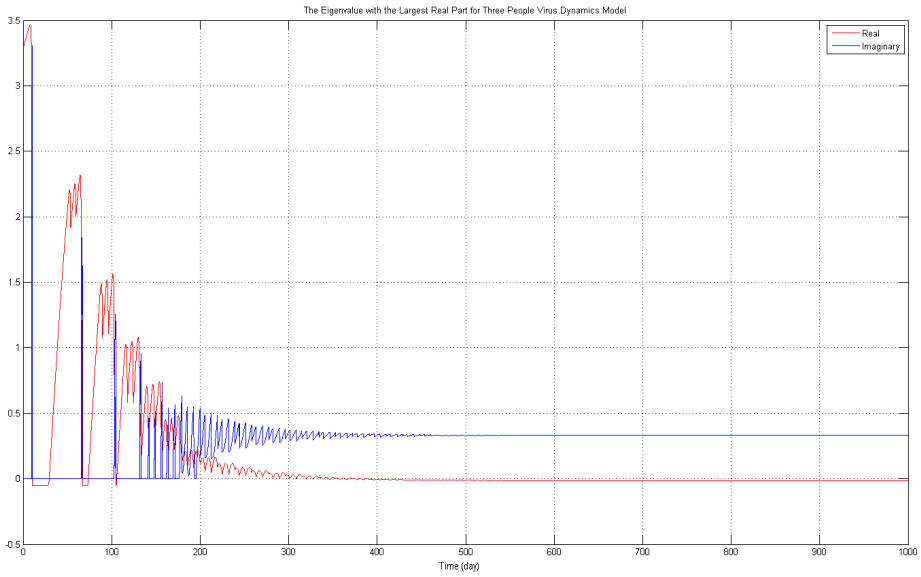

Figure 4.30: The largest real component of eigenvalues and the corresponding imaginary component over time for an individual-based viral dynamic model with 3 persons.

The largest real parts of the eigenvalues oscillate dramatically before $time = 200$, and its imaginary part is nonzero when the real part falls at the end of each period. Correspondingly, in general, behaviours of the states x_i, y_i, v_i and z_i $(i = 1, 2, 3)$ appear with pronounced oscillations during this period of time, as shown in Fig. 4.27. From $time = 200$ to $time = 300$, the magnitude of the oscillation of the imaginary parts are smaller, indicating the damping time for each oscillation is a big longer than in the previous period. After $time = 300$, both real and imaginary parts of the dominant eigenvalue became increasingly stable. Eventually, the real part of the dominant eigenvalue is below zero, and the imaginary part is around 0.35, which means the system decays toward an equilibrium with a almost constant frequency of oscillation, as shown in Fig. 4.27.

Because of the long time frame involved and the pronounced dynamics, the dy-

namics of behaviours and their corresponding eigenmodes in Fig. 4.27 is not fully clear. The following part of this section therefore focuses a short period of time when the dominant eigenvalues are complex. For example, from $time = 9.54$ to $time = 10.28$, the imaginary part of dominant eigenvalues are nonzero, and the state variables v_2 and y_2 oscillate during this period. Fig. 4.31 gives local views of state variables in this period of time. In this period, x_2 decreases while x_1 and x_3 slowly increase; y_2 increases first and declines later, while y_1 and y_3 are almost zero; v_2 increases while v_1 and v_3 are almost zero; and z_2 begins to increase at later time while z_1 and z_3 are slowly decreasing.

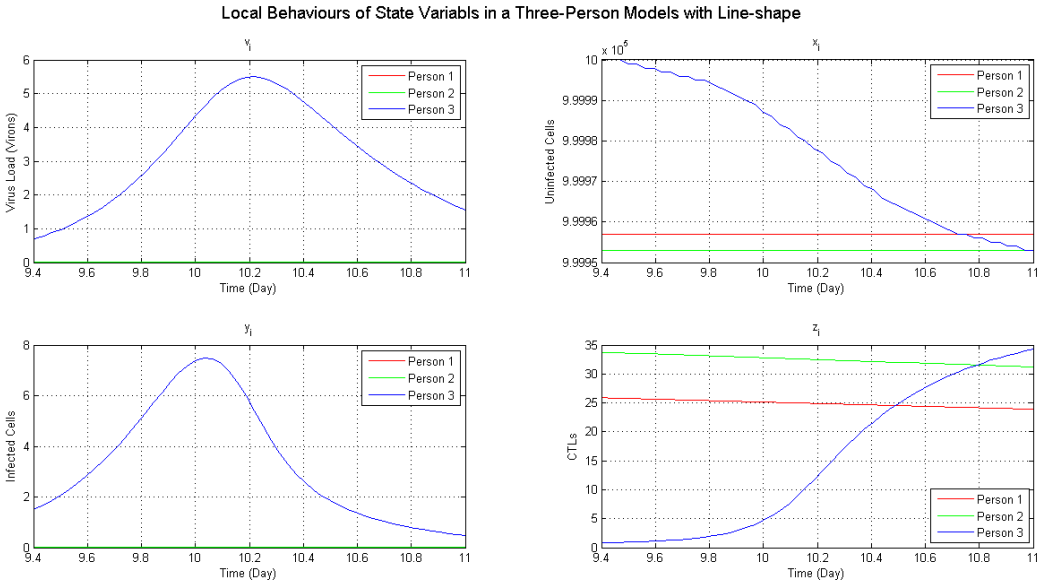

Figure 4.31: An early view of behaviours of state variables for an individual-based viral dynamics model with 3 persons, where v_1, v_2, y_1, and y_2 are near zero.

Particularly, four phases in this period are listed as: phase I ($time = 10.04$ to $time = 10.09$), phase II ($time = 10.10$ to $time = 10.15$), phase III ($time = 10.16$ to $time = 10.21$), and phase IV ($time = 10.22$ to $time = 10.28$). The dominant eigenvalues of these four phases are: $2.277 \pm 3.263i$, $1.493 \pm 3.307i$, $0.6693 \pm 3.023i$ and $0.00394 \pm 2.524i$. The real parts of the dominant eigenvectors of the four phases

are listed respectively in the following:

$$
\begin{array}{c}
x_1 \\ y_1 \\ v_1 \\ z_1 \\ x_2 \\ y_2 \\ v_2 \\ z_2 \\ x_3 \\ y_3 \\ v_3 \\ z_3
\end{array}
\begin{pmatrix}
+2.440 \times 10^{-11} \\ +2.593 \times 10^{-15} \\ +7.709 \times 10^{-15} \\ +1.674 \times 10^{-15} \\ -8.896 \times 10^{-8} \\ +1.235 \times 10^{-8} \\ +4.299 \times 10^{-8} \\ +5.287 \times 10^{-8} \\ -6.184 \times 10^{-1} \\ +3.905 \times 10^{-2} \\ +1.470 \times 10^{-1} \\ +3.740 \times 10^{-1}
\end{pmatrix},
\begin{pmatrix}
-1.398 \times 10^{-11} \\ +3.164 \times 10^{-15} \\ +8.986 \times 10^{-15} \\ -1.811 \times 10^{-15} \\ -9.466 \times 10^{-8} \\ +1.315 \times 10^{-8} \\ +4.428 \times 10^{-8} \\ +5.590 \times 10^{-8} \\ -6.432 \times 10^{-1} \\ -8.102 \times 10^{-2} \\ +1.025 \times 10^{-1} \\ +4.787 \times 10^{-1}
\end{pmatrix},
\begin{pmatrix}
-4.835 \times 10^{-11} \\ +4.143 \times 10^{-15} \\ +1.160 \times 10^{-14} \\ -8.211 \times 10^{-15} \\ -1.099 \times 10^{-7} \\ +1.402 \times 10^{-8} \\ +4.547 \times 10^{-8} \\ +6.517 \times 10^{-8} \\ -6.859 \times 10^{-1} \\ -1.444 \times 10^{-1} \\ +5.278 \times 10^{-1} \\ +5.561 \times 10^{-1}
\end{pmatrix},
\begin{pmatrix}
-6.841 \times 10^{-11} \\ +6.000 \times 10^{-15} \\ +1.607 \times 10^{-14} \\ -1.672 \times 10^{-14} \\ -1.380 \times 10^{-7} \\ +1.412 \times 10^{-8} \\ +4.429 \times 10^{-8} \\ +8.335 \times 10^{-8} \\ -7.298 \times 10^{-1} \\ -1.447 \times 10^{-1} \\ +1.018 \times 10^{-2} \\ +5.889 \times 10^{-1}
\end{pmatrix}
$$

From these eigenvectors, it can be observed that during this period of time, components in the dominant eigenvectors which represent states of `Person 3` (the final 4 components) have larger values than other components, which means in this period, the dominant eigenvalue primarily determines the behaviour mode of `Person 3`. In Fig. 4.27, the states of other two persons exhibit little change, and those of `Person 3` alter significantly. Complex eigenvalues here indicate oscillations of y_3 and v_3. In fact, x_3 and z_3 also oscillate before and after this period respectively. Because new virions are mainly produced by infected cells, the oscillation of v_3 occurs a bit later than that of y_3; meanwhile z_3 begins to grow a bit later than y_3 because CTL proliferates in response to the growth of infected cells. In phase I and II, components of y_3 in the dominant eigenvector are relatively smaller, and its change rate $\dot{y}_3$ is smaller than the change rates of other three states, as shown in Fig. 4.32. In all of these four phases, components representing x_3 in the dominant eigenvectors have relatively large absolute values, and its changing rate $\dot{x}_3$ is also very large.

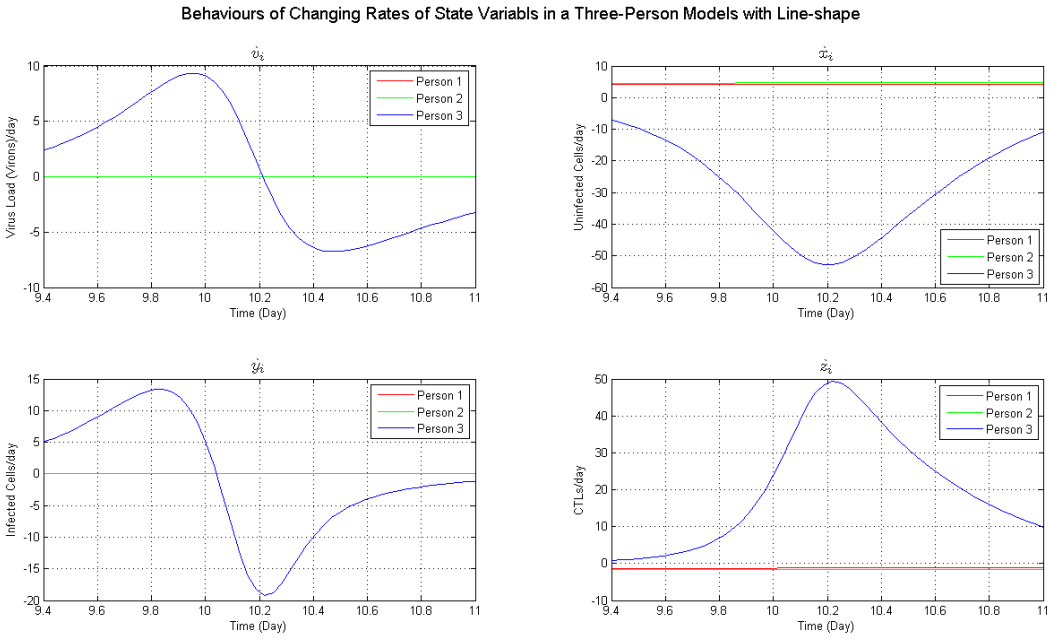

Figure 4.32: An early view of $\dot{v}_i, \dot{x}_i, \dot{y}_i, \dot{z}_i$ $i = 1, 2, 3$ for an individual-based viral dynamic model with 3 persons in line-shape.

4.2.3.3 Multiplicity of Eigenvalues

If we add another person, `Person 4` to be connected with `Person 2` in the three-person model of line-shape, who has the same connections and initial values as `Person 3` and re-analyze the model, from symmetry considerations we would expect that the final 4 entries of the eigenvectors (representing `Person 4`) and the second last 4 entries of eigenvectors (representing `Person 3`) are identical. However, for some eigenvectors (usually the last 6 eigenvectors) entries for `Person 3` and `Person 4` are not identical. One reason for that is eigenvalue multiplicity.

An eigenvalue of the square matrix A is of multiplicity of K if it is a K-fold root of the characteristic equation $|A - \lambda I| = 0$. If an eigenvalue has K linearly independent associated eigenvectors, this eigenvalue of multiplicity K is complete. However, not all multiple eigenvalues are complete, and an incomplete eigenvalue of multiplicity of $K > 1$ can be termed defective [6]. A matrix with any defective eigenvalue is called a defective matrix. The computation of eigenvalue solutions for linear differential equations with defective eigenvalues is very complicated, and its

eigenspace is also hard to analyze.

In our study, at $time = 0.5$ the last 4 eigenvectors share the same eigenvalue -0.1, associated with die-off of uninfected cells, which comes from the constant entry of Jacobian matrix, and the second last four eigenvalues of -0.05, associated with die-off of infected cells. These two eigenvalues are of multiplicity of 4. At $time = 0.5$ the rank of the matrix of eigenvectors is 16, and the matrix is of full rank[3]. Thus eigenvectors at this time point are linearly independent. We checked eigenvectors of the Jacobian matrix at several time points when the multiplicity of eigenvalues occurs, and we found that all these eigenvectors are linearly independent. Hereby we assume (though do not prove) that in our model, when there are multiple eigenvalues, they are complete and their corresponding eigenvectors are linearly independent. Thus the expansion of state variables around a point $\mathbf{x}_0$ at time t_0 could be presented as the following:

$$\mathbf{x}(t) = \sum_{i=1}^{16} c_i \mathbf{r}_i e^{-\lambda_i (t-t_0)} + \mathbf{b} \tag{4.15}$$

Where $\mathbf{x}$ is the vector of state variables, $\mathbf{r}_i$ is the ith eigenvector of the Jacobian matrix of the system, and $\mathbf{b}$ is the constant term. As we indicated in Section 3.1.3, the constant term does not affect the analysis of eigenmodes and behaviour patterns, and thus we neglect this constant term in following discussions. For this model, the last four eigenvalues are -0.1 and the second last four eigenvalues are -0.05. Therefore, we could rewrite the expansion of λs in Eq. 4.15 into the eigenmodes as:

$$\mathbf{x}(t) = \sum_{i=1}^{8} c_i \mathbf{r}_i e^{-\lambda_i (t-t_0)} + (\sum_{i=9}^{12} c_i \mathbf{r}_i) e^{-0.05(t-t_0)} + (\sum_{i=13}^{16} c_i \mathbf{r}_i) e^{-0.1(t-t_0)} \tag{4.16}$$

The last two weighted eigenvectors $\sum_{i=9}^{12} c_i \mathbf{r}_i$ and $\sum_{i=13}^{16} c_i \mathbf{r}_i$ can be calculated yielding the following:

$$\sum_{i=13}^{16} c_i \mathbf{r}_i = [\ldots, -1.49 \times 10^{-3}, -1.24 \times 10^{-17}, 2.30 \times 10^{-16}, 1.69 \times 10^{-16},$$

$$-1.49 \times 10^{-03}, -1.24 \times 10^{-17}, 2.30 \times 10^{-16}, 1.69 \times 10^{-16}]^T$$

[3]This matrix of eigenvectors is listed in Appendix B.

$$\sum_{i=9}^{12} c_i \mathbf{r}_i = [\ldots, 5.89 \times 10^{-9}, 9.86 \times 10^{-11}, -1.44 \times 10^{-9}, -4.88 \times 10^{-2},$$

$$5.89 \times 10^{-9}, 9.86 \times 10^{-11}, -1.44 \times 10^{-9}, -4.88 \times 10^{-2}]^T$$

From the above, we can see that sum of eigenvector entries for `Person 3` and `Person 4` are identical. This suggests that for an individual-based model, if several individuals share the same parameters, connections, and initial conditions we could group them together and regard them as a single individual with multiple links. In addition, because the individuals in the network share similar equations, and some of them share the same parameters and initial conditions, the multiplicity of eigenvalues occurs more frequently for the individual-based model than for the aggregate SIRS model, as shown in Fig. 4.3 and Fig. 4.28. This might be a significant limitations of eigenvalue analysis for individual-based models, and deserves our further investigations.

4.2.4 Eigenvalue Elasticity Analysis of an Individual-based Viral Dynamic Model with 3 Persons

There are ten parameters for the individual-based viral dynamics model; however, although eigenvalue elasticities with respect to parameters can be analyzed mathematically, some of these parameters are difficult to alter biologically, for example, β (`the rate at which uninfected cells are infected`). In this section, we focus on the parameter c (`the production rate of CTL`) and ω (`the connection weight`) and the eigenvalue elasticity with respect to them, because practically c might be changed by behaviour changes (e.g. exercise, smoking cessation, improved nutrition) or medical treatments (e.g. prevention of progress of kidney disease), and ω can be perturbed by social policies, such as policies to reduce risk-taking behaviours or to enhance hygiene or encourage reduced mixing.

With the symbolic expression for eigenvalue sensitivity in Eq. 3.16 and the expression of eigenvalue elasticity with respect to a parameter in Eq. 3.26, we computed the elasticities of eigenvalues with respect to ω and c. Because we have 12 eigenvalues

for this individual-based viral dynamics model, it is natural to find the eigenvalue elasticities with the largest real parts and try to perturb this parameter at the time point when the first peak of eigenvalue elasticity appears, as Section 3.2.2 suggests.

Fig. 4.33 plots the largest real parts of eigenvalue elasticity with respect to ω, and its corresponding imaginary parts. From these two figures, it can be observed that the first peak of the real parts of the eigenvalue elasticity appears from $time = 0$ to $time = 0.03$ with the value of 1.86×10^{-7}, the second significant peak appears from $time = 139.10$ to $time = 139.15$ with the value of 1.02×10^{-7}, and the elasticity arrives at the highest value of 4.53×10^{-7} when $time = 934.04$. The imaginary part of the elasticity at the first and the second peak is zero, and is 1.52×10^{-6} at the time of the third peak.

The past studies of eigenvalue elasticity, such as [7], indicated that a parameter with higher eigenvalue elasticities is more important than those with lower elasticities to the system. As a policy lever, the perturbation of this parameter might be more effective than that of other parameters. However, we also want to know proper times to change the parameter. In our study of infectious disease, it is generally desirable to intervene earlier because we want to reduce the number of infected people and delay the spread of diseases. Here, although the eigenvalue elasticity with respect to ω arrives at the highest peak at $time = 934.04$, it is nearly meaningless to perform a policy at this time in practice because the system approaches to an equilibrium after $time = 500$ and any change then will not influence the system too much. Therefore, we perturb ω at $time = 0.03$ (when the largest eigenvalue elasticity is 1.86×10^{-7}) and $time = 139.1$ (when the largest eigenvalue elasticity is 1.02×10^{-7}). A simulation of a perturbation of ω at $time = 10$ (when the largest elasticity is -3.58×10^{-12}) is performed as a control. We decrease the ω to be 90% of the original value of 10^{-6} for the perturbation.

Fig. 4.34 is the comparison of the value of average v across the population with perturbations of ω at three time points (each associated with the red, green and grey curve respectively), and the blue curve is the original value of average v in the population. Due to small values of elasticities (on the order of magnitude 10^{-7}), the

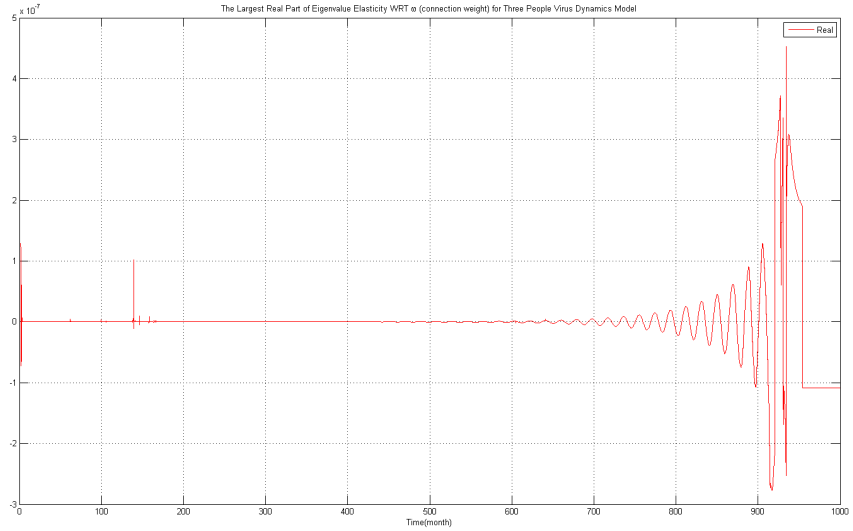

(a) Real Parts

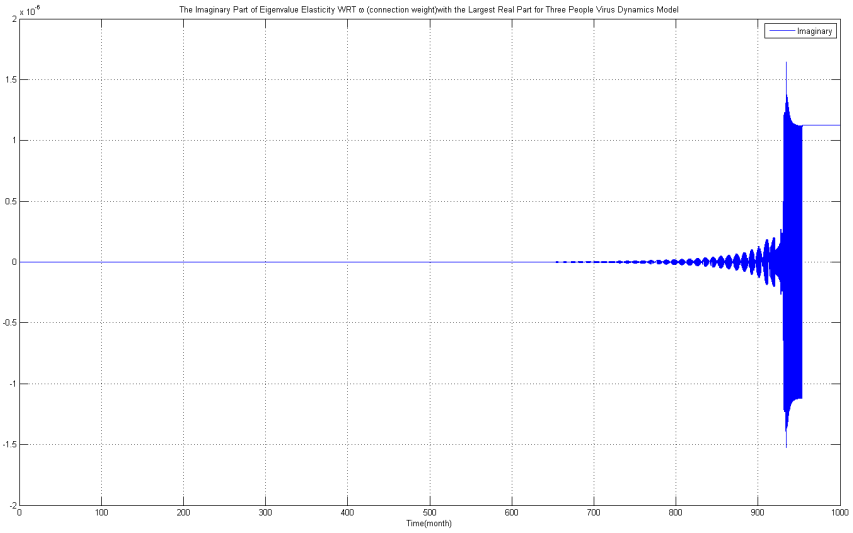

(b) Imaginary Parts

Figure 4.33: The largest real part of eigenvalue elasticity with respect to ω (`the connection weight`) for an individual-based viral dynamic model with 3 persons and the corresponding imaginary parts.

change of behaviour from the perturbation is not significant and is hard to observe in Fig. 4.34. Locally between $time = 148$ and $time = 156$, the oscillation of average v is a bit delayed with perturbation of ω at $time = 0.03$ or $time = 10$.

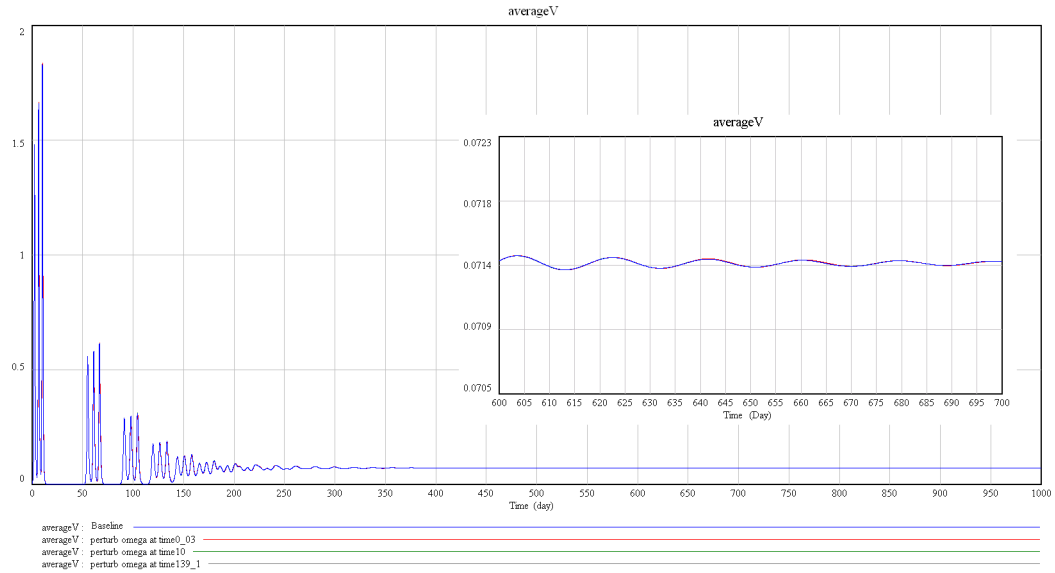

Figure 4.34: The value of average v in the population with a small perturbation of ω (`the connection weight`) at $time = 0.03$, $time = 10$, and $time = 139.1$ respectively for an individual-based viral dynamic model with 3 persons and its local view.

However, the change of behaviour is quite small and the difference between perturbations at different time points are difficult to observe because of small changes of ω and small values of the elasticities. Therefore, we give ω a bigger alteration, and change it to be 10% of its original value. Shortly after the perturbations of ω at $time = 0.03$, $time = 10$, and $time = 139.1$, the average of v in the population does not change at all. But in a bit longer term, the effects of such perturbations could be reflected.

As shown in the local view of Fig. 4.35, during the period from $time = 148$ to $time = 156$, the value of the average v in the population is a bit larger with perturbations than the original one, but the oscillations are delayed. Particularly, the perturbation at $time = 0.03$ has a longer delay of oscillation compared with the original curves than that at $time = 10$ because of the larger value of the elasticity. But this figure does not clearly show the influence of the perturbation at $time =$

139.1.

Table 4.3: The value of average v in population with perturbations of ω at different time for an individual-based viral dynamic model with 3 persons.

	average v in the population				
Time (Day)	148	148.125	148.375	148.5	148.625
Baseline	0.0433	0.0488	0.0490	0.0516	0.0547
perturbed at $time = 0.03$	0.0246	0.0241	0.0235	0.0235	0.0237
perturbed at $time = 10.0$	0.0277	0.0275	0.0278	0.0283	0.0291
perturbed at $time = 139.1$	0.0433	0.0488	0.0490	0.0516	0.0547

Table 4.3 gives the value of average v in the population at a selected set of time points. In this table, the perturbation of ω at $time = 139.1$ nearly has no effect on the value of average v, i.e., such perturbation does not apparently change the system behaviour. With Eq. 3.17, we have

$$\Delta\lambda_i \approx \epsilon_i(p_j)\frac{\Delta p_j}{p_j}\lambda_i \tag{4.17}$$

With a given change of p_j, the value of $\Delta p_j/p_j$ is fixed, and the change of λ_i is determined by both the elasticity and the eigenvalue itself. From Table 4.4, it can be observed that at $time = 139.1$, the eigenvalue corresponding to the largest elasticity is much smaller than the dominant eigenvalue. In contrast, at $time = 10$, the eigenvalue corresponding to the largest elasticity is with the same order of magnitude of the dominant eigenvalue; and at $time = 0.03$ the eigenvalue with the largest elasticity is the dominant eigenvalue at that time. Therefore, we conjecture that the perturbation at $time = 0.03$ alters the system behaviour most significantly, because the perturbation of the parameter affects the dominant eigenvalue.

At the endemic equilibrium, the average value of v in the population for three-person model in the line-shape is

$$\bar{v} = \frac{bk\,(3\,u + 4\,\omega)}{3\,(u^2 - 2\,\omega^2)\,c} \tag{4.18}$$

With the default values of parameters, the population mean value of v at the endemic equilibrium is 0.07142860. When ω is decreased to be 10% of the default value, the

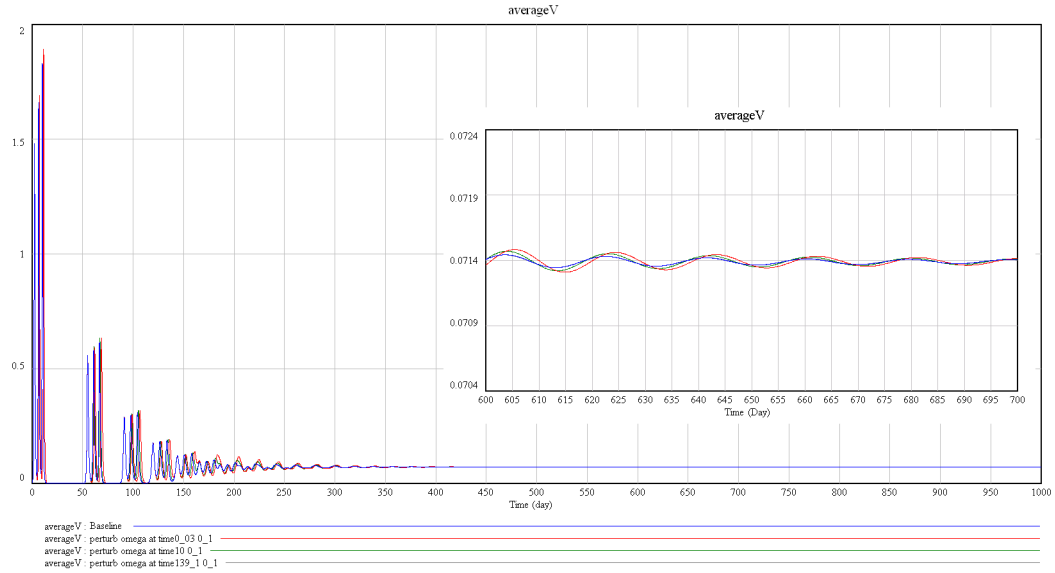

(a) Overall view and local view in the long run

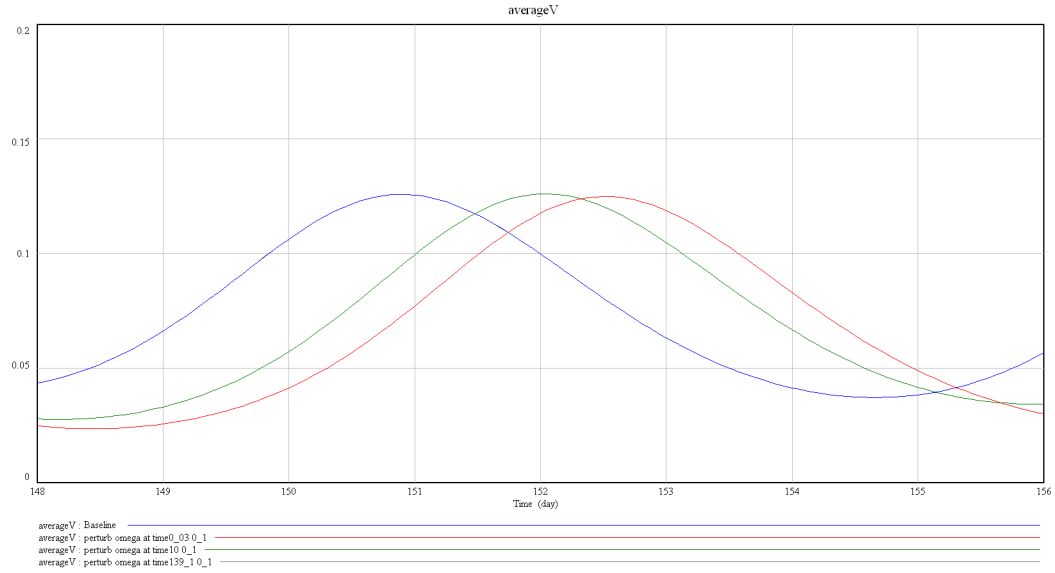

(b) Local view between $time = 148$ and $time = 156$

Figure 4.35: The value of average v in population with a large perturbation of ω (`the connection weight`) at $time = 0.03$, $time = 10$, and $time = 139.1$ respectively for an individual-based viral dynamic model with 3 persons and its local views.

Table 4.4: The dominant eigenvalues and eigenvalues with the largest elasticity at different times for an individual-based viral dynamic model with 3 persons.

Time (Day)	Eigenvalue with the Largest Elasticity	Dominant Eigenvalue	The Largest Eigenvalue Elasticity
0.03	3.278	3.278	1.86×10^{-7}
10.0	-1.744	2.814	1.02×10^{-7}
139.1	2.738×10^{-3}	6.908×10^{-1}	-3.58×10^{-12}

population mean value of v at the endemic equilibrium becomes 0.07142857. The difference between the original value and the shifted value is only of the order of magnitude of 10^{-6}. Therefore, the perturbation of ω by a small amount cannot significantly decrease the mean viral load across the population in the long-term, shown in Fig. 4.35, but could locally alter the trajectory of the average v in the population, and especially at the time points when the elasticity is high and when the eigenvalue with the large elasticity is close to the dominant eigenvalue.

The elasticity of the eigenvalue with respect to ω is of the order of magnitude of 10^{-7}, and a small change of ω does not result in a significant alteration of the system behaviour. Because the eigenvalue elasticity is dimensionless, we now choose the parameter with the largest elasticity. Fig. 4.36 illustrates the real and imaginary parts of the largest eigenvalue elasticity with respect to c (`the production rate of CTL`) respectively. The maximum elasticity of the eigenvalues with respect to c has much larger value than that with respect to ω. The first significant peak of the eigenvalue elasticity with respect to c appears from $time = 94.85$ to $time = 94.9$ with the value of -225.9, and the most significant peak of the elasticity appears from $time = 158.72$ to $time = 158.78$ with the value of -2264. The elasticity also arrives at another peak from $time = 165.97$ to $time = 166.03$ with the value of -747.34.

We perturb c to change it to be 110% of the original value 0.7 at $time = 94.85$ and $time = 158.72$. With 10% increment of c, the mean value of v in the population at the endemic equilibrium in Eq. 4.18 becomes 0.06493509, decreased by 9.1% from the original value. Such perturbation changes the behaviour of the average v in the population in the long run (Fig. 4.37).

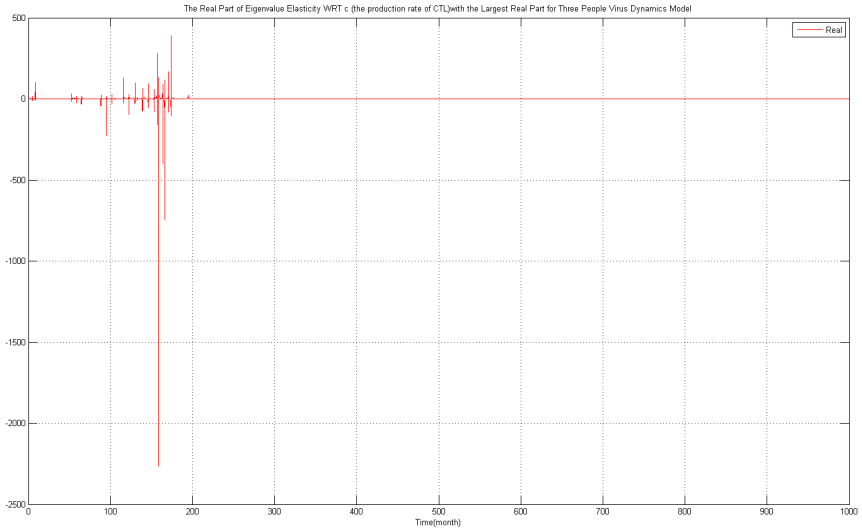

(a) Real Parts

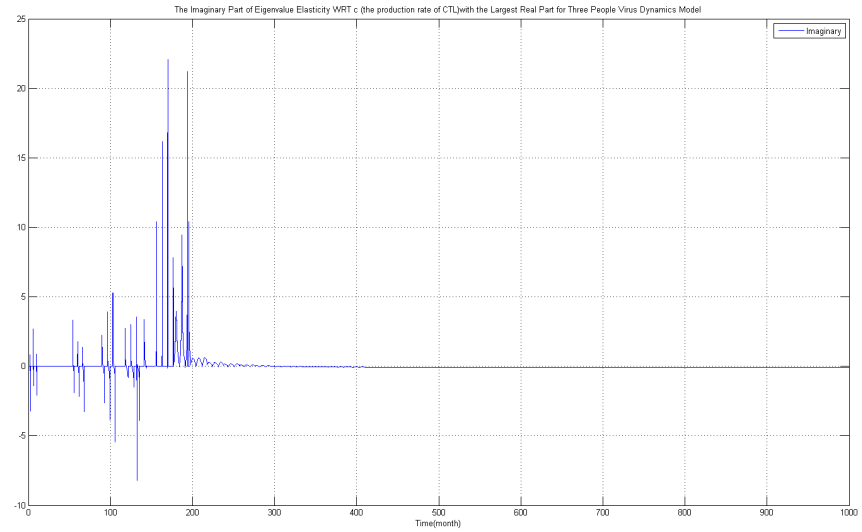

(b) Imaginary Parts

Figure 4.36: The largest real part of eigenvalue elasticity with respect to c (`the production rate of CTL`) for an individual-based viral dynamic model with 3 persons and the corresponding imaginary parts.

Similar to the perturbation of ω, we also add an experiment to perturb c at $time = 10$ as a control when the elasticity is $0.768 \pm 0.362i$. Fig. 4.37 is the comparison of the value of average v with perturbations of c at three different time points and its local view from $time = 600$ to $time = 700$, presenting by red, green and grey curves respectively, and the blue curve is the original value of average v in the population. Table 4.5 illustrates the local changes of the average v shortly after the perturbation of c. From these figures, the trajectory of average v has been changed by the perturbations. The value of the average v across the population becomes smaller in a short period of time after perturbations of c at these time points than the original values, which indicates such policy causes the mean viral loads in the population to decline. In addition, the proportional changes of the average v brought by the perturbation at $time = 158.72$ is a bit more significant than that from the perturbation at $time = 94.85$. The eigenvalue corresponding to the largest elasticity at $time = 158.72$ is the dominant eigenvalue (3.360×10^{-1}) at that time, while the eigenvalue associated with the largest elasticity at $time = 94.85$ is -3.208×10^{-4}. The coefficients of those two eigenvalues are on the order of magnitude of 10^{-1} at that time when the largest and the smallest order of magnitude of the coefficient are 10^{1} and 10^{-5}. According to Eq. 4.17, the change of the behaviour mode from the perturbation of c at $time = 158.72$ is a bit more significant than that at $time = 94.85$, as demonstrated in the local view.

However, similar to the perturbation of ω, as a control experiment the perturbation of c at $time = 10$ alters the system behaviour greatly in a short period of time after the perturbation. In fact, the eigenvalue of the largest elasticity is the dominant eigenvalue at that time ($2.814 \pm 2.989i$). In addition, the coefficient of this eigenvalue is 33.72, the largest coefficient at that time, which means the eigenvector of this eigenvalue must be an eigenvector which dominates the system significantly. Therefore, a small change of the eigenvalue from the perturbation of c can generate distinct changes of the behaviour. Because eigenvalue elasticities at a particular time point are computed with the Jacobian matrix at that time, the largest elasticity can only predict local proportional changes of eigenvalues. In a long run, eigenvectors,

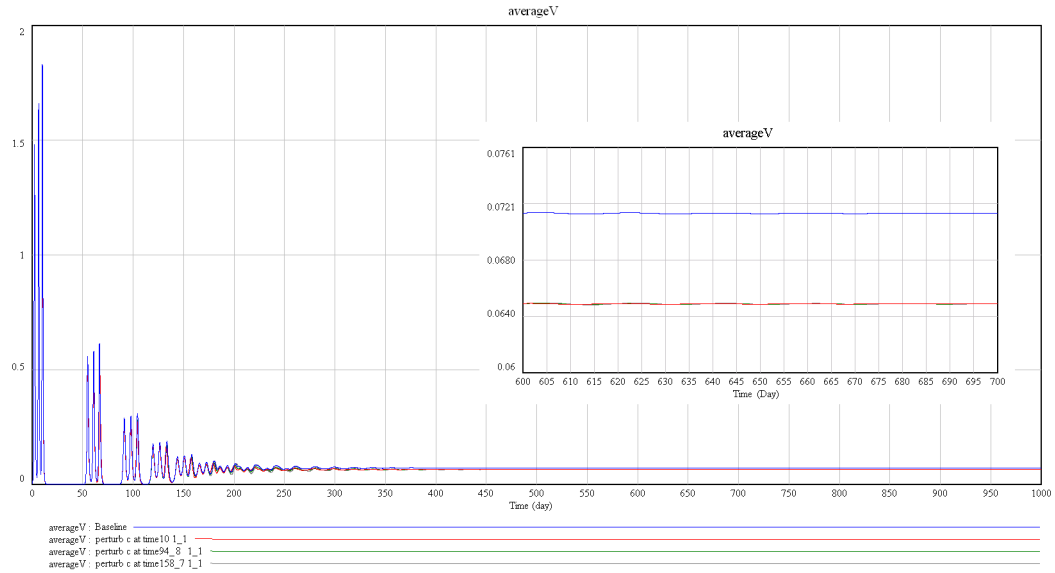

Figure 4.37: The value of average v in the population with a perturbation of c (`the production rate of CTL`) at $time = 10$, $time = 94.85$, and $time = 158.72$ respectively for an individual-based viral dynamic model with 3 persons and its local view.

as well as coefficients, can also jointly determine the evolution of the system, and locally high eigenvalue elasticities are not necessarily indications of global results of the perturbation of the parameters.

4.2.5 Discussion

We analyzed an individual-based viral dynamics model with three people with equilibria, eigenvalues, eigenvectors and eigenvalue elasticities in this section. The number of equilibria of the equations grows geometrically with the population size. With current parameter settings, the disease-free and defense-free equilibria are unstable and the endemic equilibrium is stable for both the one-person model and multi-person model. Perturbations of the connection weight ω or the production rate of CTL c in our eigenvalue elasticity analysis do not change the stability of the endemic equilibrium, but will slightly shift its position.

Unlike the SIRS model discussed in the above section, the individual-based model exhibits complexity due to relatively large number of state variables and network connections. Even for the model of three people it is hard to describe the system

Table 4.5: The value of average v in the population shortly after perturbations of c at different time for an individual-based viral dynamic model with 3 persons.

	average v in the population				
Time (Day)	10.0078	10.0391	10.0703	10.1016	10.1328
Baseline	1.47217	1.56318	1.64619	1.71767	1.77432
perturbed at $time = 10.0$	1.47217	1.56299	1.64507	1.71432	1.76699
proportional changes	0	-1.2155×10^{-4}	-6.8036×10^{-4}	-0.002	-0.004
Time (Day)	94.5859	94.6172	94.6484	94.6797	94.7109
Baseline	0.0222304	0.0219134	0.0216387	0.0213912	0.0211761
perturbed at $time = 94.58$	0.0222304	0.0219134	0.0216386	0.0213911	0.0211758
proportional changes	0	0	-4.6213×10^{-6}	-4.6748×10^{-6}	-1.4167×10^{-5}
Time (Day)	158.727	158.773	158.813	158.852	158.898
Baseline	0.122342	0.121043	0.119902	0.118709	0.117216
perturbed at $time = 158.72$	0.122341	0.121039	0.119889	0.118681	0.117162
proportional changes	-8.1738×10^{-6}	-3.3046×10^{-5}	-1.0842×10^{-4}	-2.3587×10^{-4}	-4.6069×10^{-4}

behaviours with eigenvalues alone; evolving eigenvectors and coefficients also play an important role in determining the behaviour patterns. Multiple eigenvalues of the Jacobian matrix for an individual-based model occur more frequently than for the SIRS model analyzed early in this chapter. All of these difficulties hamper the efficiency of the application of eigenvalue analysis for individual-based models of infectious disease spread.

Because the eigenvalue elasticity is dimensionless, we could compare it with respect to different parameters. In our analysis of the individual-based model, the eigenvalue elasticity with respect to c is much higher than that with respect to ω (by the order of the magnitude 10^8). When both of these two parameters are changed with the same proportion, the changes after perturbations of c are more distinct than after the perturbations of ω. The perturbations of a parameter based on eigenvalue elasticity analysis is also determined by the elasticities, the eigenvalues and their coefficients. For example, an eigenvalue with a small value may have a large elasticity with respect to a parameter, and in such a case, because the eigenvalue does not determine the major behaviour of the system, changing the value of the parameter may not result in notable alterations of the system behaviour. In addition, the per-

turbation of a parameter with a large eigenvalue and a large elasticity at a particular point might also have a very limited impact on the system because the coefficient may have a small value. Consequently, the perturbation of a parameter with a high elasticity cannot be guaranteed to yield a significant change of the system behaviour over time, even in the short-term. In next chapter, we will see how global behaviours of the system can limit effectiveness of parameter sensitivity analysis. Furthermore, if we analyze a more complex model consisting of 30 or 100 or even one thousand people, eigenvalue elasticity analysis can likely not provide instant and effective suggestions. To sum up, the eigenvalue elasticity analysis, which aims to provide policy levers, is not as powerful for a complicated infectious disease model as it can be for simple models.

Chapter 5

Global Function Elasticity and Sensitivity Analysis of Infectious Disease Models

As introduced in Section 3.3, a consideration of a global function in state space and its elasticity analysis offers an easier insight into the influence of a parameter on a system than for eigenvalue elasticity analysis. This reflects the fact discussed in Section 4.2.4 that the effects of perturbations of a parameter on eigenvalues may not directly be reflected by state variables. In this chapter, we analyze global function elasticity and sensitivity with respect to parameters for both aggregate and individual-based infectious disease models. A global function in state space is defined as a mapping from the state space of the system to the real domain $\mathfrak{R}$. Such a function summarizes state variables in the state space at a particular time. For simplicity, we call a global function in state space a "global function" for short.

5.1 Global Function Elasticity Analysis of an Individual-based Viral Dynamic Model with 30 Persons

The motivations for the analysis of parameter impact on global functions is several-fold. For an individual-based model with a large population, we believe that policy makers cannot limit their concerns to one or two individuals in the system, and

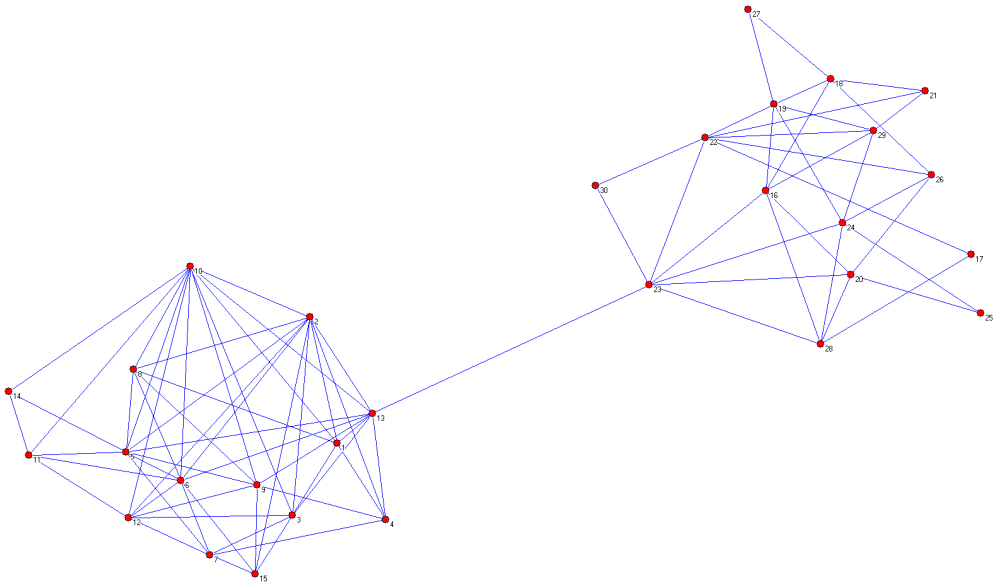

Figure 5.1: The connection network for an individual-based viral dynamic model with 30 persons.

their aim is control the disease on a macro-level. Another direct inspiration for our introduction of global function elasticity and sensitivity is the difficulty of applying eigenvalue elasticity methods to an individual-based model with a large population size, as we analyzed in the last chapter. Therefore in the following, we concentrate on an individual-based viral dynamic model with a relatively large population size (30) by global function elasticity and sensitivity. The model with the 30 persons is similar to that with 3 persons except for presence of a larger population size and the presence of a different connection matrix $(\sigma)_{ij}(i, j = 1, \cdots, 30)$. Fig. 5.1 shows the network of connection among 30 persons in this model.

For the purpose of disease control, one possible target could be decreasing the amount of virus or the rate at which the quantity of viral particles grows on a level of the whole population. Thus we define G to be the average virus load in the population. Because any change of a parameter cannot instantly influence the state variables, as Table 4.5 shows, but the changing rate of state variables and of functions of state variables can be changed immediately, in this chapter, we apply our analysis of the impact of parameter changes on the rate of change of global functions. The global function we study here is its the rate of changing: $\dot{G}$. If P is the population

size of the model, G is defined as:

$$G = \frac{1}{P}\sum_{i=1}^{P} v_i \tag{5.1}$$

According to Eq. 3.31, we have

$$\dot{G} = \frac{\partial G}{\partial t} + \sum_{i=1}^{P}\frac{\partial G}{\partial x_i}\dot{x}_i = 0 + \sum_{i=1}^{P}\frac{\partial G}{\partial x_i}\dot{x}_i \tag{5.2}$$

From the definition of G in Eq. 5.1, we have

$$\frac{\partial G}{\partial x_i} = \frac{\partial G}{\partial y_i} = \frac{\partial G}{\partial z_i} = 0$$

$$\frac{\partial G}{\partial v_i} = \frac{1}{P}$$

With Eq. 4.8, we have

$$\dot{G} = \frac{1}{P}\sum_{i=1}^{P}\dot{v}_i = \frac{1}{P}\sum_{i=1}^{P}(ky_i - uv_i + \omega\sum_{i\neq j}\sigma_{ij}v_j) \tag{5.3}$$

From Eq. 5.3, it can be observed that the global function $\dot{G}$ depends on three parameters: k (`the rate at which infected cells produce free virus`), u (`the death rate of the free virus`), and ω (`the connection weight`, dictating the rate of viral transmission between neighbours). In this section, we analyze the global function elasticity with respect to u and ω. We do so because in practice it may be possible to perturb the parameter u by biological or medical treatment, and the parameter ω by interventions focused on risk behaviour modification, hygiene, etc.

With Eq. 3.29 and Eq. 5.3, the sensitivity of $\dot{G}$ with respect to parameters u and ω is as follows:

$$\dot{g}_s(u) = -\frac{1}{P}\sum_{i=1}^{P} v_i \tag{5.4}$$

$$\dot{g}_s(\omega) = \frac{1}{P}\sum_{i=1}^{P}\sum_{i\neq j}\sigma_{ij}v_j \tag{5.5}$$

We now analyze the elasticity of the global function $\dot{G}$ with Eq. 5.4, Eq. 5.5 and Eq. 3.30. From Eq. 3.30, we have

$$\dot{g}_e(p) = \lim_{\Delta p\to 0}\frac{\frac{\Delta\dot{G}}{\dot{G}}}{\frac{\Delta p}{p}} \tag{5.6}$$

In this section, we calculate anticipated (theoretic) changes in $\dot{G}$ resulting from changing a parameter using the following approximations:

$$\frac{\Delta \dot{G}}{\dot{G}} \approx \dot{g}_e(p) \frac{\Delta p}{p} \tag{5.7}$$

$$\Delta \dot{G} \approx \dot{g}_e(p) \dot{G} \frac{\Delta p}{p} \tag{5.8}$$

Eq. 5.7 tells us that the proportional change of $\dot{G}$ approximately equals the multiplication of the elasticity of $\dot{G}$ with respect to a parameter p and the proportional change of p. In this study, one purpose of parameter perturbations is to decrease $\dot{G}$ so that the average free viral particles v could decrease faster or increase more slowly (i.e., $\Delta \dot{G} < 0$). Whether we should increase or decrease the parameter p to accomplish this depends on values of both the elasticity and $\dot{G}$.

5.1.1 Global Function Elasticity with Respect to ω

The $\dot{G}$ elasticity with respect to ω over time for the 30-person model is presented in Fig. 5.2. The elasticity has large values after $time = 300$, especially after $time = 500$. Policy makers will prefer to intervene when the disease first breaks out in order to decrease the cost brought by disease spread. Although the global function elasticity has large values in the late stage of the system evolution, it also attains relatively high absolute values in the early stage of the system evolution. From this figure we could know that there are peak values from $time = 0$ to $time = 150$ when the system first evolves, though these peaks are almost invisible compared with significant peaks in the later stages.

Three time points with apparent peak values in the time period from $time = 0$ to $time = 100$ are selected to perturb the parameter ω separately for the 30-person model. The global function elasticity with respect to ω arrives at a peak value at $time = 4.37$ ($\dot{G} = 6.73317 \times 10^{-5}$) with the value of 1.029×10^{-3}, and another peak value at $time = 9.89$ ($\dot{G} = -7.89554 \times 10^{-3}$) with the value of -1.374×10^{-3} and the third peak value at $time = 36.51$ ($\dot{G} = 5.52824 \times 10^{-17}$) with the value of 3.673×10^{-3} when other values of the elasticity are on the order of magnitude of

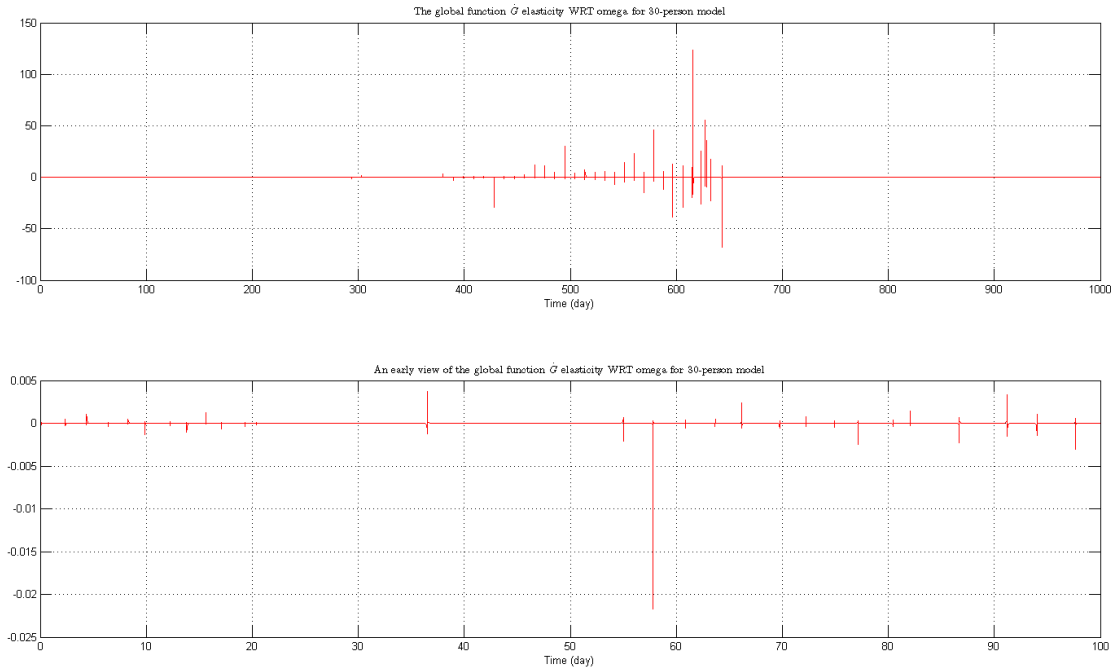

Figure 5.2: The global function elasticity with respect to ω (`the connection weight`) for an individual-based viral dynamic model with 30 persons and its early view.

10^{-5} or smaller. ω was decreased to 10% of the original value at these time points according to Eq. 5.8 so that the value of $\dot{G}$ can be decreased. With Eq. 5.7 we have at $time = 4.37$, $\frac{\Delta\dot{G}}{\dot{G}} = 1.029 \times 10^{-3} \times -0.9 = -9.2610 \times 10^{-4}$; at $time = 9.89$, $\frac{\Delta\dot{G}}{\dot{G}} = -1.374 \times 10^{-3} \times -0.9 = 0.0012$; and at $time = 36.51$, $\frac{\Delta\dot{G}}{\dot{G}} = 3.673 \times 10^{-3} \times -0.9 = -0.0033$. Initially such perturbations change the trajectory of $\dot{G}$, shown in Table 5.1, Table 5.2 and Table 5.3. From these tables, we can see that immediately after the perturbation, the proportional change of $\dot{G}$ is not far from the prediction of the global function elasticity and the proportional change of ω. We should note here and in following analysis that such immediate periods after perturbations are practically too short to control disease spread, but for methodological study, it could indicate the local effectiveness of such techniques.

Fig. 5.3 shows the views of the changes of $\dot{G}$ in later stage. The perturbation at $time = 4.37$ produces the most significant changes of the behaviour of $\dot{G}$ that perturbations at other time points: the oscillation of $\dot{G}$ is largely delayed and the magnitude is slightly reduced. The perturbation at $time = 9.89$ has similar influences

Table 5.1: The proportional change of $\dot{G}$ with a perturbation of ω at *time* = 4.37 for an individual-based viral dynamic model with 30 persons (theoretically $\Delta\dot{G}/\dot{G} \approx -9.2610 \times 10^{-4}$).

Time (Day)	$\dot{G}$	$\dot{G}$ with Perturbation	$\frac{\Delta\dot{G}}{\dot{G}}$
4.37087	1.13633×10^{-4}	1.13528×10^{-4}	-9.2403×10^{-4}
4.37287	2.06512×10^{-4}	2.06458×10^{-4}	-2.6149×10^{-4}
4.37487	2.99617×10^{-4}	2.99564×10^{-4}	-1.7689×10^{-4}
4.37687	3.92984×10^{-4}	3.92931×10^{-3}	-1.3487×10^{-4}

Table 5.2: The proportional change of $\dot{G}$ with a perturbation of ω at *time* = 9.89 for an individual-based viral dynamic model with 30 persons (theoretically $\Delta\dot{G}/\dot{G} \approx 0.0012$).

Time (Day)	$\dot{G}$	$\dot{G}$ with Perturbation	$\frac{\Delta\dot{G}}{\dot{G}}$
9.8904	-7.89544×10^{-3}	-7.90492×10^{-3}	0.0012
9.9004	-6.39224×10^{-2}	-6.39313×10^{-2}	1.3923×10^{-4}
9.9104	-0.120613	-0.120622	7.4619×10^{-5}
9.9204	-0.178024	-0.178032	4.4938×10^{-5}

Table 5.3: The proportional change of $\dot{G}$ with a perturbation of ω at *time* = 36.51 for an individual-based viral dynamic model with 30 persons (theoretically $\Delta\dot{G}/\dot{G} \approx -0.0033$).

Time (Day)	$\dot{G}$	$\dot{G}$ with Perturbation	$\frac{\Delta\dot{G}}{\dot{G}}$
36.5116	5.52797×10^{-17}	5.5174×10^{-17}	-0.0019
36.5216	2.72388×10^{-16}	2.72285×10^{-16}	-3.7814×10^{-4}
36.5316	4.88221×10^{-16}	4.88119×10^{-16}	-2.0892×10^{-4}
36.5416	7.02807×10^{-16}	7.02707×10^{-16}	-1.4229×10^{-4}

on $\dot{G}$ to the perturbation at $time = 36.51$.

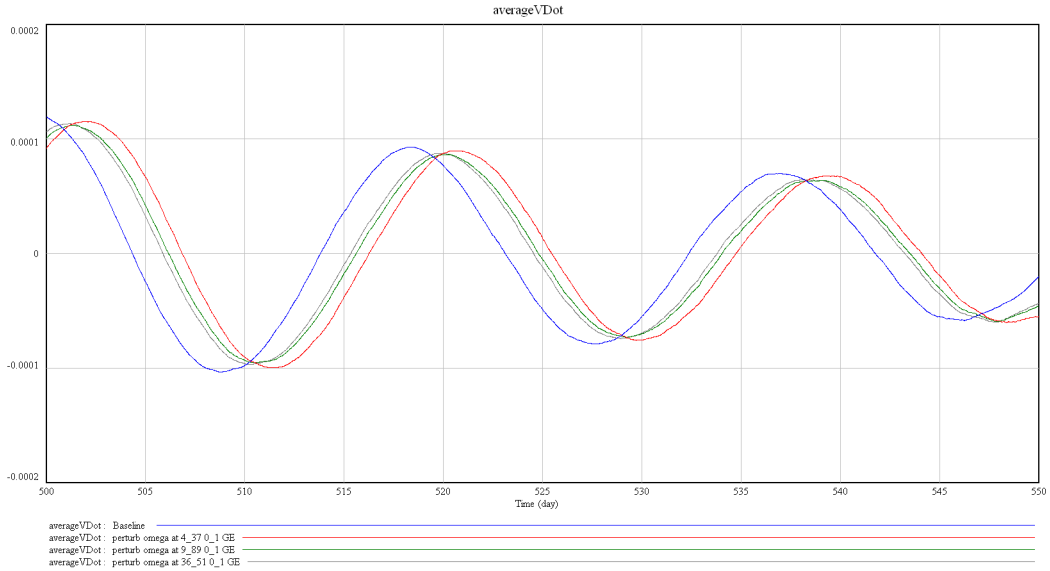

Figure 5.3: A local view of value of average $\dot{v}$ in population with a perturbation of ω (`the connection weight`) at $time = 4.37$, $time = 9.89$ and $time = 36.51$ respectively when the largest $\dot{G}$ elasticities appear in the early stage for an individual-based viral dynamic model with 30 persons.

A control experiment is added to decrease ω by 90% at $time = 5.43$ when the elasticity of the global function with respect to ω is 1.864×10^{-6} and $\dot{G} = 3.00334 \times 10^{-1}$, to compare with the perturbation at $time = 4.37$ when the perturbation produces relatively more significant changes of $\dot{G}$ for 30 people model. The proportional change of $\dot{G}$ at $time = 5.43$ should be $1.864 \times 10^{-6} \times -0.9 = -1.6776 \times 10^{-6}$. Table 5.4 gives details of the proportional changes of $\dot{G}$ in a small window of time. Compared with Table 5.1, Table 5.4 shows that in a very short period of time after changing ω, the proportional change of $\dot{G}$ at $time = 5.43$ is indeed much smaller than that at $time = 4.37$, but later on the differences of the proportional changes at two time points become less notable. As shown in Fig. 5.4, in the long run, the perturbation at an early time point with a small value of the elasticity generates similar trajectory changes of $\dot{G}$ to the perturbation at another early time point with a large elasticity value, because the state variables approaches to the equilibrium, and the changing rate of G approaches to zero.

Table 5.4: The proportional change of $\dot{G}$ with a perturbation of ω at $time = 5.43$ for an individual-based viral dynamic model with 30 persons (theoretically $\Delta\dot{G}/\dot{G} \approx -1.6776 \times 10^{-6}$).

Time (Day)	$\dot{G}$	$\dot{G}$ with Perturbation	$\frac{\Delta\dot{G}}{\dot{G}}$
5.4398	0.31028	0.3102794	-1.9337×10^{-6}
5.4498	0.320531	0.3205304	-1.8719×10^{-6}
5.4598	0.331095	0.3310945	-1.5101×10^{-6}
5.4698	0.341979	0.3419785	-1.4621×10^{-6}

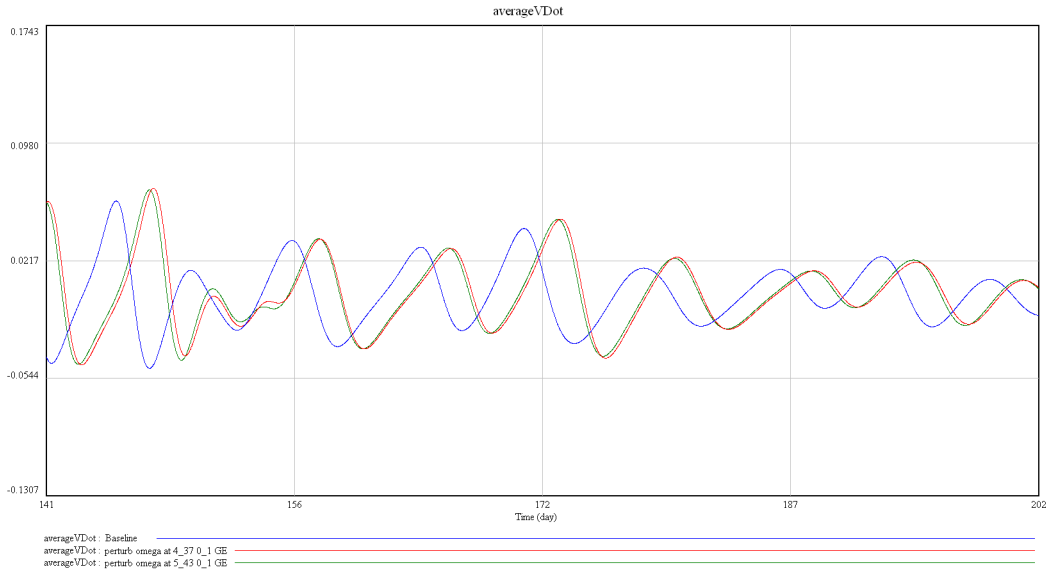

Figure 5.4: A local view of the comparison of the value of average $\dot{v}$ in the population with a perturbation of ω (`the connection weight`) at $time = 4.37$ when the largest $\dot{G}$ elasticity appears in the early stage and at $time = 5.43$ when the elasticity is small for an individual-based model with 30 persons.

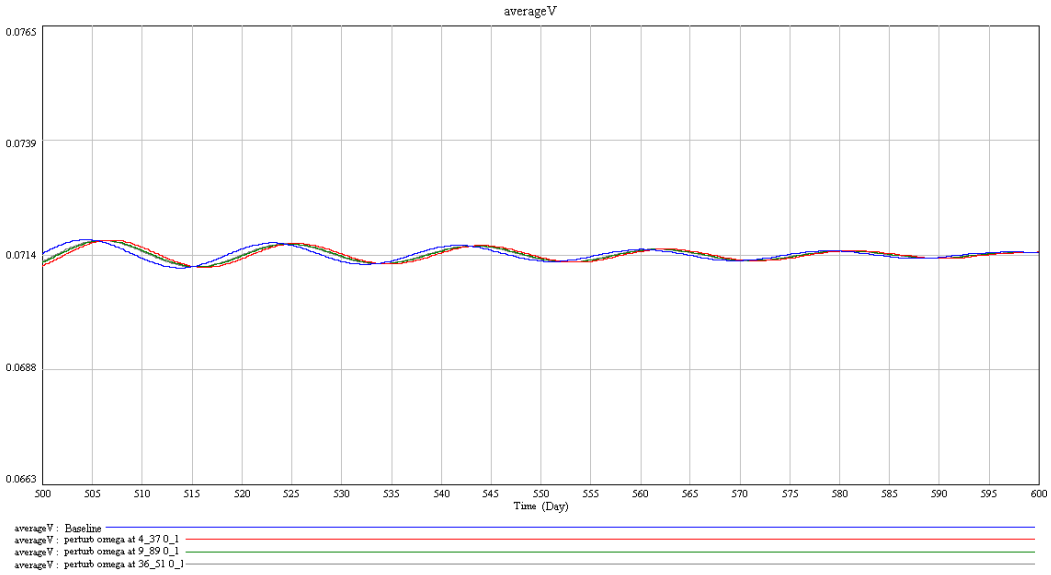

Figure 5.5: The value of average v in the population with a perturbation of ω (`the connection weight`) in the long run for an individual-based model with 30 persons.

When approaching the endemic equilibrium, $\dot{G}$ approaches to zero no matter the parameters are perturbed or not. Thus if we check the changes of G near the endemic equilibrium, we can see the impacts of the changes of a parameter in the long time. Fig. 5.5 illustrates the changes of the global function G: the average virus loads across the population in the long run with perturbations of ω. Globally the average virus loads are not changed significantly. As we analyzed in the last chapter, for an individual-based model the connection weight does not greatly influence the position of the endemic equilibrium because of its relatively low value. Here we also observe that the average virus loads near the endemic equilibrium vary little with perturbations of ω.

5.1.2 Global Function Elasticity with Respect to u

The impact of the $\dot{G}$ elasticity with respect to u over time for the 30 people model is similar to that to ω. Because the parameter u can be increased by biological or medical treatment and because the purpose of perturbation is to decrease the global function $\dot{G}$, we choose the time points when the elasticity is negative, and thus the large elasticity here means the negative values with large absolute values. Similar

to the $\dot{G}$ elasticity with respect to ω, the global function elasticity with respect to u attains relatively high absolute values in the early stage of the system evolution. There are peak values from $time = 0$ to $time = 100$ when the system first evolves and $\dot{G}$ has large values, though these peaks are almost invisible compared with significant peaks in the late stages, as described in Fig. 5.6.

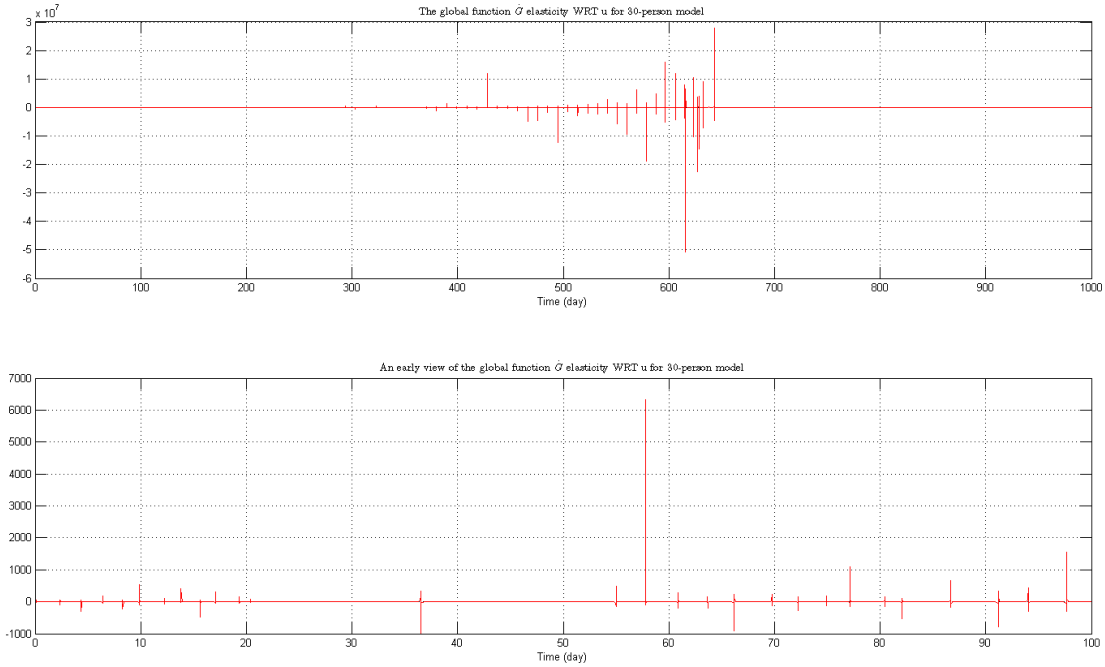

Figure 5.6: The global function elasticity with respect to u (`the death rate of the free virus`) for an individual-based viral dynamic model with 30 persons and its early view.

The global function elasticity with respect to u arrives at the peak value at the same time points as the elasticity of ω: $time = 4.37$, $time = 9.89$ and $time = 36.51$, when the value of the elasticity is -296.9, 529.1 and -993.5, while the values of the elasticities are on the order of magnitude of 10^1 or below at most of other time points during the early stage. We perturb u to increase it by 10% at these time points so that $\Delta\dot{G} < 0$. Based on Eq. 5.7, we have $\frac{\Delta\dot{G}}{\dot{G}} = -296.9 \times 0.1 = -29.69$ at $time = 4.37$, $\frac{\Delta\dot{G}}{\dot{G}} = 529.1 \times 0.1 = 52.91$ at $time = 9.89$ and $\frac{\Delta\dot{G}}{\dot{G}} = -993.5 \times 0.1 = -99.35$ at $time = 36.51$. Table 5.5, Table 5.6 and Table 5.7 provide details of the changes of $\dot{G}$ shortly after the perturbations, from which we could see that the perturbation of u at a time point of a high global function elasticity could produce a significant alteration

of $\dot{G}$ in a very short time period after the perturbation, i.e. the proportional change in a very short period after altering u produced by the perturbation at $time = 36.51$ is larger than those changes generated by the perturbation at $time = 4.37$ and $time = 9.89$.

Table 5.5: The proportional change of $\dot{G}$ with a perturbation of u at $time = 4.37$ for an individual-based viral dynamic model with 30 persons (theoretically $\Delta\dot{G}/\dot{G} \approx -29.69$).

Time (Day)	$\dot{G}$	$\dot{G}$ with Perturbation	$\frac{\Delta\dot{G}}{\dot{G}}$
4.37087	1.13633×10^{-4}	-0.0018	-16.8363
4.37287	2.06512×10^{-4}	-0.0017	-9.2320
4.37487	2.99617×10^{-4}	-0.0016	-6.3402
4.37687	3.92984×10^{-4}	-0.0015	-4.8169

The behaviour of $\dot{G}$ is changed significantly by these perturbations over a long time period. If we focus on the trajectories with perturbations in later stage of the system evolution when the system approaches an endemic equilibrium (Fig. 5.7), we find that the perturbation at $time = 9.89$ reduces the magnitude of oscillation of $\dot{G}$ greatly, while the perturbations at $time = 4.37$ and at $time = 36.51$ increase the magnitude of oscillation.

A control experiment for the perturbation of u is performed at $time = 5.43$, when

Table 5.6: The proportional change of $\dot{G}$ with a perturbation of u at $time = 9.89$ for an individual-based viral dynamic model with 30 persons (theoretically $\Delta\dot{G}/\dot{G} \approx 52.91$).

Time (Day)	$\dot{G}$	$\dot{G}$ with Perturbation	$\frac{\Delta\dot{G}}{\dot{G}}$
9.8904	-7.89544×10^{-3}	-0.425076	52.8382
9.9004	-6.39224×10^{-2}	-0.468083	6.3227
9.9104	-0.120613	-0.513025	3.2535
9.9204	-0.178024	-0.558728	2.1385

Table 5.7: The proportional change of $\dot{G}$ with a perturbation of u at $time = 36.51$ for an individual-based viral dynamic model with 30 persons (theoretically $\Delta\dot{G}/\dot{G} \approx -99.35$).

Time (Day)	$\dot{G}$	$\dot{G}$ with Perturbation	$\frac{\Delta\dot{G}}{\dot{G}}$
36.5116	5.52797×10^{-17}	-5.40869×10^{-15}	-98.8422
36.5216	2.72388×10^{-16}	-5.0248×10^{-15}	-19.4472
36.5316	4.88221×10^{-16}	-4.6619×10^{-15}	-10.5487
36.5416	7.02807×10^{-16}	-4.31748×10^{-15}	-7.1432

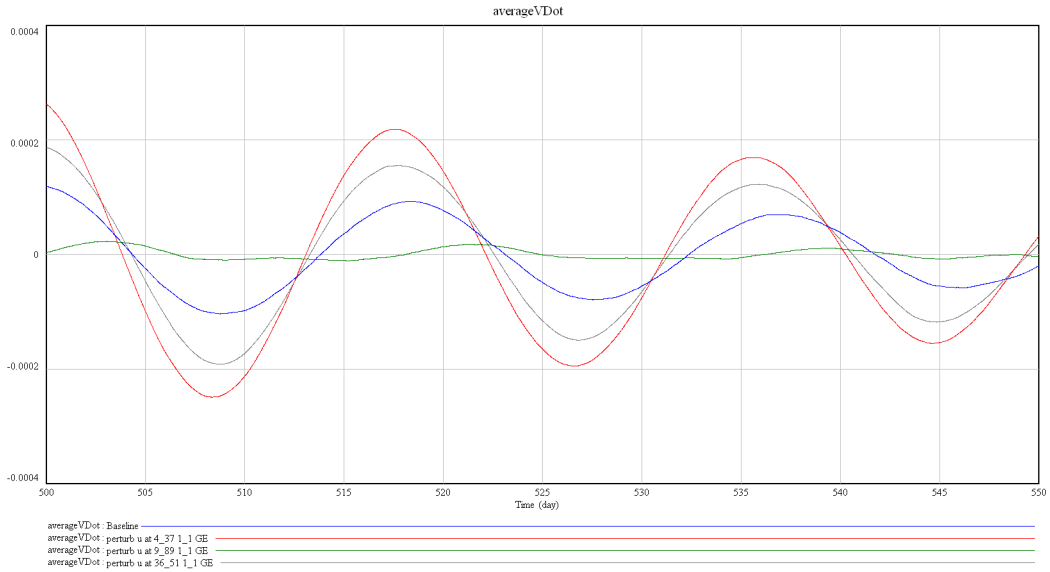

Figure 5.7: A long-term view of the value of average $\dot{v}$ in population with a perturbation of u (`the death rate of the free virus`) at $time = 4.37$, $time = 9.89$, and $time = 36.51$ respectively, when the largest $\dot{G}$ elasticities appear in the early stage for an individual-based viral dynamic model with 30 persons.

$\dot{G} = 3.00334 \times 10^{-1}$, with the value of the global function elasticity -9.089×10^{-1}. Hereby the proportional change of $\dot{G}$ approximates $\frac{\Delta\dot{G}}{\dot{G}} = -9.089 \times 10^{-1} \times 0.1 = -0.09089$. Table 5.8 shows the proportional changes of $\dot{G}$ after perturbing u at $time = 5.43$. As was predicted, immediately after the perturbation, $\frac{\Delta\dot{G}}{\dot{G}}$ is much smaller than that in the case of the perturbation at $time = 4.37$ or at $time = 9.89$.

Table 5.8: The proportional change of $\dot{G}$ with a perturbation of u at $time = 5.43$ for an individual-based viral dynamic model with 30 persons (theoretically $\Delta\dot{G}/\dot{G} \approx -0.09089$).

Time (Day)	$\dot{G}$	$\dot{G}$ with Perturbation	$\frac{\Delta\dot{G}}{\dot{G}}$
5.4398	0.31028	0.2829	−0.0882
5.4498	0.320531	0.293	−0.0859
5.4598	0.331095	0.3033	−0.0839
5.4698	0.341979	0.3138	−0.0824

However, over a long period, the perturbation in the control experiment also produces apparent changes of the behaviour of $\dot{G}$, and the changes are almost similar to the results produced by the perturbation at $time = 4.37$. In the later stage of the system evolution, shown in Fig. 5.8, the trajectory of $\dot{G}$ with perturbation at $time = 5.43$ has little difference from that at $time = 4.37$. When the state variables approaches to equilibrium, because G is associated with state variables, its changing rate $\dot{G}$ tends to be zero. In the long-term, trajectories converge and the perturbation of the parameter at any time point should result in similar behaviours of $\dot{G}$.

Fig. 5.9 describes the changes of the average virus loads with perturbations of u in the long run. Different from that with perturbations of ω, the changes of the average v is more significant around the endemic equilibrium. The perturbations of u have both local and global impacts on G and $\dot{G}$.

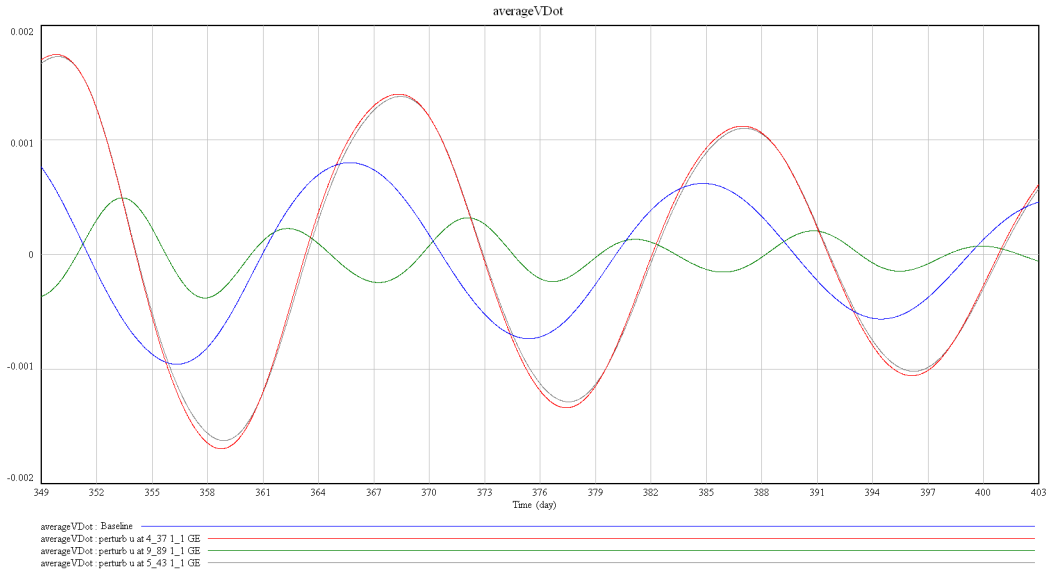

Figure 5.8: A long-term view of the comparison of the value of average $\dot{v}$ in the population with a perturbation of u (`the death rate of the free virus`) at $time = 4.37$ and $time = 9.89$ respectively, when the largest $\dot{G}$ elasticity appears in the early stage and at $time = 5.43$ when the elasticity is small for an individual-based viral dynamic model with 30 persons.

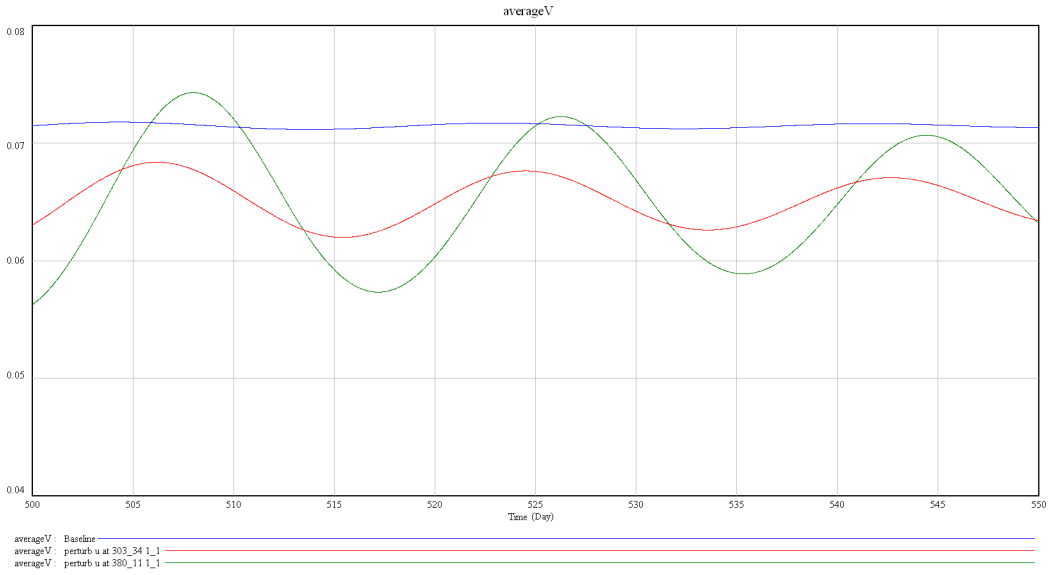

Figure 5.9: The value of average v in the population with perturbations of u (`the death rate of the free virus`) in the long run for an individual-based viral dynamic model with 30 persons.

5.1.3 Discussion

In the above two sections, a perturbation at a time point when the global function elasticity is high can result in a significant proportional change of $\dot{G}$ shortly after the perturbation. But over a long period, such high elasticity may not produce more notable proportional changes of $\dot{G}$. For the model at hand, the global function elasticity usually has large value in the late stages of the system evolution. From Eq. 3.30, we have $\dot{g}_e(p) = \frac{\partial \dot{G}}{\partial p}\frac{p}{\dot{G}}$. With a given expression of $\frac{\partial \dot{G}}{\partial p}$ and the value of p, the elasticity is large when $\dot{G}$ is small. Thus for the current model (which approaches the endemic equilibrium) the elasticity has peak values in the late stages when the global function has very small values. As we analyzed in the last chapter, changing a parameter ω or u by a small amount alters the position of the endemic equilibrium but does not alter the stability of the endemic equilibrium. Any perturbation of a parameter would produce similar trajectories of the global function in the long-term when the system is near the endemic equilibrium. Therefore, the global function elasticity analysis is only effective in a short period of time after the perturbation.

In a short period after the perturbation, the proportional changes of $\dot{G}$ follow their theoretical values, i.e., a large $\dot{G}$ elasticity could produce a significant proportional change of $\dot{G}$. Based on Eq. 5.8, we know that the absolute change of $\dot{G}$ depends on both the elasticity and the value of $\dot{G}$ with a given change of a parameter, and thus it is possible that a perturbation of a parameter at a time point when the elasticity is low can result in an apparent absolute change of $\dot{G}$ if $\dot{G}$ has a high value at that time. Therefore, because of the large values of $\dot{G}$ in the early period of time, a small change of a parameter can generate a significant alteration of the behaviour of $\dot{G}$, though the elasticities at the time points when the perturbation of the parameter is performed have small values.

A large value of the global function elasticity cannot guarantee a desired result in a relatively long time. For example, in 30-person model, we want to decrease the value of $\dot{G}$ so that the value of G (average value of viral loads across the population) is able to increase slowly or decline fast and have smaller values. As control

experiments, as Fig. 5.8 shows, the perturbation of u at $time = 5.43$, when the global function elasticity is low, also produces a desired result as perturbations at later time points. One possible reason is that for a nonlinear system its Jacobian matrix is changing over time. Great local proportional changes might become less significant because the structure of the system is changing. Another reason might be the accumulation or offset of the effects of changes of the parameter in later time points when the elasticity is high or low. Thirdly, because the trajectory is altered, the elasticity of the global function with a parameter could be changed if the value of this parameter is altered, therefore our perturbation of a parameter in a long time may neglect such changes of the elasticity. At last, because trajectories of state variables converge towards endemic equilibrium, the change rate of the global function approaches zero and any perturbation of a parameter will not change $\dot{G}$ in a long-term.

In addition, because the global function elasticity with a parameter is dimensionless, like the eigenvalue elasticity, it is helpful for indicating the significance of a parameter on the system. The $\dot{G}$ elasticity with respect to u is much larger than that to ω, and thus the small perturbations of u (10% increased) produce more significant changes of the global function that the large perturbations of ω (90% decreased).

Because the global function elasticity is defined as the ratio of proportional changes of the global function to proportional changes of parameters, as Eq. 3.30 shows, when the value of the global function is near zero, the value of the elasticity can be extremely high. We conjecture (but have not demonstrated) that this is the reason for the impulse-like values shown in Fig. 5.2 and Fig. 5.6. Although the proportional changes of the global function with perturbations of parameters at time points with those impulse-like elasticity values could be large, the absolute changes of the global function is usually very small because of its near-zero values. Practically, it is less meaningful to change the global function with tiny absolute changes at time points when its values are close to zero. There is a distinct risk of zero or near-zero values in the denominator of the eigenvalue elasticity can distract us from more practically important leverage points for changing system behaviour.

5.2 Global Function Sensitivity Analysis of an Individual-based Viral Dynamics Model with 30 Persons

In the last section, we saw that the rate of change in global function, $\dot{G}$, has great influence on the value of the global function elasticity. Motivated by that observation, in this section, we focus on the global function sensitivity with respect to a parameter. Recall from Eq. 3.29, we have

$$\dot{g}_s(p) = \lim_{\Delta p \to 0} \frac{\Delta \dot{G}}{\Delta p} \tag{5.9}$$

$$\Delta \dot{G} \approx \dot{g}_s(p) \Delta p \tag{5.10}$$

From Eq. 5.10 we know that the absolute change of $\dot{G}$ approximately equals the product of the sensitivity of $\dot{G}$ and the absolute change of the parameter p.[1] Thus we know that the global function sensitivity indicates how much the global function changes in absolute terms when the parameter changes by a given absolute change amount, as Eq. 5.10 indicates. Because a high global function sensitivity indicates a large change to $\dot{G}$ in response to a given change in a parameter *regardless of the value of* $\dot{G}$, we investigate here whether it might yield greater insight into leverage points than does the global function elasticity.

5.2.1 Global Function Sensitivity with Respect to ω

$\dot{G}$ sensitivity with respect to ω (`the connection weight`) is shown in Fig. 5.10. From this figure, we can learn that the sensitivity over time is positive and that before $time = 100$, the $\dot{G}$ sensitivity attains apparent peaks with large values, especially between $time = 0$ and $time = 50$. The first peak of the value of the elasticity appears at $time = 2.37$ with the value of 1.9239, the second peak appears around

[1] An absolute change of p here means $\Delta p = p_{\text{new}} - p$, and an absolute change of $\dot{G}$ is $\Delta \dot{G} = \dot{G}|_{p_{\text{new}}} - \dot{G}|_p$.

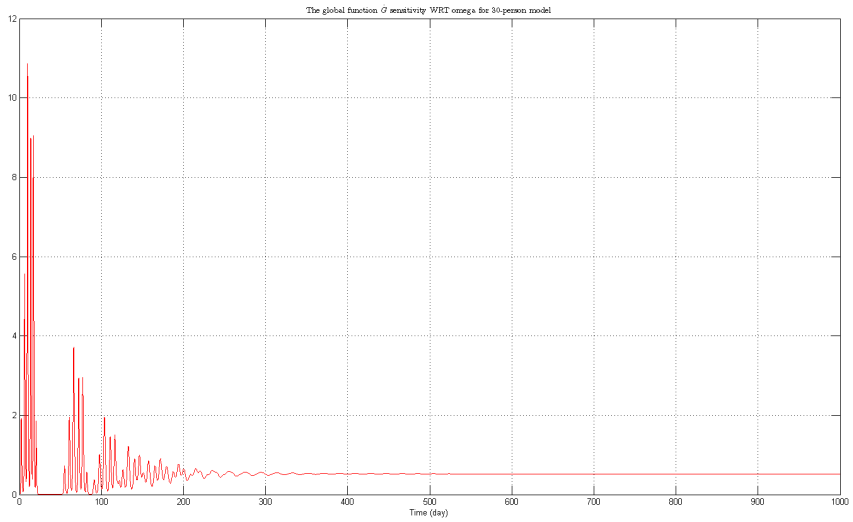

Figure 5.10: The global function sensitivity with respect to ω (`the connection weight`) for an individual-based viral dynamic model with 30 persons.

$time = 6.39$ when the value is 5.569, and the third peak is at $time = 9.87$ with the value of 10.8567.

We now test new perturbations of parameters affecting $\dot{G}$. Similar to the global function elasticity analysis, the parameter ω is changed to be 10^{-7} from the original value 10^{-6}, i.e., the absolute change of ω is -9×10^{-7}, at $time = 2.37$, $time = 6.39$, and $time = 9.87$ respectively. Based on Eq. 5.10, the absolute change of $\dot{G}$ here should be -1.7315×10^{-6}, -5.0121×10^{-6} and -9.7710×10^{-6} respectively.

Table 5.9, Table 5.10 and Table 5.11 provide the absolute change of $\dot{G}$ shortly after the perturbation, from which it can be observed that in a short period of time the absolute change of $\dot{G}$ approximates its theoretical value. The absolute change of $\dot{G}$ in the case of the perturbation at $time = 9.87$ is greater than in the case of the perturbation at $time = 2.37$ because of the higher sensitivity at $time = 9.87$. Therefore, the perturbation at a time point with a high sensitivity could produce more significant absolute changes of $\dot{G}$ in the short-term than the perturbation at time points with a low sensitivity.

Fig. 5.11 is a detailed view in the later stage of the change of the trajectory of $\dot{G}$ with perturbations. As this figure indicates, because the system is near the endemic

Table 5.9: The absolute change of $\dot{G}$ with a perturbation of ω at $time = 2.37$ for an individual-based viral dynamic model with 30 people (theoretically $\Delta\dot{G} \approx -1.7315 \times 10^{-6}$).

Time (Day)	$\dot{G}$	$\dot{G}$ with Perturbation	$\Delta\dot{G}$
2.37	4.26869×10^{-3}	4.26763×10^{-3}	-1.1×10^{-6}
2.38	-7.70133×10^{-3}	-7.70236×10^{-3}	-1.0×10^{-6}
2.39	-1.94064×10^{-2}	-1.94074×10^{-2}	-1.0×10^{-6}
2.40	-3.07938×10^{-2}	-3.07948×10^{-2}	-1.0×10^{-6}

Table 5.10: The absolute change of $\dot{G}$ with a perturbation of ω at $time = 6.39$ for an individual-based viral dynamic model with 30 people (theoretically $\Delta\dot{G} \approx -5.0121 \times 10^{-6}$).

Time (Day)	$\dot{G}$	$\dot{G}$ with Perturbation	$\Delta\dot{G}$
6.39	5.86581×10^{-2}	5.86496×10^{-2}	-8.5×10^{-6}
6.40	-1.59672×10^{-2}	-1.59755×10^{-2}	-8.3×10^{-6}
6.41	-9.00328×10^{-2}	-9.0041×10^{-2}	-8.2×10^{-6}
6.42	-1.6318×10^{-1}	-1.63188×10^{-1}	-8.0×10^{-6}

Table 5.11: The absolute change of $\dot{G}$ with a perturbation of ω at $time = 9.87$ for an individual-based viral dynamic model with 30 people (theoretically $\Delta\dot{G} \approx -9.7710 \times 10^{-6}$).

Time (Day)	$\dot{G}$	$\dot{G}$ with Perturbation	$\Delta\dot{G}$
9.87	1.02612×10^{-1}	1.02602×10^{-1}	-1×10^{-5}
9.88	4.75688×10^{-2}	4.75594×10^{-2}	-9.4×10^{-6}
9.89	-7.89544×10^{-3}	-7.90453×10^{-3}	-9.1×10^{-6}
9.90	-6.39224×10^{-2}	-6.3931×10^{-2}	-8.6×10^{-6}

equilibrium, at a later time after changing ω, the perturbation at $time = 2.37$ results in similar changes as that at other time points, despite the fact that the value of sensitivity then is not so large. The only difference is that it delays the oscillation a bit and slightly decreases the magnitude.

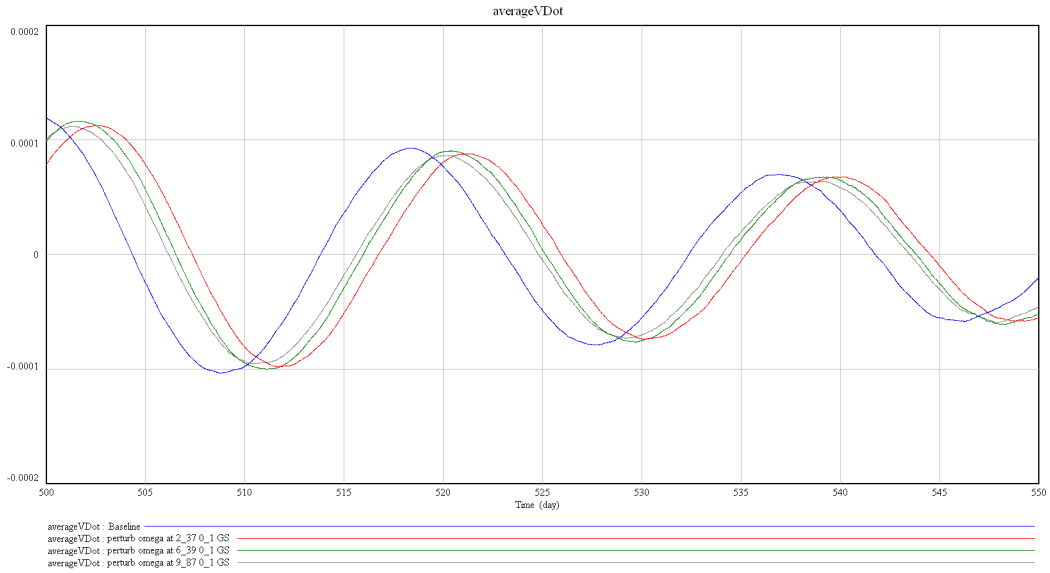

Figure 5.11: A long-term view of the value of average $\dot{v}$ in population in the long run with a perturbation of ω (`the connection weight`) at $time = 2.37$, $time = 6.39$, and $time = 9.87$ respectively, when the largest $\dot{G}$ sensitivities Appear for an individual-based viral dynamic model with 30 persons.

5.2.2 Global Function Sensitivity with Respect to u

Fig. 5.12 shows the $\dot{G}$ sensitivity with respect to u (`the death rate of the free virus`) over time for a 30-person model. In this figure, the value of the sensitivity is negative over time, and it is quite large in the early stage of the system evolution. The first peak of the value of the sensitivity appears at $time = 2.37$, with the value of -0.1489, the second peak appears at $time = 6.41$ which is -0.9593, and the third peak is at $time = 9.89$ with the value of -1.3925. We change u by 10% of the original value, i.e. increasing u by 0.3 absolutely, at these three time points to try to change the behaviour of the global function. According to Eq. 5.10, the theoretical absolute change of $\dot{G}$ should be -0.0447, -0.2878 and -0.4178, respectively.

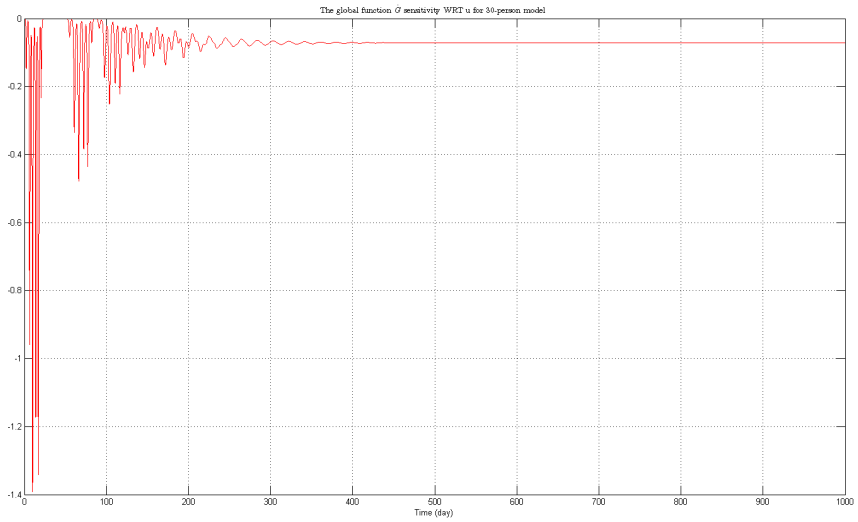

Figure 5.12: The global function sensitivity with respect to u (`the death rate of the free virus`) for an individual-based viral dynamic model with 30 persons.

Table 5.12, Table 5.13 and Table 5.14 list the absolute changes of $\dot{G}$ in a small window frame after the perturbations. During this period of time the values of $\Delta\dot{G}$ are close to the product of the global function sensitivity and the absolute change of u. The absolute changes of $\dot{G}$ with a perturbation at $time = 9.89$ are larger than the changes with a perturbation at $time = 6.41$, which are greater than the absolute changes with a perturbation at $time = 2.37$, because $\dot{g}_s(u)|_{time=9.89} > \dot{g}_s(u)|_{time=2.37}$. Therefore, locally $\dot{G}$ is mostly decreased with the perturbation of u at time point when the sensitivity is high.

Table 5.12: The absolute change of $\dot{G}$ with a perturbation of u at $time = 2.37$ for an individual-based viral dynamic model with 30 persons (theoretically $\Delta\dot{G} \approx -0.0447$).

Time (Day)	$\dot{G}$	$\dot{G}$ with Perturbation	$\Delta\dot{G}$
2.37	4.26869×10^{-3}	-4.01179×10^{-2}	-0.0443866
2.38	-7.70133×10^{-3}	-5.07052×10^{-2}	-0.0430039
2.39	-1.94064×10^{-2}	-6.11484×10^{-2}	-0.041742
2.40	-3.07938×10^{-2}	-7.13722×10^{-2}	-0.040578

Table 5.13: The absolute change of $\dot{G}$ with a perturbation of u at $time = 6.41$ for an individual-based viral dynamic model with 30 persons (theoretically $\Delta\dot{G} \approx -0.2878$).

Time (Day)	$\dot{G}$	$\dot{G}$ with Perturbation	$\Delta\dot{G}$
6.419	-9.00328×10^{-2}	-3.69063×10^{-1}	-0.27903
6.429	-1.6318×10^{-1}	-4.33865×10^{-1}	-0.27069
6.439	-2.35054×10^{-1}	-4.98038×10^{-1}	-0.26298
6.449	-3.05311×10^{-1}	-5.61106×10^{-1}	-0.25579

Table 5.14: The absolute change of $\dot{G}$ with a perturbation of u at $time = 9.89$ for an individual-based viral dynamic model with 30 persons (theoretically $\Delta\dot{G} \approx -0.4178$).

Time (Day)	$\dot{G}$	$\dot{G}$ with Perturbation	$\Delta\dot{G}$
9.89	-7.89544×10^{-3}	-4.25067×10^{-1}	-0.4172
9.90	-6.39224×10^{-2}	-4.68083×10^{-1}	-0.4042
9.91	-1.20613×10^{-1}	-5.13025×10^{-1}	-0.39241
9.92	-1.78024×10^{-1}	-5.59728×10^{-1}	-0.3817

Fig. 5.13 describes the changes of the behaviour of $\dot{G}$ in the later stage with the perturbation of u. All of these perturbations produces significant alterations of the behaviour of $\dot{G}$. The perturbation at $time = 9.89$ results in a decrease of the magnitude of the oscillation of $\dot{G}$, whereas the magnitude is enlarged by the perturbations at other time points. Therefore, it is difficult to describe the significance of the perturbation at those three time points in a long period of system evolution. In terms of the endemic equilibrium, as analyzed in Section 5.1, the perturbations of u change the position of the endemic equilibrium, and thereby change the value of G at the endemic equilibrium. But the value of $\dot{G}$ at the endemic equilibrium, where $\dot{G} = 0$, is not influenced by the perturbations of u.

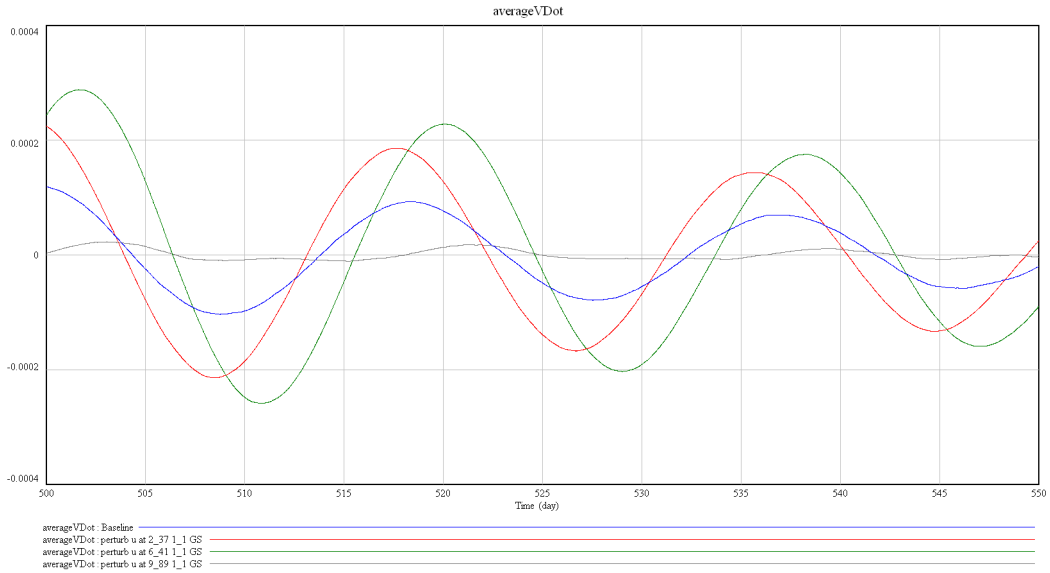

Figure 5.13: A long-term view of the value of average $\dot{v}$ in population in later stage with a perturbation of u (`the death rate of the free virus`) at $time = 2.37$, $time = 6.41$, and $time = 9.89$ respectively, when the largest $\dot{G}$ sensitivities appear for an individual-based viral dynamics model with 30 persons.

5.2.3 Discussion

The above two sections suggest that global function sensitivities are effective for indicating the ideal time for policy makers to perform the control over disease spread in a short period of time. Because the global function sensitivities are not effected by the influence of changes of the global function values, this method could indicate the early time points when the $\dot{G}$ is sensitive to parameters. The perturbation of the parameter at time point when the sensitivity is large can locally change the trajectory of the global function as the global function sensitivity indicates, but the large sensitivity is neither necessary nor a sufficient condition of significant changes of the global function in a long period of time. However, from the above sections, we can find that the early control of parameters at time points when the global function sensitivities are large can alter the behaviour of the global function. Practically, it suggests that policies performed in the early stage when the system is far from equilibrium have great influences on the system behaviours. On the disadvantage side, because the global function sensitivity is not dimensionless, we cannot use it to

compare the relative importance of parameters for the system, if those parameters have different dimensions.

5.3 Global Function Elasticity Analysis of an Aggregate Infectious Disease Model

Although the SIRS model is an aggregate model and its state variables to some degree describe global states of the system, we could also define a global function to describe the overall behaviour of the system with a measurement. For example, in Section 4.1 we define *Prevalence* to be the infected fraction of the entire population. Because some infectious diseases are already established, and because after an outbreak it is possible that an infectious disease may evade elimination in a relatively short period of time, we could consider it as the target of disease control to decrease the endemic prevalence. Therefore, in this section, we use the changing rate of *Prevalence*, $\dot{Prev}$, as the global function $\dot{G}$ for an SIRS model described by Eq. 4.1.

For the model of Eq. 4.1, there are no explicit symbolic solutions. Thus we cannot use Eq. 3.31 to derive symbolic expressions for $\dot{Prev}$ and the global function elasticity with a parameter, and we compute it numerically instead. Specifically, we increase each parameter by 1% over time to approximate the global function elasticity defined in Eq. 3.28:

$$\dot{g}_e \approx \frac{\frac{\Delta \dot{G}}{\dot{G}}}{\frac{\Delta p}{p}} \tag{5.11}$$

We computed the global function elasticity with β (`Per Infected Contact Infection Rate`) and μ (`Mortality Rate`) in the SIRS model based on Eq. 5.11, and plotted them in Fig. 5.14.

The global function elasticities with respect to β have a positive peak value 0.11 at $time = 79$, which is larger than absolute peak values of the global function elasticity with respect to μ. At $time = 73$, the elasticity with respect to μ arrives at the negative values -0.022. We choose β and μ to perturb by 10%, based on their

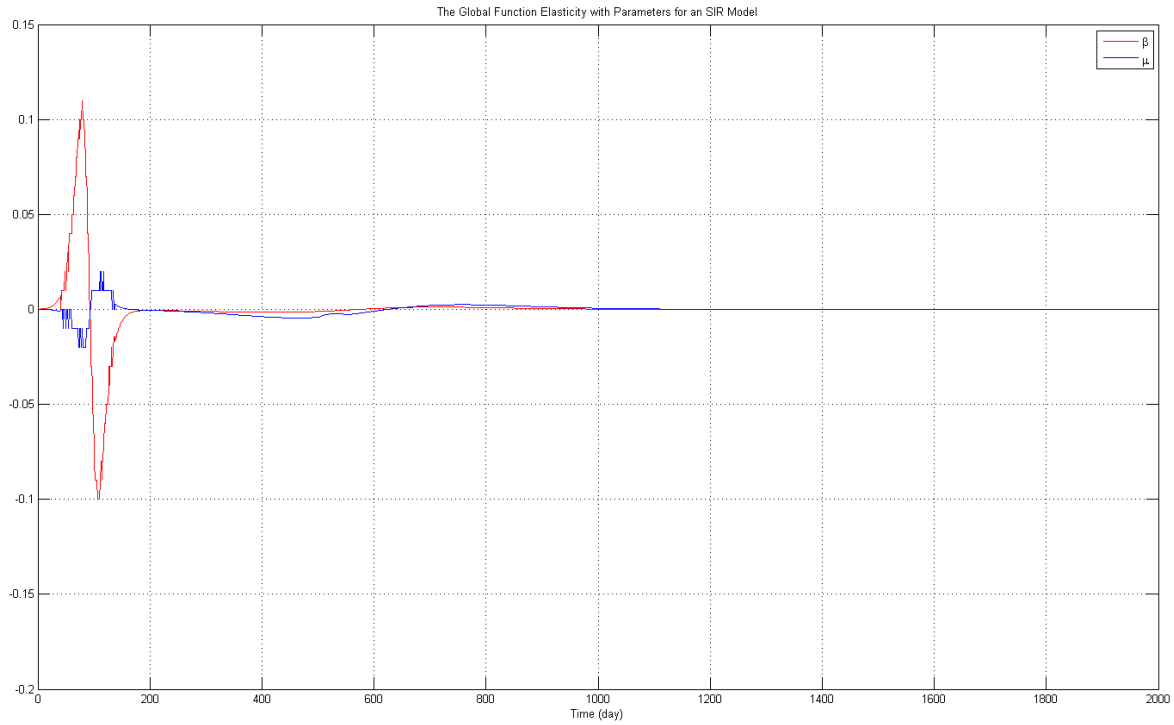

Figure 5.14: The global function elasticity with respect to β and μ in an SIRS model.

elasticities. According to the stability analysis of the SIRS model in Section 4.1, such small perturbations will not change the stability of the endemic equilibrium of the SIRS model. We decrease the value of β by 10% at $time = 79$ because of the positive value of the elasticity and $\dot{Prev}$. We add a control experiment at $time = 53$ when the elasticity is 0.02 to compare the results of perturbed trajectories of the global function.

Fig. 5.15 and Fig. 5.16 plot these altered trajectories of $\dot{Prev}$ and *Prevalence*. Immediately after the perturbation, $\dot{Prev}$ is instantaneously changed and the decrement of $\dot{Prev}$ with the perturbation of β at $time = 79$ is more significant than that at $time = 53$. In aspect of *Prevalence*, the perturbation at $time = 79$ brings a bit more decrement than the perturbation at $time = 53$ in a short period of time. However, after $time = 150$ the difference between two scenarios is little; after $time = 500$ these two trajectories of *Prevalence* and the original trajectory overlap.

We increase the value of μ to be 110% of the default value 0.02 at $time = 73$. Similarly, we add two control experiments at $time = 37$ when the elasticities are

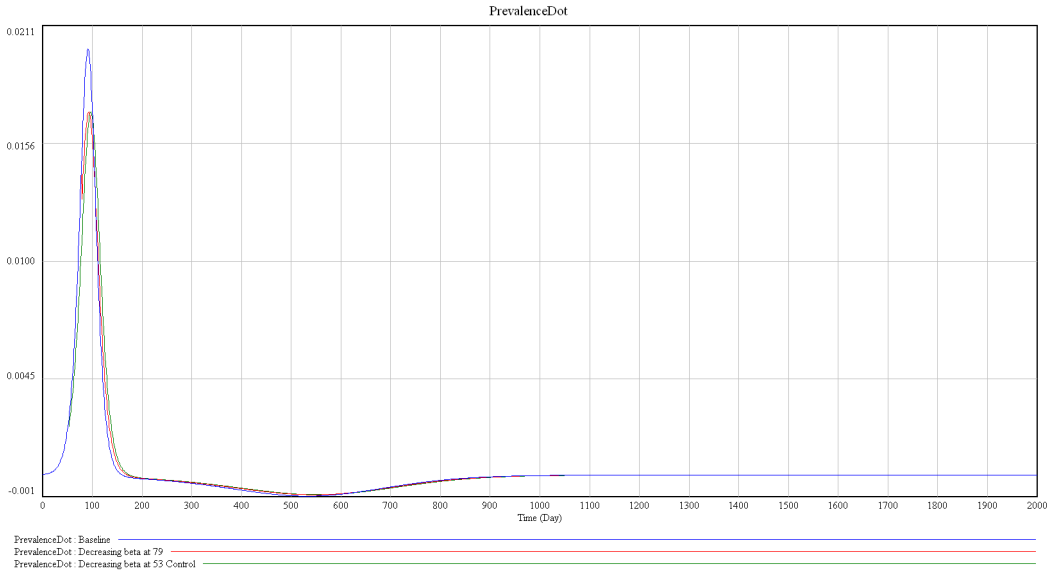

(a) Changes of $\dot{Prev}$ with perturbations in the long-term

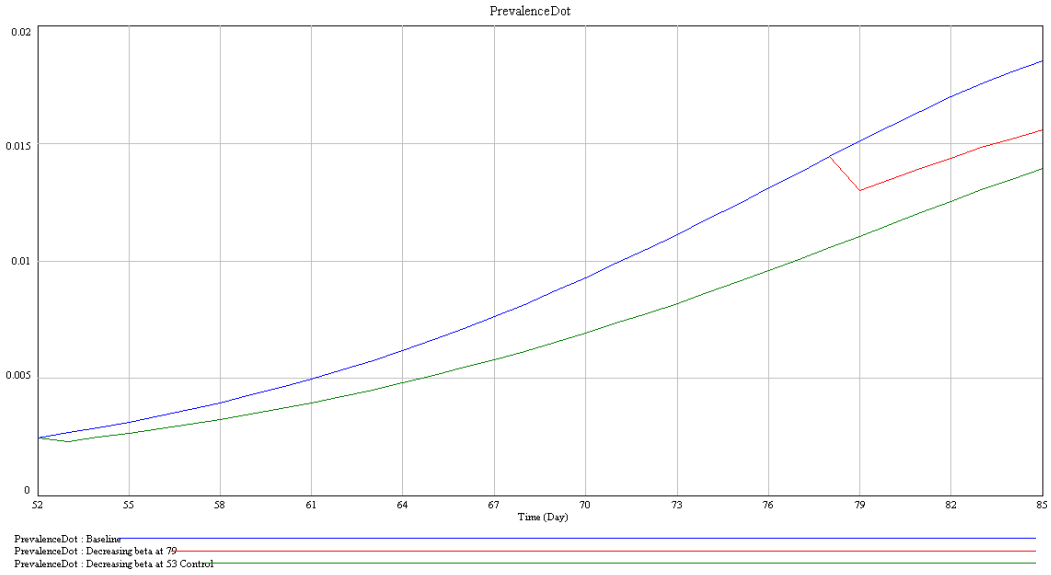

(b) Changes of $\dot{Prev}$ shortly after perturbations

Figure 5.15: Two views of the value of $\dot{Prev}$ over time for an SIRS model with a perturbation of β at $time = 79$ when the largest global function elasticity appears and at $time = 53$ when the global function elasticity is small and its early view.

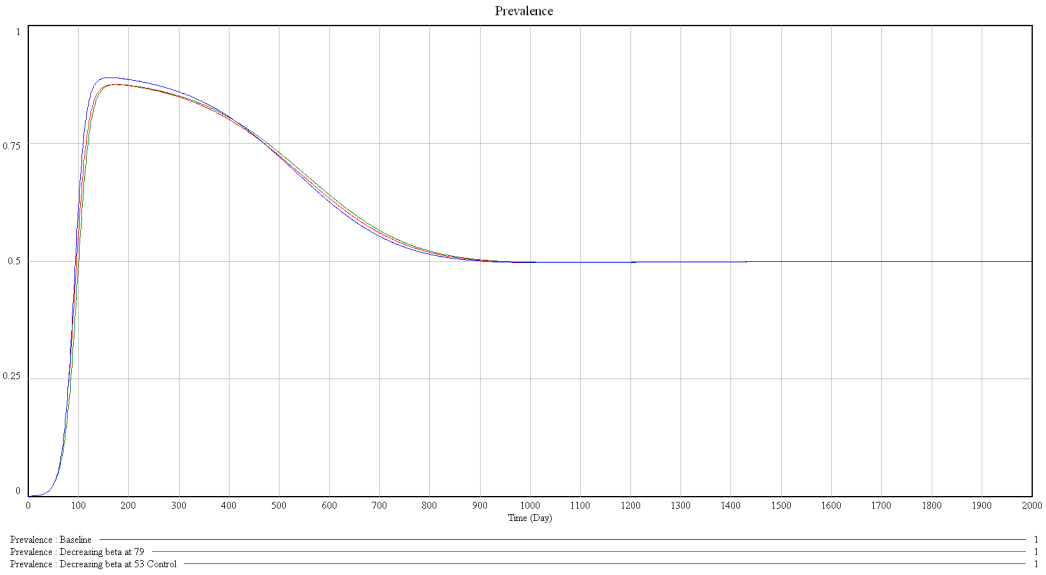

Figure 5.16: The value of *Prevalence* over time for an SIRS model with a perturbation of β at $time = 79$ when the largest global function elasticity appears and at $time = 53$ when the global function elasticity is small.

-0.00087. Fig. 5.17 shows the behaviours of $\dot{Prev}$ with perturbations at different time points. $\dot{Prev}$ is altered immediately after the perturbation. Shortly after the perturbation, $\dot{Prev}$ decreases more greatly when μ is perturbed at $time = 73$ than when perturbing it at $time = 37$ because of the high absolute value of elasticity at this time point. Compared with the perturbations of β, the local changes of $\dot{Prev}$ with a perturbation of μ at $time = 73$ because of the relatively lower value of the elasticity. However, in the long run, the perturbation of μ at any of these two time points leads $\dot{Prev}$ to approach zero.

From Fig. 5.18, we could learn that the value of *Prevalence* is decreased significantly in the later stages, though changing μ does not produce great decline of it shortly after the perturbation. In fact, the global function *Prevalence* here is the variable i in Eq. 4.6, the fractional variable of I. As we mentioned in Section 4.1.5, the fixed point of the global function *Prevalence* is equivalent to

$$\hat{i} = \frac{\sigma}{\mu}$$

The position of i at the endemic equilibrium is related with μ but has no relation with β. Thus, the perturbation of β at any time point will not change the stable

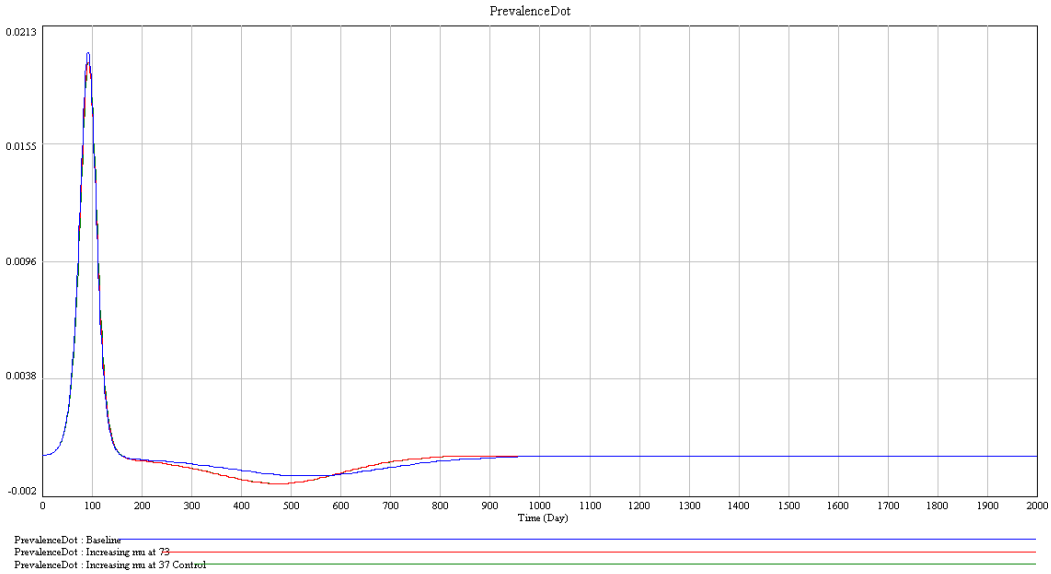

(a) Changes of $\dot{Prev}$ with perturbations in the long-term

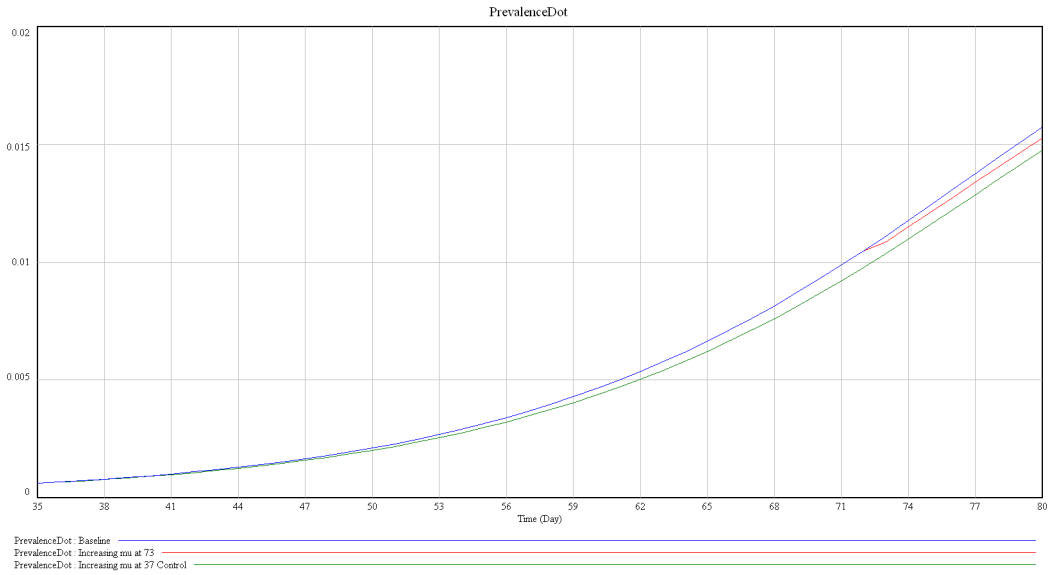

(b) Changes of $\dot{Prev}$ shortly after perturbations

Figure 5.17: Two views of the value of $\dot{Prev}$ over time for an SIRS model with a perturbation of μ at $time = 73$ when the largest global function elasticity appears and at $time = 37$ when the global function elasticity is small.

value of *Prevalence*, i.e., although *Prevalence* could be decreased temporarily in a short period of time after the perturbation, it will not be altered in the long run. In contrast, the increase of μ will change the position of i at the endemic equilibrium, which means the perturbation of μ at any time will permanently change the value of the global function *Prevalence*. Fig. 5.18 also suggest that although the perturbation of μ at other time points after $time = 73$, when the elasticity has the largest absolute value, could also lower the values of the global function, such a perturbation will delay the time for the global function to arrive at the changed stable value. Therefore, it suggests that in terms of decreasing disease prevalence, changing μ before the time point when its global function elasticity arrives at the largest absolute value could yield more rapid changes than after that time point. Practically, we cannot suggest policy makers to increase the mortality rate of infected individuals, however, based on our analysis the quarantine of infected patients in time may be meaningful to decrease the prevalence.

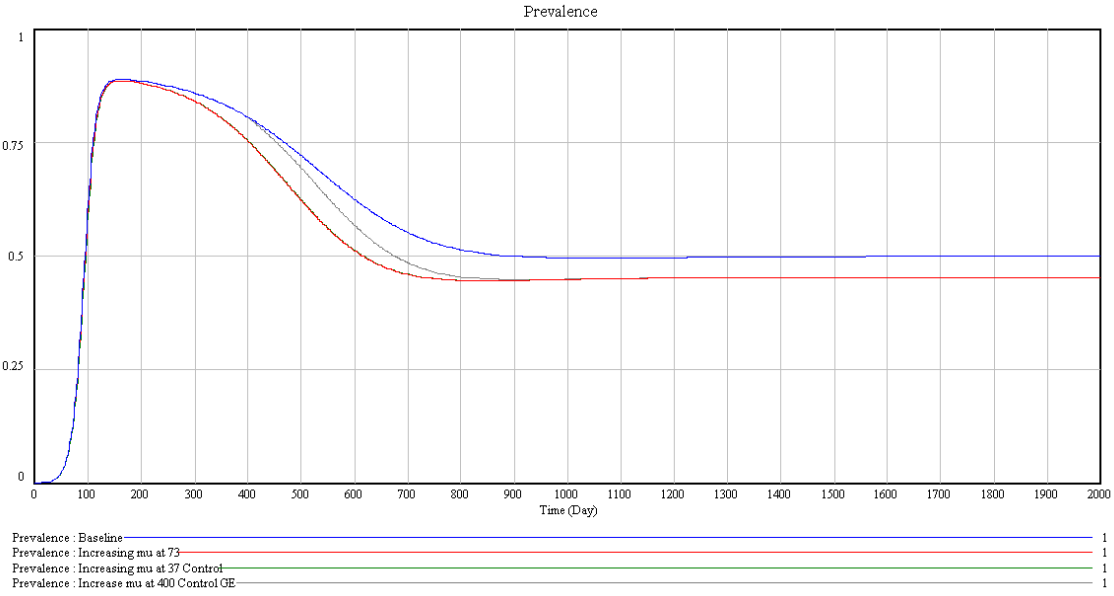

Figure 5.18: The value of *Prevalence* over time for an SIRS model with a perturbation of μ at $time = 73$ when the largest global function elasticity appears at $time = 37$ and at $time = 400$ when the global function elasticities are small.

5.4 Summary

Global function elasticity analysis for the SIRS model is clearer than that for the individual-based model. Although the SIRS model is nonlinear, it is much less complex than the individual-based model. The effectiveness of the global function elasticity method on the SIRS model might be attributed to 1) fewer state variables, 2) a less nonlinear model compared with the individual-based model, and 3) the selection of the global function. However, for a system of high nonlinearity, such as the individual-based model in this chapter, linearization of the system is local and the eigenvalues of the Jacobian matrix only present the behaviour modes of the system around the time point when the linearization is performed. Although such changes may produce significant alterations at the time points when the global function is highly sensitive to the parameter, the changes of a parameter may not alter the global structure of the system and the trajectory of the global function in a long-term (i.e., the individual-based model in our analysis), because these local attributes of a nonlinear system are changing for long period of time, and probably because 1) when we perturb a parameter based on the original value of the global function, the trajectory changes of the global function might have different global function elasticity or sensitivity from the baseline global function at the same time; 2) because of the experimental designing, the effect of the perturbation of a parameter may be accumulated or offset at later time points when the elasticities or sensitivities are high, which could diverge original proportional or absolute changes of the global function; 3) such changes of a parameter can make the trajectory shift in the state space, but these shifted trajectories might evolve to the same equilibrium and in the later stages of the system evolution, because of this convergence it is possible that the trajectory of the global function with a perturbation of a parameter at a time point when the elasticity or sensitivity is small will closely approach a trajectory with a perturbation at a time point with high elasticity or sensitivity. As a result, of all these factors, even for a simple system, local analysis is sometimes ineffective in anticipating the impacts of a change on the global behaviour of the nonlinear system.

Chapter 6

Conclusion

In this thesis, we studied two types of mathematical models of infectious disease spread, an aggregate SIR model and individual-based viral dynamic models. We applied local analysis tools, such as eigenvalue and eigenvalue elasticity analysis and developed global function elasticity and sensitivity analysis, to these two types of models to study the dynamics of the spread of diseases and the short-term influences of parameters in a short period of time, especially during a disease outbreak. Global analysis tools, like fixed points and stability analysis, are used in these two types of models to study the long-term impacts of parameters and their changes on the system evolution.

For the aggregate infectious disease model, an elaborate SIR model in our study, we developed symbolic expressions of its three equilibria in terms of parameters. We found that because of growing population size, its disease-free equilibrium is unstable when the basic reproductive ratio R_0 is less than one, that contradicts a strong requirement for stability. But when we studied the fractional model, the disease-free equilibrium becomes asymptotically stable if $R_0 < 1$. Dominant eigenvalues of the Jacobian matrix are able to describe the major behaviour modes in a short period of time, but the eigenvectors are also of the important factors to determine the behaviour patterns of state variables. The perturbations of a parameter based on the eigenvalue elasticity could bring local changes of some state variables, but eigenvectors, as well as coefficients, jointly determine which variables could be affected by the perturbations of the parameter. By applying the Routh-Hurwitz Criterion, we know that a small parameter change will not alter the stability of the endemic equilibrium for the aggregate model, when the values of other parameters are fixed.

For an individual-based viral dynamic model, both local eigenvalue analysis and its elasticity methods and global fixed points analysis are also viable. We figured out the symbolic expressions of the equilibria for models with small population size and analyzed their stability. However, for a model with large population size, the derivation of general symbolic expressions of the equilibria is difficult because 1) the number of the equilibria grows geometrically with the population size, and 2) the various network structures make the structure of the defense-free and the endemic equilibria much complicated. We found that the stability of the endemic equilibrium for a given population size can be determined by two extreme cases: the network with no connection and with full connections. The case of no connection is the least stable because medical treatments could change the states of an individual in the model in isolation; by contrast, in the full connections case, because of connections to other infected individuals, the effects of changing states by medical treatment could be offset by newly transmitted virions and the endemic equilibrium is relatively more stable. In addition, the strength of the connection weight also effects the stability. If individuals are connected more strongly, the endemic equilibrium is more stable, and vice versa. Therefore, for a model with a fixed population size, we could learn the stability of its endemic equilibrium by studying that of the model with no connections. Also following the Routh-Hurwitz Criterion, we derived a range of values of a parameter, within which the changes of this parameter will not change the stability of the endemic equilibrium, providing that the other parameters are held constant.

However, for an individual-based viral dynamic model with relatively large population size, eigenvalue analysis is less effective than for the aggregate model, and perturbations of a parameter based on high eigenvalue elasticities could not reliably change state behaviours locally. The first reason for the challenge is the large number of eigenvalues and eigenvalue multiplicity. Similar mathematical equations and parameter values for each individual make some of the eigenvalues of the Jacobian matrix identical. Because the system behaviour is determined by the superposition of eigenvalues, and because there might be more than one dominant eigenvalue that

jointly control the evolution of the system; it is in general difficult to determine the number of dominant eigenvalues. Secondly, the eigenvalue with high elasticity may have a small value of coefficient which indicates that the corresponding eigenvector is not the major direction of the system evolution or may not be a dominant eigenvalue. The perturbation of a parameter based on this elasticity thus might not alter the system behaviour significantly. Because of the large number of eigenvalues, coefficients and eigenvalue elasticities, it is difficult to understand even the short-term behaviour of a large system using the analysis of eigenvalue and their elasticities. Thirdly, the perturbation of a parameter based on the eigenvalue elasticity does not directly work on the state variables, but on the eigenvalues. Although the changes of state variables are little shortly after the perturbation, persistent changes exert their influences in a relatively long run. In terms of the disease control, especially during the outbreak of the disease, such long time effects are not as we expected. Accordingly, we used the global function elasticity to look for parameters and time points to perturb in order to change the global behaviour of the system.

Inspired by traditional eigenspace analysis for nonlinear systems, we developed global function analysis to discover the influences of the parameters on the global functions associated directly with state variables for infectious disease models. By applying this new method to both the aggregate and the individual-based models of infectious disease spread, we found that in a short period of time after the perturbation at a time point when the elasticity or the sensitivity is high, the changes of the global function are notable. Practically, this method is effective to inform the control of disease spread in a short time, such as in the period of the disease outbreak. Globally, such perturbations cannot reliably determine the changes of the $\dot{G}$ in a long period of time. This reflects the fact that for a nonlinear system, because local attributes, such as eigenvalues and eigenvectors of Jacobian matrix, vary over time, we are unable to determine global attributes of the system behaviours for long period of time. Around the endemic equilibrium, the behaviour of the global function is only determined by parameters related with the endemic equilibrium.

Because eigenvalue elasticity and the global function elasticity are dimensionless,

these methods make it possible for us to compare the importance of parameters for a model, that is capable to help policy makers to find out crucial factors for disease control in a short period of time, especially during the outbreak of an infectious disease. However, the duration of such importance may not be in a long time. An important parameter during the outbreak of a disease could have no influence or unfavorable influence on the equilibria, e.g., the perturbation of a parameter at the time point with high elasticity can lead the prevalence of disease or the virus loads decrease significantly in a short period of time, but in the long time such changes may not change or even slightly increase the prevalence or the virus loads when the system evolves to the endemic equilibrium.

Therefore, we could say that for infectious disease models, where the attention is on immediate disease control during a short time period around a disease outbreak, local analysis methods (eigenvalues, eigenvalue elasticity, and global function elasticity and sensitivity) can be effective to indicate the behaviour patterns, the importance of parameters, and the time to change parameters, so that policy makers are able to decrease the prevalence or the severity of the disease in some degree. But in the long run, these methods are not effective to predict the behaviour changes, and the analysis of fixed points, as well as other methods could help us to better anticipate the long-term behaviour patterns and parameter sensitivities.

The future work related with this study relates to three aspects. Firstly, more complicated individual-based models deserve further study with the eigenvalue method, such as the multiplicity of the eigenvalues and the independence of their corresponding eigenvectors. Secondly, we could also apply eigenvalue elasticity and network analysis methods to study the link between individuals to dynamically look for the important individuals and subgroups. This would be motivated by the fact that for a large population individual-based model, we are unable to change parameters for all persons, and the important individuals and the significant sub-structure in the whole society are valuable for policy makers to highlight particular groups of people to which more attentions should be paid. Thirdly, a stricter mathematical proof of the stability of the models at the endemic equilibrium is necessary for further

research, especially for the individual-based models. Lastly, an effective method to describe the local and global characteristics of infectious disease models deserves to be developed. We make a balance between local eigenvalue and global function analysis and the long-term fixed points analysis, but we are also interested in investigating other methods (such as those from control theory) that could be effective to indicate the parameter sensitivities both locally and globally.

References

[1] R. M. Anderson and R. M. May. *Infectious Diseases of Humans: Dynamics and Control*. Oxford University Press, 1991.

[2] P. Bearman, J. Moody, and K. Stovel. Chains of affection: The structure of adolescent romantic and sexual networks. *American Journal of Sociology*, 110(1), 2004.

[3] S. Busenberg and P. van den Driessche. Analysis of a Disease Transmission Model in a Population with Varying Size. *Journal of Mathematical Biology*, 28:257–270, 1990.

[4] G. Demirel. Aggregated and Disaggregated Modeling Approaches to Multiple Agent Dynamics. In *Proceedings of the 25th International Conference of the System Dynamics Society*, Boston, MA, 2007.

[5] O. Diekmann, J. A. P. Heesterbeek, and J. A. J. Metz. On the Definition and the Computation of the Basic Reproduction Ratio R_0 in Models for Infectious Disease in Heterogeneous Population. *Journal of Mathematical Biololgy*, 28(365), 1990.

[6] C. H. Edwards and D. E. Penney. *Differential Equations and Boundary Value Problems: Computing and Modeling*. Pearson Education, 3rd edition, 2004.

[7] N. Forrester. *A Dynamic Synthesis of Basic Macroeconomic Theory: Implacations for Stabilization and Policy Analysis*. PhD thesis, MIT, Cambridge, MA, 1982.

[8] F. R. Gantmacher. *The Theory of Matrix*, volume II. Chelsea Publishers, 1959.

[9] J. W. Glasser, S. O. Foster, J. D. Millar, and J. M. Lane. Evaluating Public Health Responses to Reintroduced Smallpox via Dynamic, Socially Structured, and Spatially Distributed Metapopulation Models. *Clinical Infectious Disease*, 46:S182–194, 2008.

[10] B. Guneralp. Progress in Eigenvalue Elasticity Analysis as a Coherent Loop Dominance Analysis Tool. In *Proc. The 23rd International Conference of the System Dynamics Society*, Boston, MA, July 2005.

[11] B. Guneralp. *Exploring Structure-Behavior Relations in Nonlinear Dynamic Feedback Models*. PhD thesis, University of Illinois at Urbana-Champaign, 2006.

[12] M. S. D. in Education Project (SDEP). System Dynamics. http://sysdyn.clexchange.org/.

[13] D. Kaplan and L. Glass. *Understanding Nonlinear Dynamics*. Springer-Verlag New York, 1995.

[14] W. O. Kermack and A. G. McKendrick. A Contribution to the Mathematical Theory of Epidemics. In *Proceedings of The Royal Society of London*, volume 115 of *A*, pages 700–721, 1927.

[15] J. Koopman. Modeling Infection Transmission. *Annual Review of Public Health*, 25:303–326, 2004.

[16] G. A. Korn and T. M. Korn. *Mathematical Handbook for Scientists and Engineers: Definitions, Theorems, and Formulas for Reference and Review*. Dover Publications, 2nd revised edition, 2000.

[17] A. Korobeinikov and P. K. Maini. Non-linear Incidence and Stability of Infectious Disease Models. *Mathematical Medicine and Biology*, 22:113–128, 2005.

[18] T. Kostova. Persistence of Viral Infections on the Population Level Explained by an Immunoepidemiological Model. *Mathematical Biosciences*, 206:309–319, 2007.

[19] J. M. Last. *A Dictionary of Epidemiology*. Oxford University Press, 4th edition, 2001.

[20] L. A. Meyers, B. Pourbohloul, M. E. J. Newman, D. M. Skowronski, and R. C. Brunham. Network Theory and SARS: Predicting outbreak diversity. *Journal of Theoretical Biology*, 232:71–81, 2005.

[21] S. M. Moghadas and A. B. Gumel. Stability of a Two-stage Epidemic Model with Generalized Non-linear Incidence. *Mathematics and Computers in Simulation*, 60:107–118, 2002.

[22] M. A. Nowak and R. M. May. *Virus Dynamics: Mathematical Principles of Immunology and Virology*. Oxford University Press, 2000.

[23] N. Osgood. Individual-Based Models: Advantages and Tradeoffs. Technical report, Department of Computer Science, University of Saskatchewan, 2008.

[24] N. Osgood. The Impact of Healthcare Delays on Infectious Disease Spread: A Simple Model. Presentation for the Saskatoon Chapter of the Canadian Operational Research Society, April 2008.

[25] B. Porter and R. Crossley. *Modal Control: Theory and Application*. Taylor and Francis, London, UK, 1972.

[26] D. Powell, J. Fiar, R. L. L. Moore, and D. Thompson. Sensitivity Analysis of an Infectious Disease Model. In *Proceedings of the 23rd International Conference of the System Dynamics Society*, Boston, MA, July 2005.

[27] R. C. Robinson. *An Introduction to Dynamical Systems: Continuous and Discrete*. Prentice Hall, 2004.

[28] M. Saleh. *The Characterization of Model Behavior and its Causal Foundation*. PhD thesis, University of Bergen, Bergen, Norway, 2002.

[29] M. Saleh, P. Davidsen, and K. Bayoumi. A Comprehensive Eigenvalue Analysis of System Dynamics Models. In *Proc. The 23rd International Conference of the System Dynamics Society*, Boston, MA, July 2005.

[30] L. F. Shampine, I. Gladwell, and S. Thompson. *Solving ODEs with MATLAB*, chapter 2, page 65. Cambridge University Press, 2003.

[31] J. D. Sterman. *Business Dynamics: Systems thinking and modeling for a complex world*. McGraw Hill, 2000.

[32] P. van den Driessche and J. Watmough. Reproduction Numbers and Subthreshold Endemic Equilibria for Compartmental Models of Disease Transmission. *Mathematical Biosciences*, 180:29–48, 2002.

[33] D. Vickers and N. Osgood. A Unified Framework of Immunological and Epidemiological Dynamics for the Spread of Viral Infections in a Simple Network-based Population. *Theoretical Biology and Medical Modelling*, 4(49), 2007.

[34] E. W. Weisstein. SIR Model. MathWorld-A Wolfram Web Resource http://mathworld.wolfram.com/SIRModel.html.

[35] M. Wooldridge. *An Introduction to Multiagent Systems*. John Wiley and Sons Ltd., 2002.

Appendix A

Flowchart of Analysis Implementation

To analyze eigenvalue elasticities and global function elasticities, Vensim® is used to simulate a system and to get all values of state variables over time. Matlab® codes are run to calculate eigenvalue elasticities and global function elasticities where symbolic expressions of them are generated from Maple®. The flowchart is shown as Fig. A.1.

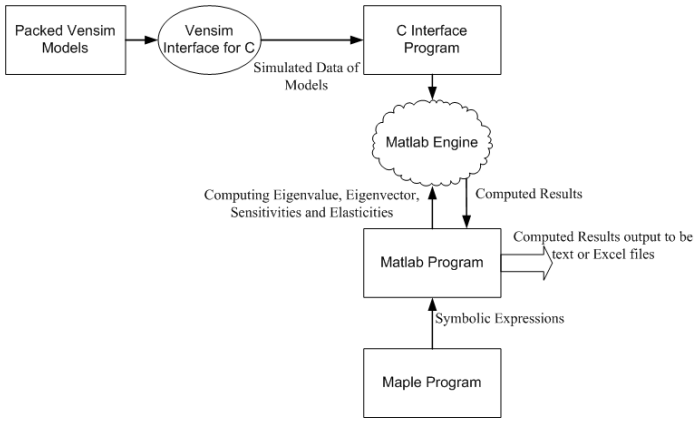

Figure A.1: The flowchart of implementing analysis programs.

Appendix B

Eigenvectors of an Individual-based Viral Dynamic Model with 4 Persons

The row vectors of the matrix below are eigenvectors of the Jacobian matrix at $time = 0.5$ for the individual-based viral dynamics model with four people in Section Section 4.2.3.3, where `Person 3` and `Person 4` are identical.

$$
\begin{bmatrix}
0.000000093964 & -0.0000010974 & 0.000044936 & 0.000000077934 & -0.020881 & 0.046578 & -0.99856 & -0.016538 & -4.2284 \times 10^{-11} & 4.9385 \times 10^{-11} & -0.0000000020221 & -3.5068 \times 10^{-12} & -4.2284 \times 10^{-11} & 4.9385 \times 10^{-11} & -0.0000000020221 & -3.5068 \times 10^{-12} \\
-0.018522 & 0.022400 & -0.73577 & -0.0019130 & -0.000000041605 & 0.00000123390 & -0.000016527 & -0.000000052903 & 0.012035 & -0.014554 & 0.47806 & 0.0012429 & 0.012035 & -0.014554 & 0.47806 & 0.0012429 \\
-0.017020 & 0.020584 & -0.67608 & -0.0017579 & -0.000000038225 & 0.00000011383 & -0.000001184 & -0.000000048608 & -0.013098 & 0.015840 & -0.52027 & -0.0013527 & -0.013098 & 0.015840 & -0.52027 & -0.0013527 \\
0.000001013857 & 0.000000111112 & 0.00000042395 & -0.000000114457 & -0.30379 & -0.039856 & -0.92946 & 0.20552 & -6.3245×10^{-12} & -5.0692×10^{-12} & -1.9349×10^{-11} & 5.2286×10^{-12} & -6.3242×10^{-12} & -5.0692×10^{-12} & -1.9349×10^{-11} & 5.2286×10^{-12} \\
-1.6884×10^{-12} & 4.6473×10^{-13} & -1.5264×10^{-11} & -4.0157×10^{-14} & -2.2780×10^{-12} & 3.5423×10^{-17} & -5.1753×10^{-16} & -2.1919×10^{-16} & -0.017787 & 0.021511 & -0.70655 & -0.0018370 & 0.017787 & -0.021511 & 0.70655 & 0.0018370 \\
-0.11586 & 0.063511 & 0.96682 & 0.026790 & -0.00000331400 & 0.000000075447 & 0.0000226203 & 0.0000015909 & 0.018211 & -0.0099840 & -0.15197 & -0.0042101 & 0.018211 & -0.0099840 & -0.15197 & -0.0042101 \\
-0.025756 & 0.014120 & 0.21496 & 0.0059552 & -0.00000069800 & 0.00000016773 & 0.0000058256 & 0.00000035365 & -0.081912 & 0.044909 & 0.68364 & 0.018935 & -0.081912 & 0.044909 & 0.68364 & 0.018935 \\
-1.8207×10^{-12} & 3.5342×10^{-13} & 5.3803×10^{-12} & 1.4857×10^{-13} & 2.3823×10^{-12} & 1.7883×10^{-18} & 2.3166×10^{-16} & -3.0318×10^{-15} & 0.083912 & -0.046006 & -0.70033 & -0.019398 & -0.083912 & 0.046006 & 0.70033 & 0.019398 \\
0.013807 & -0.00017236 & -0.00034817 & -0.99990 & 0.00000066888 & -0.000000048681 & -0.00000016867 & -0.000059074 & -0.000000015211 & 0.000000053805 & 0.000000038356 & 0.0000084810 & -0.000000015211 & 0.000000053805 & 0.000000038356 & 0.0000084810 \\
0.000000057886 & -0.000000003174 & -0.000000014410 & 0.00000034634 & -0.0096747 & 0.00011900 & 0.0024042 & -0.99995 & 0.000000000939939 & 2.2259 $\times 10^{-14}$ & 1.5863 $\times 10^{-13}$ & -5.0865 $\times 10^{-11}$ & -5.7583 $\times 10^{-13}$ & 2.2262 $\times 10^{-14}$ & 1.5863 $\times 10^{-13}$ & -5.0850 $\times 10^{-11}$ \\
1.0032×10^{-13} & -1.0885×10^{-14} & -2.4491×10^{-14} & 2.3562 $\times 10^{-11}$ & -5.2927×10^{-17} & 2.3511 $\times 10^{-20}$ & -1.8387×10^{-20} & -8.4465×10^{-16} & -0.000000021029 & 0.000000000926023 & 0.000000052572 & 0.77478 & 0.000000017159 & -0.000000021235 & -0.000000042899 & -0.63222 \\
-9.6983×10^{-13} & 1.0780×10^{-13} & 2.4253 $\times 10^{-13}$ & -0.000000000023334 & 4.6579 $\times 10^{-14}$ & -2.3496×10^{-19} & 1.3916 $\times 10^{-19}$ & 8.3829 $\times 10^{-15}$ & 0.000000020285 & -0.000000000025102 & -0.000000050710 & -0.74735 & 0.000000018034 & -0.000000022316 & -0.000000045084 & -0.66443 \\
-1.0 & 0.000000000051905 & 0.000000010593 & -0.000000070435 & -0.00000048737 & 6.4155 $\times 10^{-15}$ & 3.4711 $\times 10^{-13}$ & -4.3708×10^{-13} & 0.000003775 & -1.5977 $\times 10^{-14}$ & -1.0987 $\times 10^{-13}$ & 2.1838 $\times 10^{-13}$ & 0.000038766 & -1.5977 $\times 10^{-14}$ & -1.0987 $\times 10^{-13}$ & 2.1827×10^{-13} \\
-0.000006976 & -1.5529×10^{-14} & -5.9878×10^{-14} & 2.1073×10^{-13} & 1.0 & 0.000000000061717 & 0.000000012595 & -0.000000000042047 & 0.000003391 & -3.9754 $\times 10^{-19}$ & -9.3401 $\times 10^{-18}$ & 1.7541 $\times 10^{-16}$ & 0.000000052785 & 9.4015 $\times 10^{-20}$ & 7.2605 $\times 10^{-19}$ & 2.9765 $\times 10^{-16}$ \\
-0.000000000093861 & 9.0870 $\times 10^{-22}$ & 6.6133 $\times 10^{-18}$ & -1.2331×10^{-20} & -8.8239×10^{-12} & -5.4231×10^{-21} & -1.1054×10^{-19} & 3.7024 $\times 10^{-19}$ & -0.014379 & 2.2448 $\times 10^{-16}$ & 4.5812 $\times 10^{-15}$ & -3.0666 $\times 10^{-15}$ & -0.99990 & 1.5610 $\times 10^{-14}$ & 3.1856 $\times 10^{-13}$ & -2.1314×10^{-13} \\
-0.000000000091112 & 8.8440 $\times 10^{-22}$ & 6.4196 $\times 10^{-18}$ & -1.2006×10^{-20} & -0.000000000050687 & -3.1283×10^{-19} & -6.3837×10^{-18} & 2.1349 $\times 10^{-17}$ & -0.99988 & 1.5609 $\times 10^{-14}$ & 3.1856 $\times 10^{-13}$ & -2.1314×10^{-13} & 0.015298 & -2.3882×10^{-16} & -4.8740×10^{-15} & 3.2600×10^{-15}
\end{bmatrix}
$$